Hot-electron transport and ultrafast magnetization dynamics in magnetic multilayers induced by femtosecond laser pulse excitation

Grégory Malinowski

Habilitation à Diriger des Recherches

Spécialité: Physique

Par

Grégory Malinowski

Hot-electron transport and ultrafast magnetization dynamics in magnetic multilayers induced by femtosecond laser pulse excitation

Habilitation soutenue publiquement le 25 janvier 2023 à Nancy devant le jury composé de :

Rapporteurs :	
Dr. Stefania Pizzini	Institut Néel (Grenoble, France)
Pr. Chiara Ciccarelli	Cavendish Laboratory (Cambridge, United Kingdom)
Dr. Michel Viret	SPEC CEA Saclay (Saclay, France)
Examinateurs :	
Pr. Bert Koopmans	Eindhoven University of Technology (Eindhoven, The Netherlands)
Pr. Matias Bargheer	University of Potsdam (Potsdam, Germany)
Dr. Fausto Sirotti	Ecole Polytechnique (Palaiseau, France)
Dr. André Thiaville	Université Paris-Saclay (Orsay, France)
Pr. Michel Hehn	Université de Lorraine (Nancy, France)

Institut Jean Lamour - UMR 7198 - CNRS
Université de Lorraine – Pôle M4 : matière, matériaux, métallurgie, mécanique

Table of Contents

Preamble

Since I joined the CNRS as a research fellow in 2010 in the Laboratory of Solide State Physics in Orsay, my research activities were focusing on studying laser induced ultrafast magnetization dynamics and especially the role of hot electrons transport at the femtosecond timescale. When I joined the Institut Jean Lamour (IJL) Spintronics and Nanomagnetism group in 2013, I had the opportunity to setup a complete research laboratory and to start this research activity in the group which has strongly developed during the last few years.

In this manuscript, I summarize some of my research activities I have been doing during the last decade. I deliberately chose not to present everything to maintain a certain coherence and hopefully makes the reading more pleasant.

The first chapter gives an overview of the history and state-of-the-art of the research in the field of ultrafast magnetization dynamics and spin transport as well as laser induced all-optical switching. The resulst we obtained regarding these two topics are presented in chapter 2 and 3. Some perspectives are presented in chapter 4. The last chapter summarizes other research related activities.

Chapter 1

Introduction

Manipulating and controlling the magnetic state of a material have been the focus of intensive researches for decades. The desire to understand the physics behind magnetization dynamics was clearly motivated by numerous possible technological applications, such as magnetic hard-disk drives, magnetic memories, and sensors. Within the purpose of ever increasing the speed and density of data storage and decreasing its energy consumption, different levers were proposed to control the magnetization, for instance magnetic field pulses [1], spin polarized currents [2, 3], temperature gradient [4, 5], electric fields [6, 7], strains [8], and more recently THz excitations [9, 10].

In 1996 Jean-Yves Bigot and Eric Beaurepaire from the University of Strasbourg [11] set the ground to a whole new research area in the field of magnetism : femtomagnetism, pushing the ability to alter the magnetic state on the sub-picosecond timescale. Indeed, they showed using the time-resolved magneto-optical Kerr effect (TRMOKE) that the magnetization quenching of a Ni thin film following a 60 fs laser pulse excitation proceeds within less than a picosecond. To date, these results have been confirmed and extended to all pure transition metals (TM) (Fe, Co, Ni) but also different magnetic alloys including rare-earth (RE) elements by using different time-resolved techniques such as, second-harmonic generation [12–19], photoemission [20–23], X-ray magnetic circular dichroism (XMCD) [24–28], or time-resolved x-ray resonant magnetic reflectometry (XRMR) [29, 30].

Less than a decade later, Kimel *et al.* demonstrated that an ultrafast spin reorientation in the antiferromagnet $TmFeO_3$ can be induced by an ultrashort laser pulse due to a sub-picosecond change of the anisotropy axis. Moreover, they showed that the spin dynamics in $DyFeO_3$ could be excited in a non-thermal way using circularly polarized 200 fs laser pulses, leading to a coherent control of the magnetization by way of the inverse Faraday effect [31]. While these experiments were performed at low temperature, a ground breaking result was obtained a couple of years later by Stanciu *et al.* [32]. Indeed, they reported that the magnetization of ferrimagnetic GdFeCo alloys could be deterministically reversed by a single 40 fs circularly polarized laser pulse. In this first demonstration, the direction of this opto-magnetic switching was only determined by the helicity of light which defines the helicity dependent all-optical switching (HD-AOS). Since then, HD-AOS was observed in a large variety of magnetic thin films, including ferrimagnets, synthetic ferrimagnets, and even thin ferromagnetic films including granular media [33–37]. Later on, Radu *et al.* revealed that the magnetization of a 30 nm thick GdFeCo films could be reversed using a single lin-

early polarized pulse [27]. This phenomenon known as the helicity independent all-optical switching (HI-AOS) was reproduced by Ostler *et al.* who showed that, independently of the initial magnetization state, each laser pulse switches the magnetization in the opposite direction [38]. In the following, I give a short introduction on the ultrafast magnetization dynamics triggered by femtosecond laser pulse excitation. I explicitly focus on the role of hot electrons since it is related to a large part of the work I have been doing and that will be presented in 2.1[1]. In the last part of this chapter, I introduce the field of all-optical switching, starting with the discovery of single shot toggle switching in GdFeCo alloys before presenting multiple shots helicity-dependent all-optical switching which has been witnessed in a large variety of magnetic materials.

1.1 Ultrafast magnetization dynamics and ultrafast spin transport

At the beginning of the 1990s, Vaterlaus and co-workers performed the first experiments where the time evolution of the out-of-equilibrium magnetization of the rare earth (RE) Gd was measured using time- and spin-resolved photoemission (TSPE). They estimated the spin-lattice relaxation time, i.e. the characteristic time to reach thermal equilibrium between the spin and lattice, to 100 ± 80 ps [40]). This value was then confirmed theoretically [41]. In 1996, the first measurements of laser induced demagnetization was performed on a transition metal (TM) and the results were quite surprising. Indeed, Beaurepaire *et al.* exploited the time-resolved magneto-optical Kerr effect (TRMOKE) to study nickel thin films [11]. They found that demagnetization after 60 fs pulsed-laser excitation takes place in few hundreds of femtoseconds. Nowadays, it has been widely confirmed that the demagnetization time of TM and their alloys lies in the 100 fs timescale. Moreover, different experimental techniques have been develloped and used to study ultrafast magnetization dynamics including second-harmonic generation (SHG) [12, 42], two-photon or time- and spin-resolved photoemission [20, 43] and later by element specific techniques such as X-ray magnetic circular Dichroism (XMCD) [24] or MOKE using XUVs to probe the $M_{2,3}$ edges [44].

Since then, numerous experiments have been performed to identify the origin of the ultrafast loss of magnetization. Despite this large experimental efforts, the microscopic mechanisms are still heavily debated. Lately, different models have been suggested, for instance based on a direct coupling between the photon field and the spin bath [45, 46] or considering the loss of magnetization due to thermal mechanisms [47, 48]. However, the most notable candidate to explain the ultrafast magnetization dynamics is scattering between particles and quasi-particles to accommodate the transfer of angular momentum out of the spin system [24, 49–56]. In these mechanisms, the electrons are strongly heated by the absorption of the laser pulse and subsequent scattering of hot electrons with energies higher than the Fermi energy thermalizes the spin system resulting in the transfer of spin angular momentum to another reservoir. However, the creation of hot electrons in a ferromagnet generates a spin-current which can have a very high spin-polarization due to the spin-filtering effect. Indeed the lifetime and velocities, as well as reflectivities and transmission of excited

[1]This part of the introduction is largely based on a review paper we published [39]

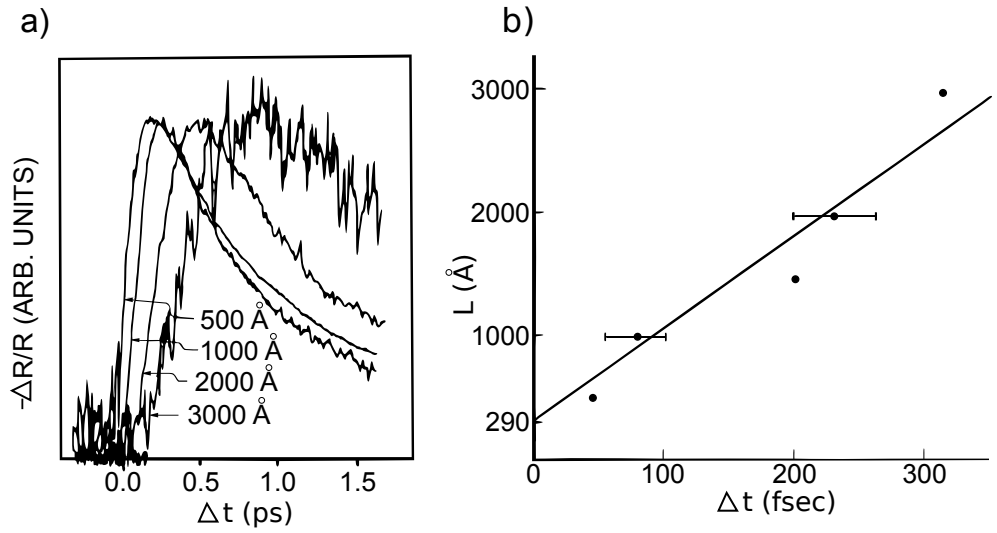

Figure 1.1: (a) Variation of the reflectivity at the back side of Au films of different thicknesses while excited at the front surface. (b) Sample thickness as a function of the time of flight for various Au films of 500, 1000, 15000, 2000 and 3000 Å thick (adapted from Brorson *et al.* [60]).

carriers are spin-dependent and significantly higher for majority spins compared to minority [57, 58]. Based on these facts, Battiato *et al.* proposed that superdiffusive transport could solely explain the ultrafast loss of magnetization [59].

1.1.1 Ultrafast demagnetization and hot electron transport

The first experimental evidence of ultrafast electronic transport following a laser pulse excitation was observed in a single Au layer by Brorson *et al.* [60]. The experiment was relatively simple. Various thicknesses of Au were deposited on a sapphire substrate. The laser excitation was focused on the front of the sample while probing the change in reflectivity induced at the back by electronic temperature changes. The results are showed in Figure 1.1.a. A clear delay in the onset of the signal was reported when increasing the Au layer thickness (Fig. 1.1.b). However, the delay remained shorter than the electron phonon relaxation time suggesting that the heat transport was carried by electrons that are out of equilibrium. It was lately shown that scattering of the excited electrons depends on the crystal structures of the samples, a larger scattering being observed in polycrystalline samples compared to single-crystals resulting in an average slower effective velocity in the case of thick films [61]. From this moment, it was clear that ballistic and diffusive electronic transports had to be taken into account when dealing with ultrafast laser excitation in metallic systems [62–64].

In magnetic materials, as presented previously, it was suggested that spin-dependent transport of optically excited hot electrons could result in a modification of the magnetization due to a redistribution of minority and majority spins within the ferromagnetic layer itself or within an adjacent metallic layer [59]. Following the statement of Battiato *et al.* "that superdiffusive processes play a main role, and can explain wholly the ultrafast demag-

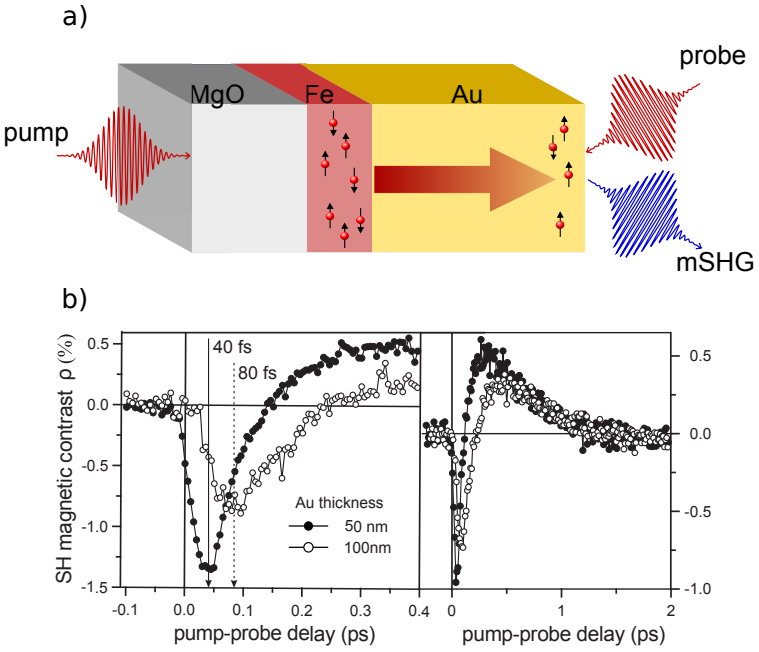

Figure 1.2: (a) Schematic representation of the experimental configuration using a back pump excitation and a front probe to measure the magnetic contribution to the second harmonic generation (mSHG) due to hot electron propagation into a Au layer. (b) Second harmonic magnetic contrast measured at the Au top surface for two different Au thicknesses.(adapted from Melnikov *et al.* [16]).

netization process during the first few hundred femtoseconds", the quest for experimental demonstration started; even though a clear evidence of the influence of hot electron transport on the ultrafast magnetization dynamics was already reported within the work I performed during my postdoctoral stay in the group of Bert Koopmans which will be discussed later on [65]. Thereafter, researchers tried to quantify the relative contribution of hot electron transport and local dissipation of angular momentum by spin-flip scattering.

The simplest structure to explore this phenomenon consists of a single ferromagnetic layer. The first attempt to provide an answer to this fundamental question in such a system was undertaken by Melnikov *et al.* [16]. Using an epitaxial system consisting of Au/Fe/MgO(001), Melnikov and collaborators chose to excite the Fe layer by shining a laser pulse through the MgO substrate. By probing the transient spin polarization at the top Au surface with second harmonic generation, they evidence the existence of a spin-polarized current of hot carriers going from the Fe to the Au layer (Fig. 1.2). They also showed that the transport was a mixture of ballistic and diffusive propagation due to the energy-dependent hot carriers relaxation time which was found to be about 1 ps.

In order to control the spin transport and verify the prediction of Battiato *et al.* [66], Schellekens *et al.* grew a Ni thin film on an insulating sapphire substrate and they measured the ultrafast demagnetization by exciting the Ni layer with a laser pulse hitting the front or the back of the sample while constantly probing from the front (Fig. 1.3 (a)) [67]. The idea behind the experiment is the following: in the case of local angular momentum dissipation, both front and back-pump experiments should result in a similar demagnetization. In the case of ultrafast demagnetization induced solely by transport of excited carriers, a front-pump configuration should lead to a decrease of the magnetization due to a flow of majority electrons toward the substrate. When pumped from the sample's back side, an increase of the magnetization is expected due to a flow of majority electrons towards the probe spot.

First of all, they showed that both front and back-pump excitations lead to a demagnetization of the Ni layer (Fig. 1.3 (b) and (c)). By analyzing the demagnetization curves

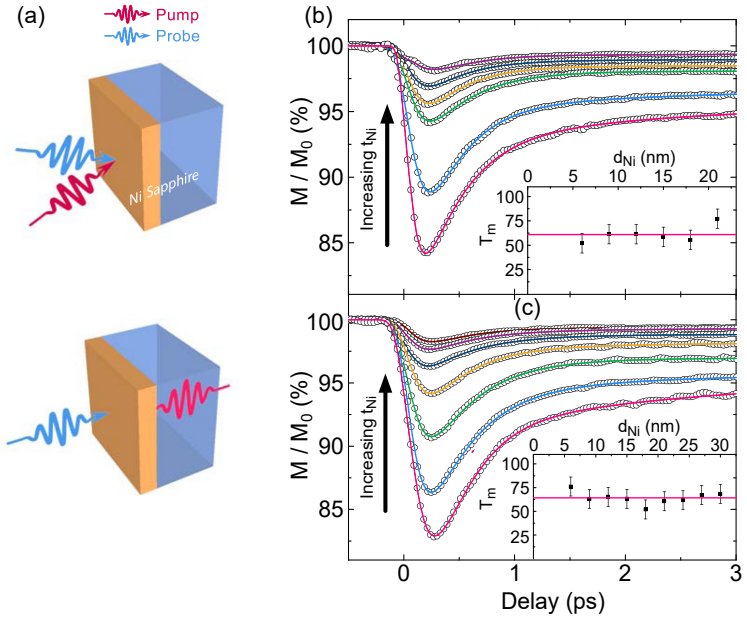

Figure 1.3: (a) Schematic representation of the sample excitation and measurement configurations. Magnetization dynamic as a function of the time delay for (b) a front and (c) a back pulsed laser excitation for various thicknesses of a Ni thin film deposited on Sapphire. Insets show the extracted demagnetization times as a function of the Ni thickness (adapted from Schellekens *et al.* [67]).

in more details, they extracted the timescale for demagnetization and they found out that there is no difference between the two scenarios. Moreover, they clearly showed that the reduction of the magneto-optical quenching as a function of the Ni thickness can be attributed to a decrease in the absorption when the Ni thickness is increased for both configurations. Therefore, all these results demonstrate that transport plays no significant role in the demagnetization of ferromagnetic Ni thin films on insulating substrates. By combining pump-probe TR-MOKE experiments with time-resolved density functional theory calculations, Shokeen *et al.* confirmed that in Ni, spin flips are the main mechanism leading to global demagnetization [68].

To confirm those results, Schellekens *et al.* finally grew a thin film of Ni on top of a wedge of Al [67]. In the case of ultrafast demagnetization governed by hot electron transport, the presence of such a metallic layer should lead to an enhancement of the quenching due to transport of spins outside of the ferromagnet. Results of the measurements showed that the characteristic demagnetization time is not influenced by the presence of the metallic layer. Moreover, increasing the Al thickness results in a decrease of the maximum quenching which does not support a significant role of transport in the demagnetization process of ferromagnetic thin films.

Surprisingly, the study of Hofherr *et al.* provides clear evidences of femtosecond injection of spin current from a Ni layer into a metallic Au substrate [69]. They concluded that the demagnetization dynamics in this system is equally due to spin transport into the adjacent Au layer and a loss of magnetization within the Ni layer itself due to spin-flip scattering or spins that are initially part of the optically excited spin current but which are scattered at the Ni/Au interface. These results are in clear contradiction with previous works presented above.

More recently, Wieczorek *et al.* investigated the relative contribution of transport and local angular momentum dissipation in another system, namely Co/Cu(100), using the complex magneto-optical Kerr effect as described in section 2.1 [70]. By comparing their mea-

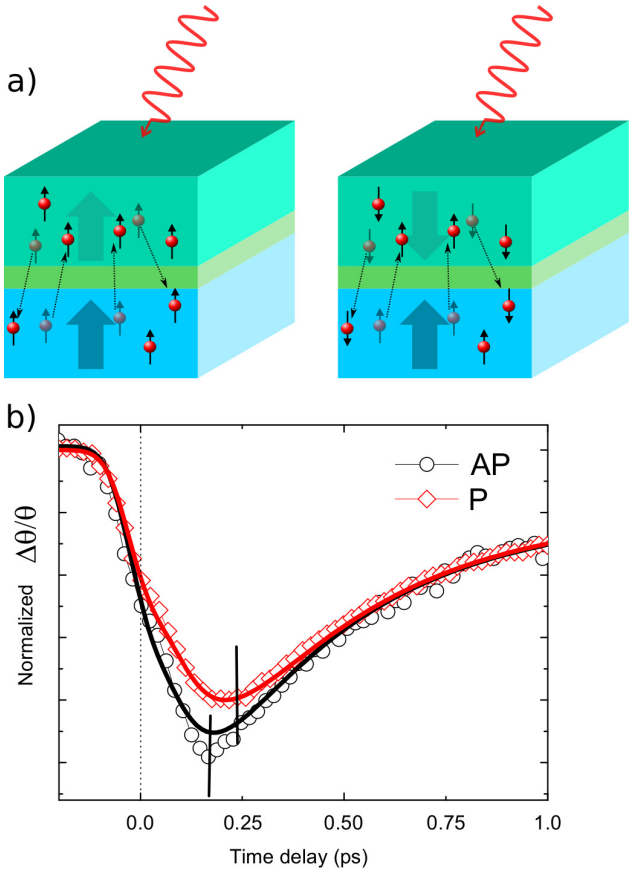

Figure 1.4: (a) Schematic representation of laser excited electrons transport in magnetic heterostructures. (b) TR-MOKE signal measured on Pt(10)/[Co(0.4)/Pt(0.7)]$_4$Co(0.4)/Ru(0.4)/Co(0.4)/[Pt(0.7)/Co(0.4)]$_4$/Pt(2) (units in nm) for parallel (P - diamonds) or antiparallel (AP - circles) alignment of the magnetizations (adapted from Malinowski *et al.* [65]).

surements to calculations based on the microscopic three-temperature model (M3TM) and on spin diffusion equation, they revealed that spin-flip plays a major role in the near-surface region at delays just above 200 fs while spin transport processes are located near the bottom Co-Cu interface and took place on a shorter timescale, earlier than 100 fs when the hot electrons are not thermalized yet. Unlike the previous reports in the case of Ni films by Schellekens *et al.* [67], spin transport processes play a significant role in Co films.

A similar behavior has been recently confirmed by Shokeen *et al.* [68]. Combining TR-MOKE measurements on Ni and Co thin films and *ab initio* calculations performed using time-dependent density functional theory, they showed that spin flips play the most significant role in the process of demagnetization. Moreover, they elucidated the nature of the differences observed for these two ferromagnets. Indeed, their theoretical results showed a temporal separation between a significant amount of spin flips and majority spin diffusion in Co. In Ni, on the other hand, both of these processes occur at the same time. They concluded that the demagnetization induced by femtosecond optical pulses in the two transition metals Ni and Co behave differently during the thermalization process of the spins.

All these results might seem contradictory but altogether, they suggest that the nature of the ferromagnetic layer and the metallic adjacent layer have to be taken into account as well as the role played by the interface in the ability to inject spin-polarized hot electrons. While the precedent paragraphs were focused on heterostructures containing a single ferromagnetic layer, evidence of hot electron transport and its influence on the ultrafast demagnetization was mostly studied in magnetic multilayers.

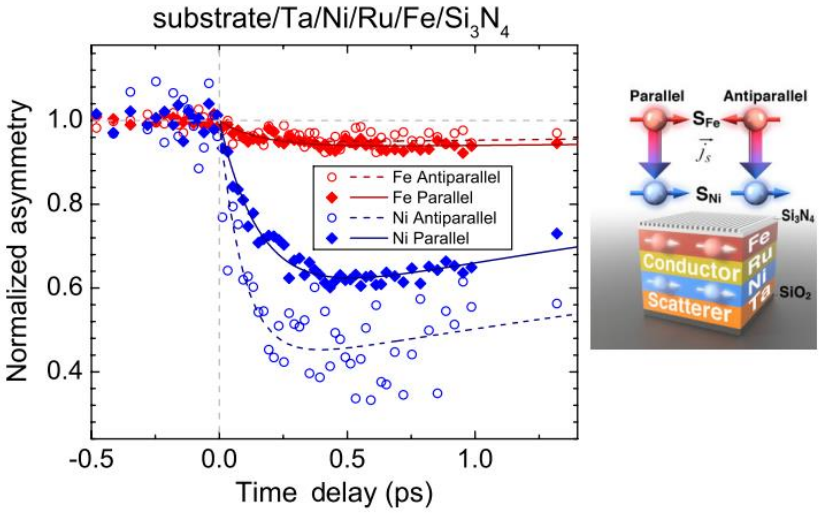

Figure 1.5: Layer-selective magnetization dynamics measured by T-MOKE using high-harmonics in substrate / Ta(3 nm) / Ni(5 nm) / Ru(1.7 nm) / Fe(4 nm) / Si3N4(6 nm). The observed demagnetization in the Fe layer does not change as a function of the relative magnetic orientation. In contrast, demagnetization in the Ni layer increases from $\sim$ 40% to $\sim$ 60% for antiparallel orientation, because spin currents from the top (Fe) layer to the bottom (Ni) layer favor spin-flip scattering processes. (Adapted from Turgut *et al.* [71]).

During my postdoctoral position in the group of Bert Koopmans, I demonstrated for the first time that a femtosecond excitation of a ferromagnetic thin layer can induce a non-local transfer of angular momentum [65]. A schematic description of the experiment and the principal results are reported in Figure 1.4.a . The original idea was to use a multilayer made of two identical out-of-plane magnetized [Co/Pt] ferromagnetic layers separated by either a metallic layer (Ru) or an insulating layer (NiO) in order to control the hot electrons flow between them. Laser excited spin-polarized hot electrons are created in both magnetic layers and travel ballistically from one layer to the other, transferring angular momentum. In the case of an insulating spacer, no difference in the ultrafast magnetization dynamics was observed between a parallel or antiparallel alignment of the magnetizations. In the case of a metallic spacer, the maximum demagnetization is larger and the dynamics is faster in the case of an anti-parallel alignment compared to a parallel alignment of both layers magnetization (Fig. 1.4). We explained this difference by hot spin-polarized electron flow, allowing for interlayer transfer of spin angular momentum between the ferromagnetic layers (Fig. 1.4).

Later on, similar results were reported by Wei *et al.* who studied the ultrafast demagnetization in CoFeB/MgO/CoFeB magnetic tunnel junctions [72]. Beside a more efficient ultrafast demagnetization observed for an antiparallel alignment of both CoFeB magnetizations, they showed that the enhancement due to spin transport becomes more efficient with increasing the laser fluence before saturating to a maximum value. These results seem contradictory with our results in which no transport of excited electrons was evidenced in the case of a NiO spacer [65]. This could be explained by the different tunneling barriers obtained with MgO and NiO. Indeed, It was demonstrated that localized states induced by defects in

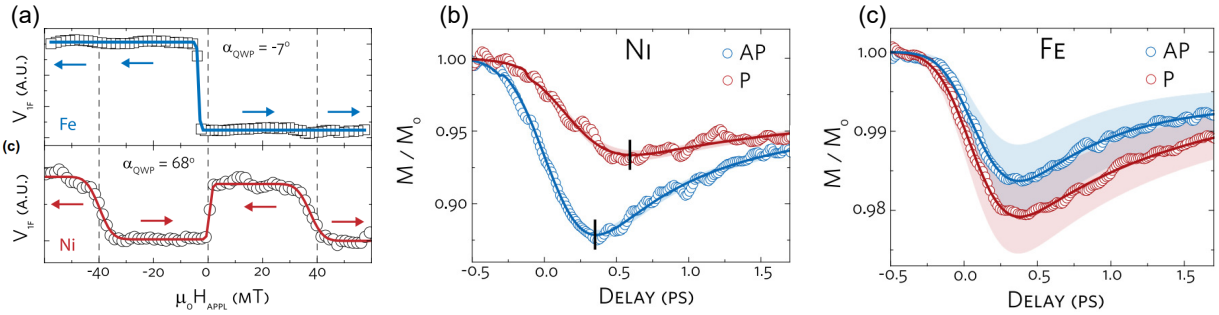

Figure 1.6: (a) One branch of the hysteresis loop is shown for an angle of the quarter wave plate (QWP) $\alpha = -7\,\text{deg}$, showing only the contribution to the MO contrast from Fe and the same is shown in the case of $\alpha = -68\,\text{deg}$, showing only the contribution to the MO contrast from Ni. Demagnetization traces of Ni(b) and Fe (c). The lines are fit to the data and the shaded areas represent the errors due to the mixing of the Ni and Fe MO signals (adapted from Schellekens *et al.* [75]).

MgO barriers strongly influence its electrical properties and spin transport [73]. Moreover, the antiferromagnetic order in the NiO thin layer might increase the spin scattering.

The advent of ultrafast x-ray and extreme-ultraviolet sources allowed for probing spin dynamics in different magnetic layers within the same heterostructure using chemical selectivity (cf section 2.1). Using table-top laser-based high-harmonic generation sources, Rudolph *et al.* simultaneously measured the spin dynamic of Fe and Ni in a Ni/Ru/Fe trilayer using the transverse magneto-opticla Kerr effect (T-MOKE)(Fig. 1.5) [71, 74]. They showed that the demagnetization in the Fe layer does not change as a function of the relative magnetic orientation. In contrast, demagnetization in the Ni layer increases by $\sim 50\%$ in the antiparallel orientation, because spin currents from the top (Fe) layer to the bottom (Ni) layer favor spin-flip scattering processes.

The same group performed complementary experiments to disentangle the contributions of spin-flip scattering and spin-transport processes in similar multilayers. In order to modify the ratio between both processes, they used different spacer layers with different spin lifetime or even an insulating Si_3N_4 to fully suppress spin currents [71]. Their results could only be explained by the simultaneous presence of both interlayer spin-current flow and spin-flip processes. By inverting the Ni and Fe layer in the structure, they have also noticed that the spin current is directional. Indeed, it preferentially flows towards the bottom of the sample. A plausible explanation would rely on the fact that the top interface would reflects the spins while the Ta seed layer would act as a strong spin scatterer, therefore reducing the majority spins flowing from the buried ferromagnetic layer. Another explanation might be related to the occurrence of time dependent thermal gradient due to the absorption profile of the laser pulse within the multilayer.

Schellekens *et al.* investigated a similar structure by TR-MOKE using a material- and/or depth-resolved technique [75]. They could access to both layers magneto-optical signal independently (Fig. 1.6.a) and measured the ultrafast magnetization of both Ni and Fe layers (Fig. 1.6.b and c). Their results unambiguously showed a more effective and faster demagnetization when both layers magnetizations are antiparallel. They estimated that roughly 30% of the Ni demagnetization was due to superdiffusive spin currents coming from the Fe layer.

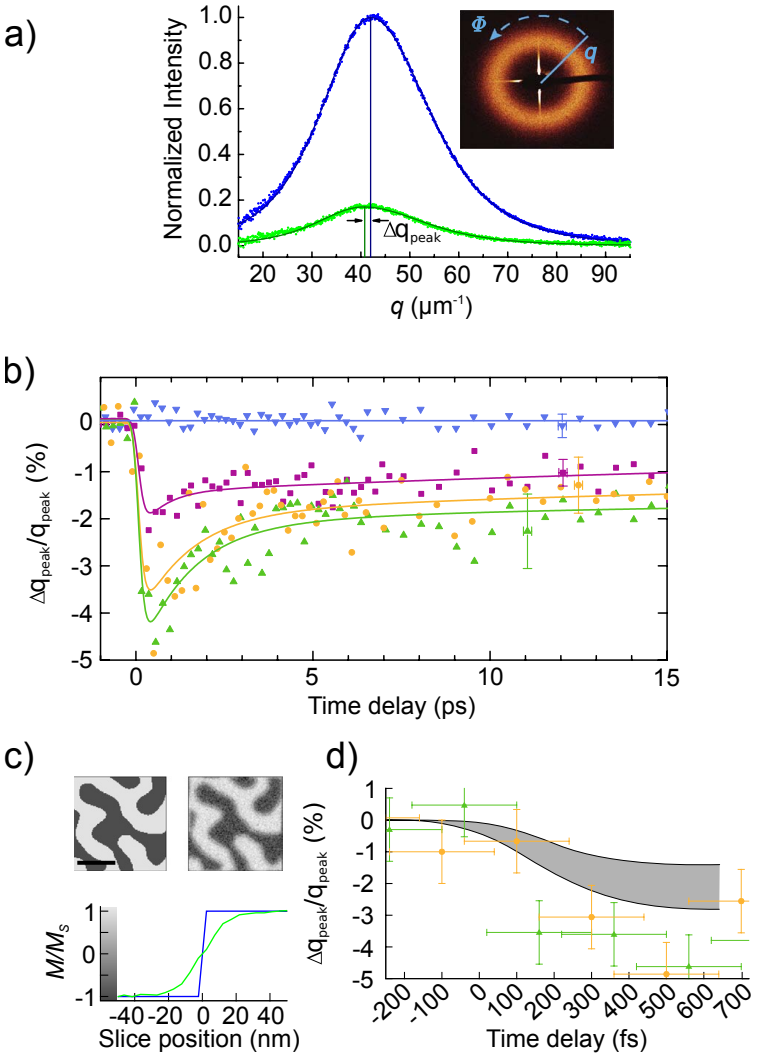

Figure 1.7: (a) Azimuthally integrated SAXS intensity (see inset) probed by a delayed X-ray pulse produced by the FEL. (b) Time evolution of the shift of the integrated SAXS maximum intensity. (c) Temporal evolution of the magnetization in a selected area at the start (top left) and after 300 fs (top right) calculated by Monte-Carlo simulation of the superdiffusive spin-transport (scale bar, 200 nm) and resulting domain-wall profile (bottom). The blue line corresponds to the initial profile while the green one is obtained after 300 fs. (d) Temporal evolution of the shift of the SAXS maximum intensity obtained by simulation (line) and from the experiment (points and error bars). The grey area reflects the uncertainties of the simulations (adapted from Pfau *et al.* [76]).

Moreover, they found that the Fe transient demagnetization was similar for both parallel and antiparallel alignments, in agreement with the work of Turgut *et al.* [71].

The role of superdiffusive transport was also investigated in single ferromagnetic layers showing a magnetic domain structure. In such a system, magnetic domain walls separate domains with opposite magnetization. Hence, they play a similar role as the spacer that is used in a multilayer structure. However, two principal differences can be pointed out when comparing this approach with a multilayer one. First, the sample is chemically homogenous avoiding therefore any disruption in the band structure. Second, in this configuration, any effect of ultrafast electronic transport mainly comes from lateral electronic motion.

Pfau *et al.* used time resolved magnetic small-angle X-ray scattering (SAXS) to study the magnetic response to ultrafast laser excitation of a lateral maze domain pattern [76]. They showed that the SAXS intensity decreases after exposure to laser excitation which reflects the decrease of the average domain magnetization. What is more remarkable is the presence of a shift in the momentum transfer showing similar dynamic to the loss of magnetization on the femtosecond timescale (Fig. 1.7). In order to explain the spatial modification of the maze structure following laser excitation, they proposed that spin-dependent transport of

optically excited hot electrons across the domain walls strongly modifies the magnetization profile of the domain walls, therefore changing the domain's scattering form factor.

Using a similar system presenting a nanoscale magnetic domain network, Vodungbo *et al.* did not observe any modification of the magnetic structure [77] . However, they showed that the demagnetization is significantly faster compared to a uniformly magnetized system of similar composition. Moreover, the characteristic demagnetization time has been shown to be independent of the amplitude of magnetization quenching in contradiction with experimental reports on similar systems uniformely magnetized [78]. To explain these results, they also came to the conclusion that there is a direct spin angular momentum transfer between neighboring domains.

In order to verify this explanation, we investigated the dynamics of similar samples for different magnetic configurations [79]. By changing the applied magnetic field during the experiment, we modified the magnetic domain structure going from a periodic system in the absence of magnetic field to a fully saturated system at high magnetic field. In the case of an intermediate magnetic field, one kind of domain was favored and these domains expanded at the expense of the other. The presence of hot electron spin transport between neighboring domains should result in the alteration of the demagnetization dynamics and in a larger demagnetization amplitude. However, no contribution either to the characteristic demagnetization time or to the demagnetization amplitude was observed. Therefore we concluded that the demagnetization was mainly due to spin flip processes.

Although the spin-polarized transport of hot electrons plays a significant role on the time scale of hot electrons thermalization, the huge experimental efforts provided so far have shown that such mechanism alone cannot explain the whole complexity of laser induced demagnetization.

1.1.2 Ultrafast magnetization dynamics induced by unpolarized hot electrons

New interest in the role of hot electrons transport has emerged since Eschenlohr *et al.* reported sub-picoseconds magnetization dynamics induced by optically generated hot electrons [80]. The authors used IR laser pulses to excite an out of equilibrium distribution of hot electrons in a Au(30nm) layer deposited on top of a Ni(15nm) layer. The Au capping layer was supposed to absorb more than 90% of incident IR laser pulses and thus to avoid direct laser excitation in the buried Ni layer. The subsequent magnetization dynamics of the Ni layer, as well as the direct laser induced dynamics in a uncapped Ni thin film used as reference, were monitored by time-resolved XMCD at the femtoslicing beamline at BESSYII (Fig. 1.8). The laser fluences for the capped and uncapped samples were tuned in order to ensure equivalent absorbed energy. The authors reported ultrafast quenching of the 3d magnetic order in the Ni layer for both the direct and indirect IR laser excitation, with similar demagnetization amplitudes and characteristic times. In the case of indirect excitation, they have attributed the demagnetization to the excited hot electrons transport from the Au layer towards the Ni layer. The slight delay revealed by the comparison of the direct and indirect excitations was attributed to the time required for the hot electrons to cross the Au layer before interacting with the Ni magnetization. Their scenario was corroborated by numerical calculation based on the superdiffusive spin transport theory of hot electrons [59,81].

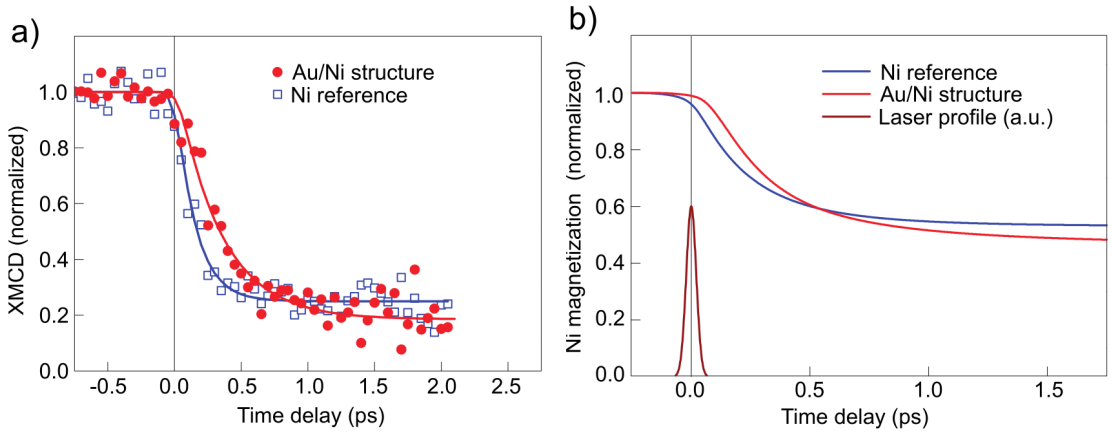

Figure 1.8: (a) Time evolution of the magnetization of Ni reference sample (open symbols) and Au/Ni sample (filled symbols) after excitation with a femtosecond laser pulse. (b) Calculated time evolution of the average magnetization of the Ni film, in the Ni reference layer and Au/Ni sample (adapted from Eschenlohr *et al.* [80]).

The authors concluded that the direct interaction of IR photons with the electronic bath of the excited magnetic material is not the only source of ultrafast dynamics and those hot electrons are as efficient as direct IR laser excitation to induce demagnetization. However, the interpretations extracted from these exciting pioneer results were contested due to the under estimation of transmitted light through the Au capping layer.

Later on, Eschenlohr's conclusions were strengthened by Vodungbo *et al.* who performed time-resolved resonant magnetic small-angle X-ray scattering, at the SXR instruments (LCLS-Stanford), on two ferromagnetic (Co0.4nm/Pd0.2nm) x 30 multilayers (ML) capped either with Al(3nm) or with Al(40nm) [82]. The former is referred as the uncapped ML while the latter is referred as the capped ML. The authors made sure that the IR intensity transmitted through the Al(40nm) capping layer was negligible. The uncapped Co/Pd ML presented a conventional demagnetization upon direct laser excitation, similar to what was previously measured in such samples [25, 77]. On the contrary, the capped Co/Pd ML showed a delayed onset, a lower demagnetization amplitude, and a slower demagnetization rate (Fig. 1.9). Following Eschenlohr's claim [80], they attributed these features to the hot electrons induced demagnetization in the capped ML. The discrepancies between both studies [80], such as the slower demagnetization rate and the longer delay for the demagnetization onset, were attributed to both the broadening of the electron distribution and the thicker capping layer. Although in qualitative agreements in respect with the overall scenario, Vodungbo *et al.* remained cautious regarding the mechanisms by which the hot electrons triggered the demagnetization in the buried Co/Pd ML. They also pointed out that the shorter hot electron lifetime in Al compared to Au could be responsible for the pulse stretching. This work has definitely settled the controversy raised by Khorsand *et al.* [83] concerning the hot electrons induced demagnetization but it has called for further investigations to reveal the transport regime of hot electrons and the microscopic mechanisms that allow transferring angular momentum on the femtosecond timescale.

Salvatella *et al.* [84] published almost simultaneously investigations of hot-electrons in-

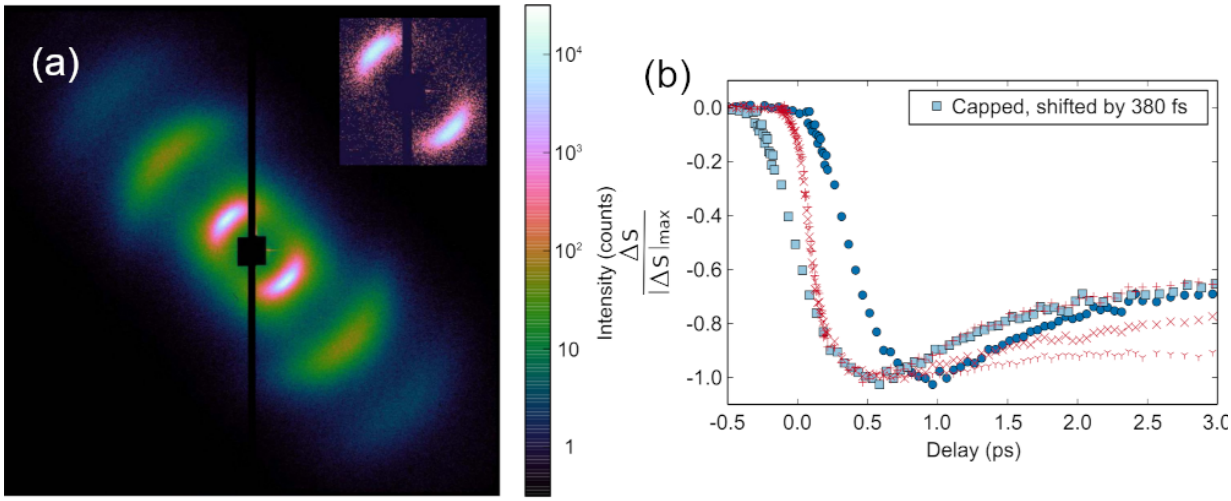

Figure 1.9: (a) Resonant magnetic scattering pattern recorded at the Co L3 edge. The pattern in inset was obtained with a single X-ray pulse. Averaging over about thousands shots reveals scattering up to the fifth order (even orders are suppressed). (b) Normalized magnetic scattering intensity as a function of the delay for capped (blue symbols) and uncapped (red symbols) samples (adapted from [77]).

duced demagnetization performed by tuning the thickness of the non-magnetic capping layer. In their work, the data acquisition was based on table-top time-resolved magneto-optical Kerr effect (TR-MOKE) which is well suited for such systematic investigations. The authors have investigated Al(d nm)/Ni(10nm) bi-layers. They showed that a 30 nm thick Al capping layer is sufficient to avoid direct excitation of the ferromagnet. Above this threshold thickness, hot electrons induced demagnetization became predominant. Their interpretation was supported by solving the heat diffusion equation within the electron gas, coupled to the lattice diffusion equation and are in good agreement with Vodungbo *et al.* results [82].

1.1.3 Manipulation of spin with hot electrons : towards femtosecond spintronics

This growing field of hot electron induced demagnetization opens the route towards femtosecond spintronics using the spin transfer torque effect [85, 86]. In the following, I present recent studies that took advantage of hot electron transport not only to demagnetize a magnetic film but also to manipulate its magnetization. Manipulation of magnetization by ultrafast spin-transfer torque (STT) either by ballistic or diffusive hot electrons were reported by different groups [87–89]. In these articles, femtosecond IR laser pulses were used in order to generate spin-polarized hot electron pulses that propagate towards a ferromagnetic layer whose magnetization dynamics was recorded by means of TR-MOKE. The authors used spin valves structures in which the first ferromagnetic layer is used as a spin-polarizer while the second magnetic layer is used as a detector (Fig. 1.10(a)). Since both experiments aimed at revealing the spin-torque exerted by the spin-polarized hot electrons on the magnetization of the detector layer, the two ferromagnetic layers possessed crossed magnetic anisotropies,

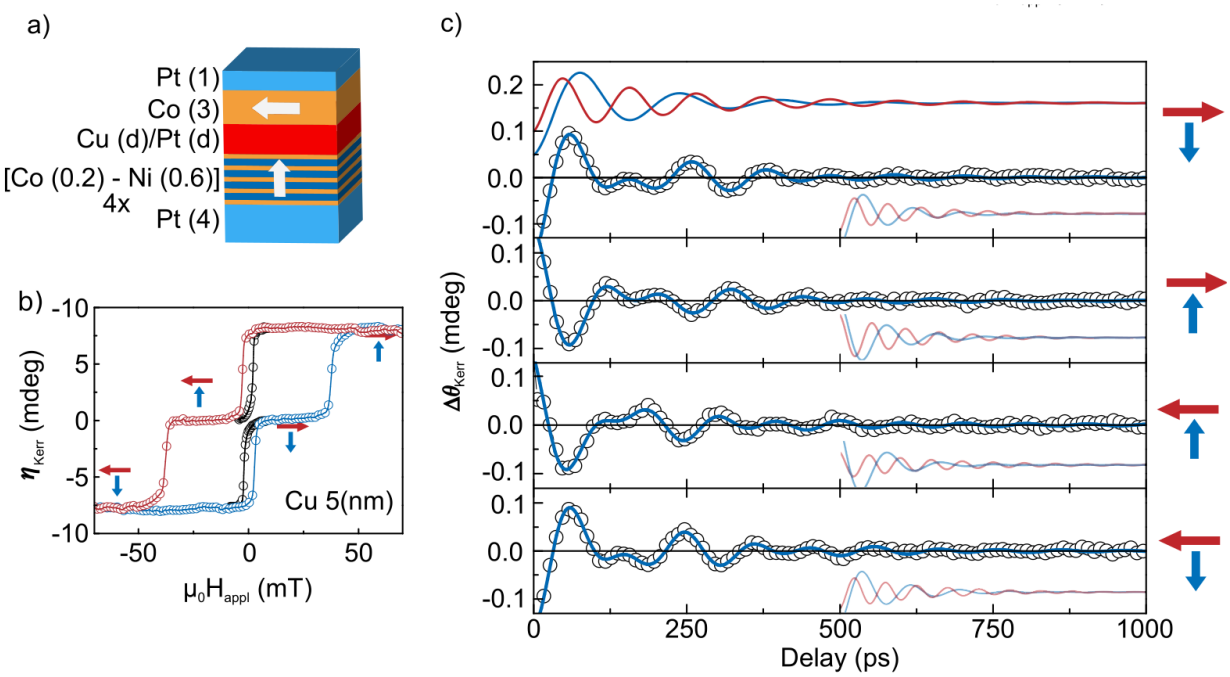

Figure 1.10: (a) Structure used to investigate ultrafast STT. (b) Longitudinal MOKE measurements for a 5 nm Cu spacing layer. The field is applied at 30 degres angle from the film plane. (c) Time-resolved measurements of the out-of-plane component of the magnetization for different magnetic configurations as depicted by the arrows on the right hand-side. (Adapted from [89].).

one pointing in the sample plane while the second one being out-of-plane. This crossed configuration enhanced the torque and avoided any threshold, inherent to parallel anisotropies configuration [2].

In the experiment proposed by Schellekens *et al.* [89], the whole sample was fully excited by the laser pulse, just as in previous experiments [65]. They reported two oscillation regimes that are superimposed with the conventional laser induced demagnetization (Fig. 1.10(c)). They presented a detailed investigation by varying the non-magnetic inter-layer and their thicknesses, the amplitude of the magnetic field as well as the magnetic configurations of both magnetic layers. Finally, they concluded that the precessional phase of the in-plane magnetized layer was determined by the orientation of the out-of-plane magnetized layer, which is fully consistent with an ultrafast laser-induced spin transfer torque. The second contribution was assigned to a precession in the out-of-plane magnetized layer due to a laser induced modification of the local anisotropy. Furthermore, they extracted the amount of angular momentum transferred from the out-of-plane to the in-plane magnetized layer. A maximum of only 2% of the spin participating in the demagnetization of the top out-of-plane layer are absorbed in the bottom layer for a Cu spacing layer of 2 nm. This amount decreases exponentially when the thickness increases due to the enhancement of spin flip scattering with a spin transfer length of about 13 nm for Cu. This length is strongly reduced to 3 nm in the case of Pt.

Choi *et al.* made use of the presence of temperature gradients within the sample thickness

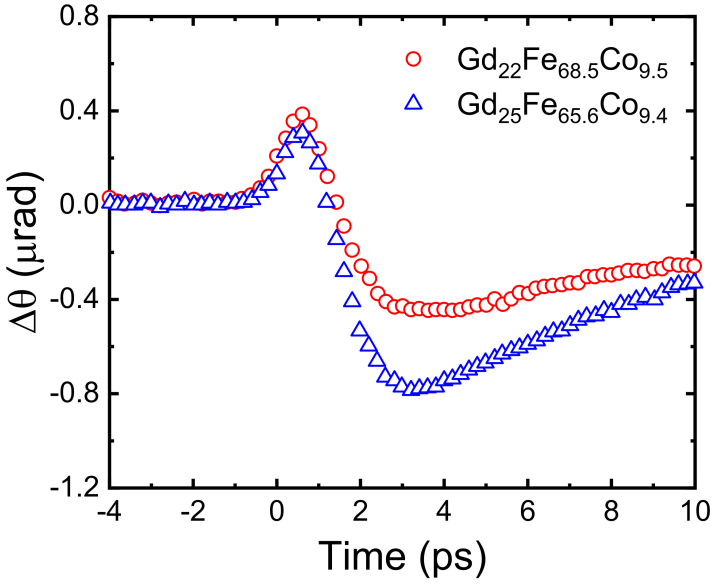

Figure 1.11: TRMOKE measurements of spin accumulation at the Cu surface of $Gd_{22}Fe_{68.5}Co_{9.5}$/Cu (red circles) and $Gd_{25}Fe_{65.6}Co_{9.4}$/Cu (blue triangles) samples.(Adapted from Choi *et al.* [90]).

to trigger a thermal spin transfer torque driven by the spin-dependent Seebeck effect in metallic spin-vales with the structure Pt/FM1/Cu/FM2 [88]. FM1 was made of [Co/Pt] or [Co/Ni] multilayers with perpendicular magnetic anisotropy (PMA) while FM2 was made of CoFeB with in plane anisotropy. A transient heat current was created by exciting the 20 nm thick Pt layer with a laser pulse of 0.8 ps. This Pt thickness insures thermalization of the hot electrons allowing for a pure diffusive description of the electronic transport. The crossed magnetic configuration of magnetization was chosen to optimize the torque exerted by the spin generated in FM1 and diffusing into FM2 through the Cu layer. They observed a clear precession of the CoFeB magnetization due to STT. Moreover, they showed that the precession phase depends on the composition of FM1 demonstrating that [Co/Pt] multilayers have a positive spin-dependent Seebeck effect while [Co/Ni] multilayers have a negative one.

Later on, they investigated the spin generation in conduction bands of ferrimagnetic materials, i.e. TbFeCo and GdFeCo alloys, by measuring spin transport induced after laser excitation into an adjacent Cu layer [90]. They observed that both sublattices composed by the rare-earth element (Tb or Gd) and the transition metals (FeCo) generate spins in the conduction band leading to a spin accumulation in the Cu layer. As plotted in figure 1.11, these two contributions are characterized by two different peaks, a positive peak at ≈ 0.5 ps and a negative peak at ≈ 3 ps. Considering that the spin generation rate is given by $g_S = -dM/dt$ [87], they attributed the positive and negative spin accumulations to the demagnetization of the FeCo and Gd sublattices, respectively. However, the remagnetization of the transition metal also contributes to the negative peak. Nevertheless, a large increase in the negative peak by almost a factor of 2 is observed when increasing the Gd concentration by only 3%. When incorporating the GdFeCo layer into a spin valve structure GdFeCo/Cu/CoFeB, they observed once again a precession of the CoFeB magnetization after laser pulse excitation. The phase of the precession was controlled by the spin current generated by the Gd sublattice occuring on a longer timescale.

Razdolski *et al.* used a similar structure composed of two Fe layers separated by a thick Au layer (55 nm) [91]. A subpicosecond spin current pulse is generated by exciting the top Fe

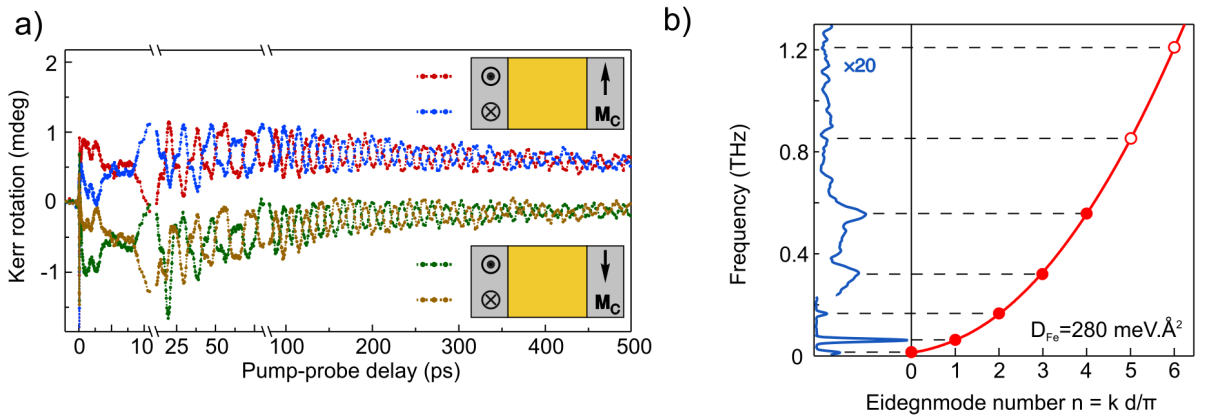

Figure 1.12: (a) Time resolved MOKE measured in four different geometries depicted on the right handside. (b) Fourier spectrum of some similar measurements (left panel). The red line shows the calculated spin wave dispersion curve where D_{Fe} is the magnon stiffness (right panel). Adapted from [91].

layer. The magnetization of both Fe layers were orthogonal in order to optimize the torque exerted by the hot electrons entering the bottom Fe layer. This results in the excitation of spin dynamics in the bottom Fe layer. Due to the very short penetration depth of spin-polarized hot electrons into the Fe layer, confined high frequency perpendicular spin-waves with non-zero k vectors are excited. From their measurements (Fig. 1.12), excitations up to the mode n=4 were observed with a frequency as large as 0.56 THz. Therefore, hot electron induced spin transfer torque is one of the most efficient mechanisms for exciting spin-waves with high k vectors. The same group demonstrated that the generation of ultrashort spin current pulses in this sample was related to the existence of a nonthermal spin-dependent Seebeck effect [58]. They give clear evidence of ballistic transport of spin-polarized electrons in the Au layer. Using a sample structure similar to the one presented in figure 1.10(a), and varying the number of repetitions of the [Co/Ni] multilayer, Lalieu *et al.* showed that the efficiency of STT does not depends on the number of repetition of [Co/Ni] bilayers [92]. In other words, the amount of angular momentum absorbed in the Co layer is similar to the one lost in the [Co/Ni]. This raises question about the mechanism involved in the optical-STT and more specially on the generation of spin current by utrashort laser pulse excitations.

1.2 Laser induced all-optical switching

In 2007, Stanciu *et al.* reported a remarkable discovery; the possibility to reverse the magnetic state of a thin GdFeCo ferrimagnetic layer using a single 40 femtosecond circularly polarized laser pulse [32]. This discovery opened up a new path toward the manipulation of magnetization using light. After 15 years of experiments and theoretical studies, tremendous progress have been obtained regarding our understanding of this phenomenon. In the following, I will present the most relevant results.

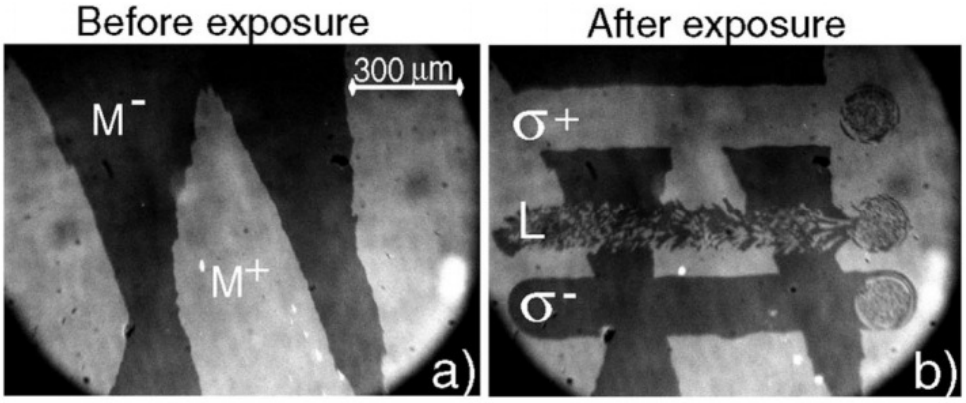

Figure 1.13: (a) Magneto-optical image of the initial magnetic state of the sample before laser exposure. Bright and dark areas correspond to up (M+) and down (M-) magnetic domains, respectively. (b) Domain pattern obtained by sweeping at low speed 30 µm/s linear (L), right-handed (σ+), and left- handed (σ-) circularly polarized beams across the surface of the sample, with a laser fluence of about 11.4 mJ/cm^2. The central area of the remaining spots at the end of each scan line consists of small magnetic domains, where the ratio of up to down magnetic domains is close to 1. Adapted from [32].

1.2.1 The peculiar case of GdFeCo ferrimagnetic alloys

1.2.2 Multiple and single pulse induced helicity dependent switching

In their first reported work, the group of Nijmegen demonstrated that the magnetization of a 30 nm thick $Gd_{22}Fe_{74.6}Co_{3.4}$ alloy with perpendicular magnetic anisotropy could be reversed but the direction of the reversed magnetization was imposed by the light helicity. As depicted in figure 1.13 (a), they performed the experiment by placing a sample under a polarizing microscope, where magnetic domains with opposite direction can be visualize as dark and bright regions. A laser beam was then swept on the sample using 40 fs laser pulses at a repetition rate of 1 kHz for different light polarization. Figure 1.13 (b) shows that $\sigma+$ (resp. $\sigma-$) pulses switch the magnetization in the dark (resp. bright) domain, without affecting the magnetization of other domain. This reversal with circularly polarized light is called all-optical helicity-dependent switching (AO-HDS). The region exposed to linearly polarized light shows a multidomain state with domains randomly oriented up or down. They also showed that exposing the sample to excitation at a 1 kHz rate, the effect of the helicity only appears in a ring area while the center of the region exposed to the gaussian laser beam revealed a demagnetized or multidomain state. Finally, they demonstrated the possibility to reverse the magnetization using a single circularly polarized pulse of 40 fs.

1.2.3 Single pulse induced helicity independent switching

In 2011, Radu *et al.* used the newly available technique of femtoslicing at the synchrotron BESSY to measure the magnetization dynamics of both Gd and Fe sublattices

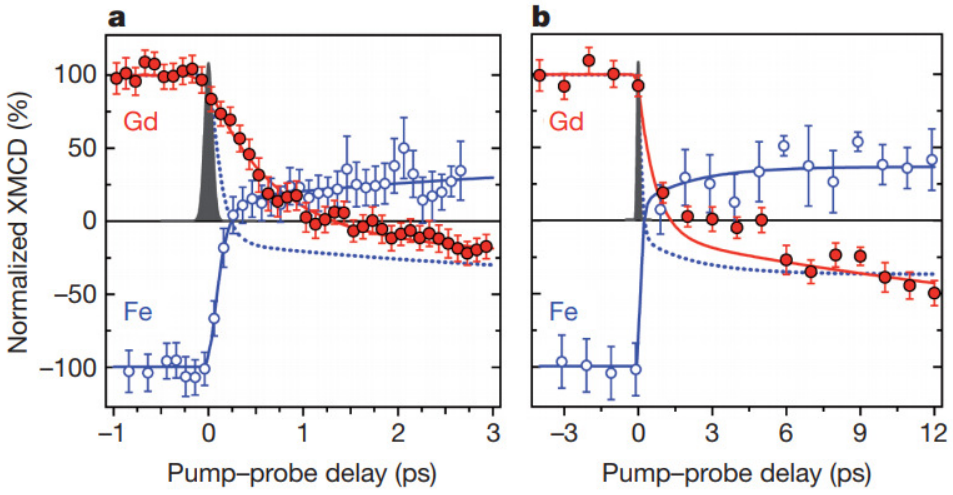

Figure 1.14: (a) and (b) Transient dynamics of the Fe (open circles) and Gd (filled circles) magnetic moments measured within the first 3 ps or 12 ps. The measurements were performed at a sample temperature of 83 K for an incident laser fluence of 4.4 mJ cm^2. Experimental time resolution of 100 fs is depicted by the solid Gaussian profile. The solid lines are fits according to a double exponential fit function. The dashed line in both panels depicts the magnetization of the Fe sublattice taken with the opposite sign. Adapted from [27].

using element-specific time resolved Xray magnetic circular dichroism (TR-XMCD) [27]. In this ferrimagnetic alloy, the magnetization of both rare earth (Gd) and transition metals (Fe and Co) sublattices are antiferromagnetically exchange coupled. The time evolution of the XMCD signal measured at the Fe L_3 and the Gd M_5 absorption edges are depicted in figure 1.14. In this experiment, they only used linearly polarized light. A clear difference between both sublattices is observed with the Fe demagnetizing much faster than the Gd. The most astonishing fact is the presence of a transient ferromagnetic like state with the reversal of the Fe net magnetization within 300 fs while the Gd switches much later at 1.5 ps. This finally ends up in the reversal of the net magnetization of the alloy proving the possibility to all-optical helicity-independent switching (AO-HIS). These measurements were performed at a temperature at which the magnetization is strongly dominated by the Gd sublattice. One may expect Gd to reverse first when the magnetization is (sufficiently) dominated by FeCo as predicted theoretically. However, this has not been experimentally demonstrated yet.

The effect of AO-HIS was then confirmed by Ostler *et al.* [38]. In their experiments, they used a single laser pulse with a duration of 100 fs and a photon energy of 1.55 eV (800 nm) to excite a $Gd_{24}Fe_{66.5}Co_{9.5}$ alloy thin film at room temperature. The magneto-optical images taken after consecutive laser pulses undoubtedly show deterministic toggle magnetization switching. The absence of dependence on the light polarization attests that ultrafast heating delivered by the laser pulse excitation is sufficient to trigger the magnetization reversal. Furthermore, Khorsand *et al.* demonstrated that the light polarization only modifies the threshold fluences required to switch the magnetization due to the existence of magnetic circular dichroism which alters the absorption of light within a magnetic media [93].

Since then, AO-HIS has not only been observed in different ferrimagnetic alloys based on rare earth elements like GdCo [94], GdTbCo [95, 96] but also in half-metallic ferrimagnetic

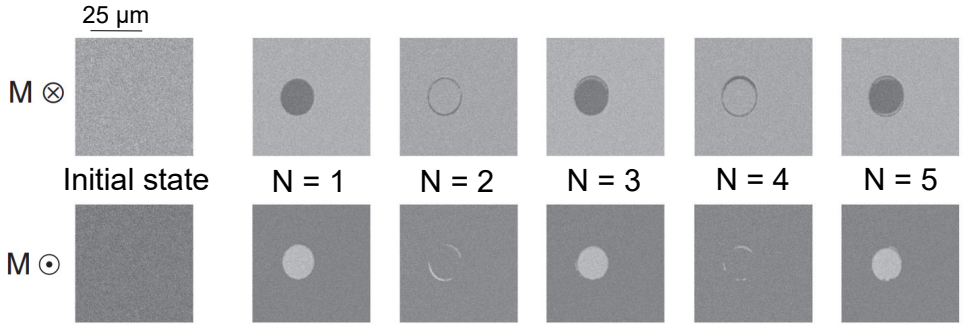

Figure 1.15: Magneto-optical images obtained after exposing a $Gd_{24}Fe_{66.5}Co_{9.5}$ alloy thin film to 5 consecutive laser pulses with a fluence of 2.3 mJ/cm^2 for both initial magnetization orientation. Adapted from [38].

Heusler alloys Mn_2Ru_xGa [97]. Furthermore, it was also reported in synthetic ferrimagnetic multilayers such as Co/Gd [98–100] and more surprisingly in Tb/Co multilayers [101, 102].

In order to unravel the microscopic mechanisms and improve the understanding of AO-HIS, different experimental and theoretical studies have been carried out to investigate the influence of the GdFeCo alloy composition [103–107], the laser pulse duration [104–106, 108] as well as the excitation energy [105, 106, 108, 109].

The pulse duration is one of the critical parameters in the observation of AO-HIS. Initially, short pulses of the 100 fs were used but the possibility to reverse the magnetization with longer pulses was first demonstrated by Steil *et al.* [108]. In their experiments, AO-HIS was achieved using a 13 ps long pulse allowing them to conclude that no strong out-of-equilibrium between the electronic and the lattice is required to achieve magnetization switching. A similar conclusion was obtained the same year by the Nijmegen group [104]. Gorchon *et al.* confirmed that AO-HIS could be observed for pulses of more than 10 ps. They reach the same conclusion that the peak in the electronic temperature and the lattice temperature are not major parameters [105]. Furthermore, they demonstrated that the pulse duration threshold above which multidomain starts appearing varies from about 1 ps for $Gd_{24}FeCo$ to about 15 ps for $Gd_{27}FeCo$. Davies *et al.* observed a similar trend with an increase of the pulsed duration threshold when increasing the Gd content [106].

The influence of the excitation energy was also investigated. Steil *et al.* varied the central wavelength of the laser excitation between 400 and 780 nm [108]. AO-HIS was observed for each wavelength with no clear evolution in the fluence threshold, raising some doubts on the inverse Faraday effect as the origin of the magnetization reversal. More recently, Davies *et al.* showed that AO-HIS could be observed for photon energy varying between 70 meV up to 1.55 eV [106]. These results confirm that a relatively small heating of the electronic system in GdFeCo is sufficient to achieve the required nonequilibrium state to reach magnetization switching.

A significant result, both from a fundamental and applied point of view was obtained by Yang *et al.* [109]. Using an Auston switch to generate individual ~ 9 ps electrical pulses with a peak current density of $\sim 7 \times 10^8$ A/cm^2, they demonstrated deterministic repeatable magnetization switching of GdFeCo. They estimated the energy required to switch a cell of 20 nm^2, which is typical for memory devices, to be $\sim 4fJ$, corresponding to a peak current of

3 mA. Therefore, picosecond electrical switching of magnetization could be as efficient as spin transfer torque or spin orbit torque based devices but more than an order of magnitude faster. Moreover, current complementary metal oxide semiconductor (CMOS) transistor nodes can generate such picosecond electrical pulses, opening the way of integrating ultrafast electrical switching in spintronics devices [110]. For more information about the recent advances in the futur integration of combined spintronics and ultrafast magnetism, we refer the interested reader to the review written by El-Ghazaly and collaborators [111].

Finally, the frequency at which AO-HIS can be used is of paramount importance regarding its applicability to high speed data processing. A first attempt to quantify this value was performed by Wang *et al.* [112]. Using 40 fs excitation pulse width, they showed that, even though writing is completed after 100 ps in GdFeCo, a reliable rewriting by a subsequent shot requires a delay of 300 ps between both pulses. This delay was attributed to the time required for the magnetic layer to cool down. By using optimized substrates to optimize the cooling rate, Steinbach *et al.* were able to strongly increase the writing frequency in GdCo alloys [113]. They also showed that the intrinsic switching dynamics of the ferrimagnetic materials sets a lower limit for the highest achievable repetition rates. A reliable re-switching for a pulse-to-pulse separation of 7 ps was obtained in the case of GdCo, which pushes write/erase cycles of magnetic bits towards the THz frequencies. Similar results were obtained by van Hees *et al.* [114]. Similarly, Banerjee *et al.* demonstrated that reswitching in Mn_2Ru_xGa could be obtained for delay time between two pulses of $\sim$ 10 ps [97].

Finally, non-local spin current can also affect the effciciency of AO-HIS. This was demonstrated by van Hees *et al.* who showed that the spin current generated by the demagnetization of a Co/Ni multilayers can either help or hinder the reversal of a Co/Gd bilayer [115]. This breaking in the symmetry allows for deterministic magnetization writing therefore overcoming the restriction of toggle switching.

Theoretical approaches to AO-HIS

Two important ingredients seem to be mandatory for the observation of AO-HIS. Actually, all the systems showing AO-HIS of magnetization exhibit an antiferromagnetic coupling between different magnetic sublattices. Moreover, both sublattices exhibit their own dynamics as reported by Radu *et al.* in the case of GdFeCo alloys [27] and by Bonfiglio *et al.* in the case of Mn_2Ru_xGa [116]. This particularity is fundamental for AO-HIS to happen since it prevents the loss of memory of the initial magnetic state allowing for a deterministic switching to take place. Bergeard *et al.* demonstrated that the total angular momentum in a GdCo alloy is conserved over a picosecond while it starts being transferred to another degree of freedom (i.e. the lattice) after 150 fs in CoTb [28]. From these results, we could thus conclude that during the first picosecond, there is an exchange of angular momentum between the Gd and the Fe (and Co) sublattices which allows for the appearance of the transient ferromagnetic like state [27]. This mechanism was previously proposed by Medapali *et al.* arguing that a direct transfer of angular momentum occurs between the TM to the RE sublattices when the temperature of the sample is below the temperature of magnetic compensation (T_{comp}) [117]. It was also proposed by Graves *et al.* who discussed the possibility to have a non-local transfer between chemicaly different areas in GdFeCo thin films [118]. However, Hennecke *et al.* demonstrated experimentally in the case of GdFeCo that there is

no transfer of angular momentum between the Fe and Gd sublattices [119]. Therefore, the loss of angular momentum can only be explained by a complete transfer to the lattice during the first hundreds of femtosecond of the demagnetization process, in opposition to what was observed by Bergeard *et al.* in GdCo alloys [28].

Different theoretical approaches have been successfully used to account for AO-HIS. Mentink *et al.* treated the multi-sublattice switching mode in a phenomenological theoretical framework in which they distinguish relaxation of spin-orbit and exchange origin [120]. Longitudinal relaxation originating from the exchange term is the key ingredient in their model since it is only present in magnetic materials with more than one sublattice. They showed that for $T \ll T_{comp}$, when relativistic relaxation mechanisms dominate, both sublattices have distinct dynamics in spite of their strong exchange coupling which follows a Bloch relaxation with a relaxation time $\tau_i = \mu_i/(2\alpha_i\gamma k_B T)$, where μ is the atomic magnetic moment, α is a microscopic parameter determining the loss of angular momentum to the lattice via all possible mechanisms (i.e. Gilbert damping) and γ is the gyromagnetic ratio. When $T < T_{comp}$, the exchange dominates allowing for transfer of angular momentum between the different sublattices, leading therefore to the reversal of one magnetic sublattice spin when it approaches zero.

Atxitia *et al.* derived the Landau-Lifshitz-Bloch (LLB) equation for a two-component magnetic system [121]. In their macroscopic approach, each sublattice is represented by a macrospin varying in length and direction. A mean field approximation is used to derive a macroscopic equation of motion for each sublattice. By complementing their calculations by large scale many-body computer simulations based on the stochastic Landau-Lifshitz-Gilbert (LLG) equation of motion for an atomistic spin model [103], they showed that the distinct element specific demagnetization rate is related to the shape of the equilibrium magnetization curve as function of temperature, suggesting that a strong temperature dependence of the net magnetization is necessary [122].

Schellekens *et al.* developped a microscopic model for ultrafast magnetization dynamics in multisublattice magnets [123]. Their approach originates from the microscopic 3 temperatures model (M3TM) [53] which describes three interacting subsystems of (spinless) electrons, phonons, and $S = 1/2$ spin excitations. They extended the model to $S = N/2$, introduced more than one spin system and added exchange scattering allowing for angular momentum to be transferred between the two magnetic sublattices when an interband electron-electron scattering event occurs. By simulating a fictitious ferrimagnet, they could reproduce the transient ferromagnetic like state as well as the reversal of the magnetization within few picosecond following the laser excitation. Once again, opening the chanel for transfer of angular momentum between both sublattices seems to be the key ingredient.

Different models have been further developed to directly take into account the exchange of angular momentum between the conduction electrons and localized spins [124–126]. In these models, they either described both magnetic sublattices as originating from localized spins which are exchange coupled to conduction electrons [125, 126] or they considered localized spins antiferromagnetically coupled to an itinerant carrier system with a Stoner gap [124]. Anyway, the exchange scattering is directly mediated by the conduction electrons. These models allowed for reproducing the transient ferromagnetic like state as well as the magnetization reversal as observed in the case of GdFeCo.

Gorchon *et al.* proposed a very elegant three-step scenario in which the magnetization

switching can occur without reaching the Curie temeprature of the sample [105]. First, the heat has to be preferentially absorbed by one sublattice, Fe in the present alloy, as suggested by Wienholdt *et al.* [127]. Then, Fe and Gd sublattices exchange energy and angular mometum. Because of the semiadiabatic nature of the process, the temporary equilibrium state will become ferromagnetic to maximize the entropy of the system. In the last step, the Gd magnetization reverses to satisfy the antiferromagnetic coupling with the dominating Fe magnetization.

Recently, Davies *et al.* demonstrated that the exact composition of the ferrimagnetic alloys affects the kinetic reversal of the magnetization [106]. Their model showed that, even for slow heating of the system with no sharp elevation of the electronic temperature, reversal can be obtained by exchange between both sublattices as long as one of them carries more angular momentum than the other and that the spin-mattice relaxation time is slower than the timescale of the intersublattice exchange relaxation.

1.2.4 Helicity dependent switching in magnetic materials

GdFeCo was for a long time the only material exhibiting AOS. However, since 2012 and the work of Alebrand *et al.*, it was shown that AO-HDS is a much more general phenomenon [33]. In this section, I will review some of the works reported in the litterature showing that it can be observed in a large variety of materials.

Ferrimagnetic alloys ans synthetic ferrimagnetic structures

Alebrand *et al.* were the first to report AO-HDS in a high perpendicular anisotropy Tb_xCo_{1-x} ferrimagnetic alloy [33]. The possibility of switching the magnetization using circularly polarized laser pulses was examined by sweeping a laser beam on the sample surface using 400 fs and 10 ps long pulses. They showed that AO-HDS could only be observed when the compensation temperature of the alloy was between room temperature and the Curie temperature.

Similar results were obtained one year later by Hassdenteufel *et al.* who studied Tb_xFe_{1-x} alloys [34]. They found that AO-HDS occurs in a Tb concentration range of $22\% < x < 34\%$. For $x < 25\%$, the compensation temperature remains below room temperature invalidating it as a critical parameter for AO-HIS. They later argued instead that the remanent magnetization is the relevant parameter [128].

The list of materials exhibiting AO-HDS was vastly extended by the work of Mangin[2] *et al.* [35] . In their work, they studied a large variety of RE-TM alloys and multilayers with RE = Gd, Tb, Dy and Ho and TM = Fe, Co or FeCo alloy as well as RE-free synthetic ferrimagnets. They have explored the response in more than 400 separate samples that span a range of fundamental magnetic properties such as spin–orbit coupling, exchange coupling, magnetization and magnetocrystalline anisotropy. AO-HDS was observed in four different magnetic alloys Gd_xFeCo_{1-x}, Tb_xCo_{1-x}, Dy_xCo_{1-x}, and Ho_xFeCo_{1-x}. However, only HoFeCo alloy exhibits AO-HDS while its compensation temperature is above room temperature.

[2]Even though I am among the authors, this work was performed before I joined the group in Nancy.

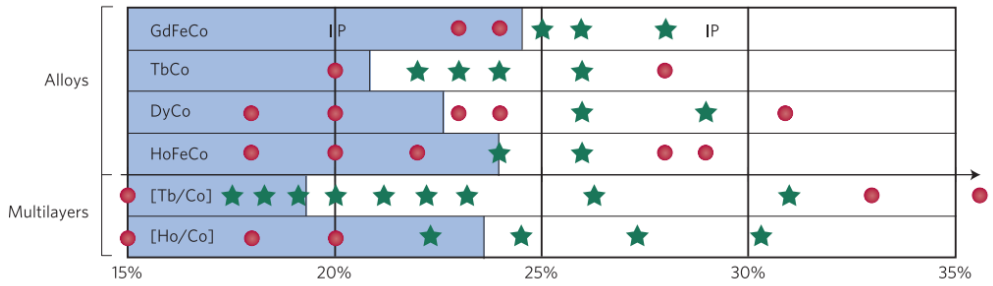

Figure 1.16: Response to optical excitation for RE–TM alloys (Gd_xFeCo_{1-x}, Tb_xCo_{1-x}, Dy_xCo_{1-x}, Ho_xFeCo_{1-x}) and two types of RE–TM multilayer ([Tb/Co] and [Ho/CoFe]) as a function of the RE concentration (different x). Red dots indicate thermal demagnetization and green stars AO–HDS. All of these alloys show perpendicular anisotropy except the two GdFeCo alloys marked as IP (for in-plane anisotropy). The shaded regions correspond to alloy compositions for which T_{comp} is below room temperature. For the multilayers the RE layer thicknesses varied from 0.3 to 0.5 nm and the TM layers varied from 0.25 to 1.0 nm. Image and caption from [35].

They then extended their studies to RE-TM multilayers in which they varied the relative thicknesses of both Re and TM as well as the number of repetition on the RE/TM bilayer. They concluded that AO-HDS can be observed only when the compensation temperature of the multilayer was above room temperature.

Finally and more surprisingly, AO-HDS was demonstrated in RE free synthetic ferrimagnetic heterostructures exhibiting magnetic properties similar to the one of RE-TM alloys and multilayers. Indeed, they exhibit perpendicular anisotropy and two distinct and antiferromagnetically coupled sublattices. Moreover, the structures composed of Ta(4 nm)/Pd(3 nm)/[Co(1 nm)/Ir/Co(0.4 nm)/Ni(0.6 nm)/Pt(0.3 nm)/Co(0.4 nm)/Ir]5/Pd(3 nm) was engineered in order for both Co(1 nm) and Co(0.4 nm)/Ni(0.6 nm)/Pt(0.3 nm)/Co(0.4 nm) layers to have different Curie temperature and therefore different evolution of the magnetization with temperature in order to exhibit a compensation temperature near or above room tempereature.

Similar results were obtained by Schubert *et al.* who used artificial zero moment magnets consisting of two ferrimagnetic layers designed to yield a zero magnetic remanent net magnetization at room temperature [37]. Both layers are made of $Tb_{36}Fe_{64}$ and $Tb_{19}Fe_{81}$ which are Tb and Co dominated respectively. When used indpendently, they both showed thermal demagnetization under femtosecond circularly polarized laser pulse excitations. However, the studies of a bilayer $Tb_{36}Fe_{64}/Tb_{19}Fe_{81}$ resulted in the demonstration of HI-AOS, proving once again that low remanence is a criterion for its observation.

Ferromagnetic materials

The results of Lambert *et al.* provoked a substantial interest due to the crucial demonstration that AO-HDS can also be observed in ferromagnetic materials [36].

They investigated the AO-HDS ability in different magnetic multilayers with PMA including, Co/Pt, Co/Pd, CoNi/Pd and Co/Ni multilayers. Figure 1.17 shows the magneto-

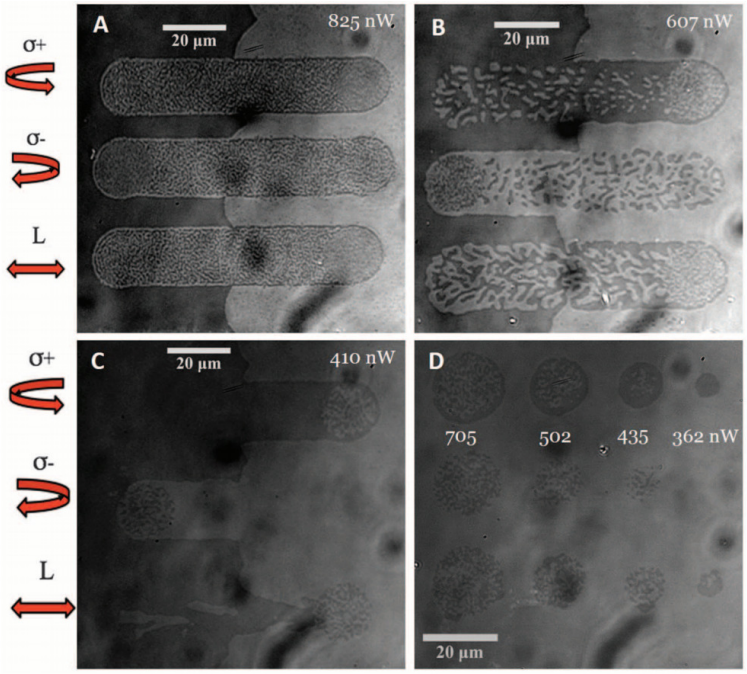

Figure 1.17: Magneto-optical response in zero applied magnetic field of [Co(0.4 nm)/Pt(0.7 nm)]$_N$ multilayer samples to various laser polarizations. (A) N = 8 repeats. (B) N =5 repeats. (C and D) N =3 repeats. For each image, the laser is circularly polarized ($\sigma+$ or $\sigma-$) or linear polarized (L). For (A) to (C), the laser beam was swept over a region of the sample while in (D), the laser was fixed at individual spots over a region of the sample with uniform magnetization. Image and caption from [36].

optical response of [Co(0.4 nm)/Pt(0.7 nm)]$_N$ multilayer samples after being excited by a 100 fs laser pulse with three different laser polarizations. The laser is scanned across a region of the films having both magnetization directions.

For N=8 and 5, a clear thermal demagnetization is observed independently of the light polarization. However, decreasing the number of repetition leads to an increase of the magnetic domains within the excited areas. This is due to the reduction of the field thickness causing a diminution of the dipolar energy. For N=3, a clear AO-HDS is observed as depicted in figure 1.17 (C). The multiple domains created with the linear polarization are much larger, in agreement with a small dipolar energy gain due to domain formation. Furthermore, the effect of the helicity can also be observed when the beam is kept at a fixed position (Figure 1.17 (D)). However, the effect of the helicity appears only in a ring surrounding a demagnetized area. A complete reversal of the excited area could be obtained by decreasing the excitation energy. Similar results were obtained for the other multilayers. However, they did not study the possibility to reverse the magnetization using a single femtosecond laser pulse, making therefore impossible any interpretation on the microscopic mechanism governing AO-HDS.

Finally, they explored the response of high anisotropy granular FePt media to the excitation of femtosecond laser beam with the presence of applied magnetic fields. These are considered as most promising candidates in heat assisted magneto-recording (HAMR) to replace the actual systems and achieve higher storage densities. Figure 1.18 shows both the sweeping and static experiments performed on FePtAgC granular film. Starting from a randomly magnetized state with equal numbers of up and down magnetic domains, a clear net magnetization was achieved whose orientation depends on the laser polarization used during the sweeping (figure 1.18(a)). However, a saturation of only $10-20\%$ of the saturation magnetization was achieved. The lack of saturation can arise from at least two effects. The first is that AO-HDS is only affecting a subset of the grains. The second, and more likely, is that

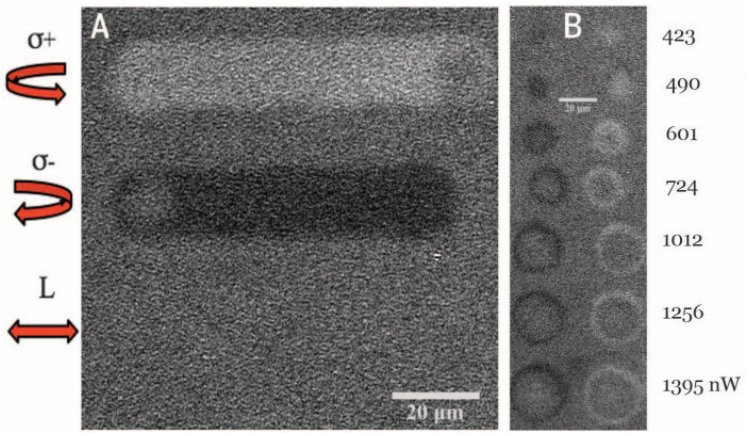

Figure 1.18: Magneto–optical response in zero applied magnetic field of a 15 nm FePtAgC granular film sample starting with an initially demagnetized sample. (A) Line scans for $\sigma+$, σ- , and linear polarized light (L). The laser beam was swept over the sample, and the magnetization pattern was subsequently imaged. (B) Images of magnetic domains written by keeping the laser spot at a fixed position on the sample. The laser was either $\sigma+$ polarized (left column) or σ- polarized (right column). The laser power was 677 nW. Image and caption from [36].

the magnetic grains are highly thermally activated. No effect was observed in the case of linearly polarized light. Static exposure also revealed the presence of AO-HDS (figure 1.18(b)). Similarly to what was observed in Co/Pt multilayers, the helicity dependence occurs only in a ring corresponding to the optimum laser intensity. Furthermore, they quantified the role of the thermal activation on AO-HDS, by applying an external magnetic field while the sample is excited by the polarized light. They demonstrated that a modest applied field of 70 mT (to be compared with the 7T coercive field) is sufficient to suppress the effects of the helicity, indicating that the laser is heating the sample near the Curie temperature T_C. It should be noted that all the results presented in this section were obtained for a large number of laser pulses, shedding light on the cumulative nature of AO-HDS.

Possible mechanisms for AO-HDS

The mechansims underlying the phenomenon AO-HDS are still heavily debated and, up to this date, there is no clear consensus. Several candidates have been proposed in the literature to account for the required symmetry breaking that ultimately leads to the magnetization reversal[3].

The first one is only a thermal effect, namely the magnetic circular dichroism which results from the difference in light absorption in magnetic media as function of the light polarization. It was successfully used to reproduced AO-HDS in granular media [130, 131].

The second one is the so-called inverse Faraday effect. The Faraday effect discovered in 1845, results from the circular birefringence, which is the optical property of a material

[3]I choose to limit the description of the different mechanisms that could explain the HD-AOS to essential. The interested readers are referred to the recent review of Scheid *et al.* [129].

having different refractive indices for left- and right-circularly polarized light resulting in different propagation velocities and therefore a phase shift between both circularly polarized light called the Faraday rotation. A reciprocal effect was proposed by Pitaevskii in 1961 for non-dissipative media and called the inverse Faraday effect (IFE) [132]. Even though this theory was developed for transparent media, it has been widely used to explain the AO-HDS even in dissipative and magnetic materials, notably by the addition of an "optomagnetic field" in micromagnetic simulations [93, 104, 131, 133]. However, these studies tend to show that the IFE might not be suitable to explain AO-HDS, because the effect of the excitation has to be longer than the laser pulse affecting the magnetization dynamics. Moreover, it is not clear whether the IFE should be considered as an effective field acting on the magnetization or as an induced magnetization as in the work of Pitaevskii [81, 132, 134].

Finally, magnetization induced during light absorption (MILA) has been proposed by Scheid *et al.* [135]. They used density functional theory to quantitatively compute the effect of light absorption in ferromagnetic materials and show that, in the presence of spin-orbit coupling, optically induced transitions do not conserve the magnetization and that a systematic induced demagnetization, whose magnitude depends on both the helicity of the light and the direction of the magnetization, is obtained. This mechanism due to the absorption of light, depends on the magnetic state of each atom, and therefore cannot be described by an effective optomagnetic field. Furthermore, contrary to the IFE, the induced magnetization remains long after the laser pulse.

Chapter 2

Hot-electron induced ultrafast magnetization dynamics

During the last 25 years, transport and relaxation mechanisms of photogenerated carriers in metals have been extensively studied [64, 136]. However, the ability to generate and use laser induced polarized or unpolarized hot electron flow to manipulate the magnetic state of a nanometer thin layer is much more recent. In this chapter, I will present some of the work we have been doing related to this thematic since I joined the Institut Jean Lamour. I will start by focusing on ultrafast spin dynamics induced by unpolarized hot electrons before addressing the case of polarized hot electrons.

2.1 Ultrafast spin dynamics induced by unpolarized hot electrons

2.1.1 Hot electrons induced ultrafast demagnetization in Co/Pt multilayers

In 2016, following the work of Eschenlohr *et al.* [80] presented in 1.1.2, we decided to investigate the ultrafast demagnetization induced by hot electrons. Our aim was to settle the the controversy concerning the efficiency of ultrafast magnetization induced by hot electrons. This work was performed during Nicolas Bergeard postdoctoral fellowship [137].

The investigated samples consisting of Glass/Ta(3)/Pt(3)/$[\text{Co}(0.6)/\text{Pt}(1.1)]_2$/Co(0.6)/Cu($d$)/Pt(3) (numbers in bracket correspond to nm) were grown by DC magnetron sputtering, with d the Cu thickness varying from 0 to 300 nm 2.1 (a). Cu was chosen since it has one of the highest hot electrons lifetime [136]. TR-MOKE experiments were realized using a pump-probe technique. The pump consists of 800 nm laser pulses, corresponding to a photon energy of 1.55 eV, with a 35 fs duration. The probe is frequency doubled to 400 nm. The laser repetition rate is 5 kHz. Both beams hit the sample at almost normal incidence and they are focused down to 300 μm and 60 μm for the pump and the probe respectively. Measurements were performed for both directions of the magnetization by pumping the sample from the top Pt/Cu face, while probing the magneto-optical Kerr effect through the glass substrate. In order to accurately determine the zero time delay, samples were patterned to have areas

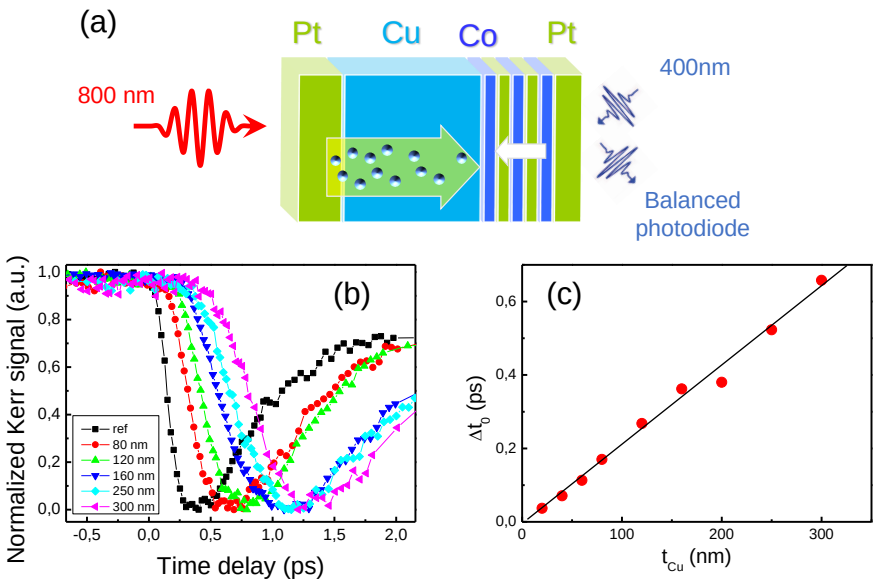

Figure 2.1: (a) Schematic representation of the multilayer structure. (b) Time evolution of the magneto-optical signal measurements for different Cu thicknesses. The laser power was adjusted to keep the maximum demagnetization constant for all samples, allowing for a normalization of the signal. (c) Cu thickness dependence of the induced time delay in the onset of demagnetization $\Delta t_0 = t_0(d) - t_0(d = 0)$. The full line is a linear fit to the data.

with and without the Cu layer.

In order to quantitatively separate direct photon excitation from the one due to hot electron transport, we carefully measured the optical transmission in samples consisting of Glass/Ta(3)/Cu(d)/Pt(3) (units in nm) and we compared them to calculations based on absorption profiles [83]. Furthermore, absorption profiles were calculated for the full stack containing the [Co/Pt] multilayer. Because of the high absorption of Pt compared to Cu, the majority of the light is absorbed in the top Pt layer. Since its thickness is smaller than the hot electrons relaxation length at this energy, hot electrons generated in Pt can propagate to the Cu layer without experiencing significant scattering. As the Cu thickness increases, direct laser excitation of the Co/Pt multilayers is strongly reduced, since photon transmission decreases exponentially with the Cu thickness. The absorption in the Co/Pt multilayers is reduced by a factor of 100 for 60 nm of Cu, while hot electrons can pass such a layer almost without any loss.

Figure 2.1 (b) shows the evolution of the transient Kerr rotation as function of the Cu thickness. We extracted the modification of the delay time in the onset of demagnetization $\Delta t_0(d) = t_0(d) - t_0(d = 0)$ where $t_0(d)$ is measured at 10% of the total signal, as function of the Cu thickness(Figure 2.1 (c)). A linear evolution of the delay time in the onset of demagnetization with the Cu thickness is observed from 0 up to 300 nm of Cu. The slope corresponds to a constant velocity of $0.68 \times 10^6 \pm 0.05 \times 10^6$ m/s assuming ballistic trajec-

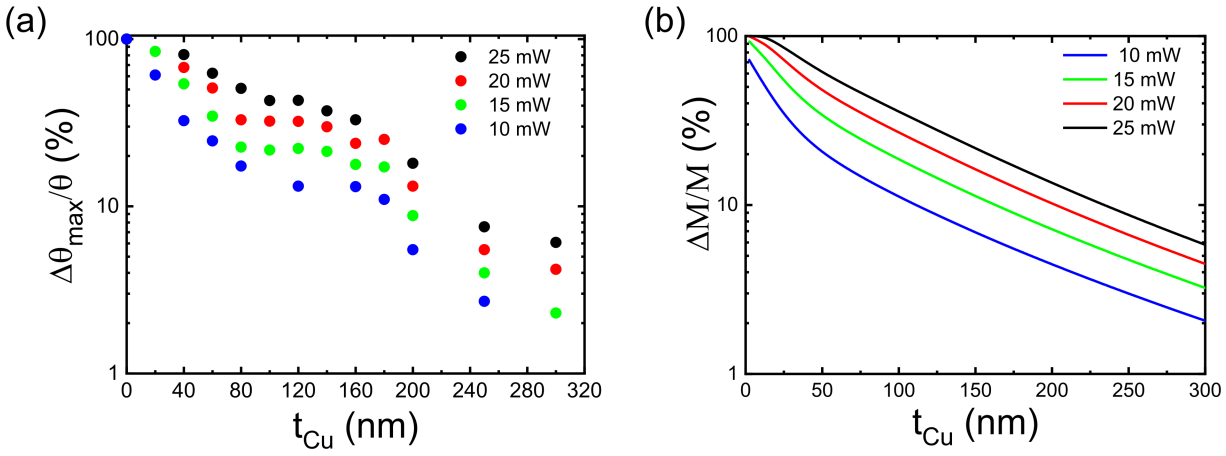

Figure 2.2: (a) Experimental and (b) simulated variation of the maximum induced Kerr rotation as function of the Cu thickness for different laser power.

tory perpendicular to the Cu layer. Such a linear variation and high velocity can only be attributed to hot electron transport. We first attributed this linear dependence to a proof of ballistic electron transport, as it was initially suggested by Brorson *et al.* [60]. However, in a collaborating study with the group of Mathias Bargheer, it was clearly demonstrated that the presence of a linear space-time relationship in the experimental data is not sufficient to identify a ballistic transport mechanism [138].

In order to study the decay of demagnetization efficiency more quantitatively, we extracted the maximum demagnetization at fixed laser power as a function of Cu spacer thickness, whereby clearly distinct regimes can be found in figure 2.2 (a). A separation between demagnetization due to direct photon excitation and hot electron excitation can be observed which occurs around 60 nm of Cu. For Cu layers thinner than 60 nm, the decay is rather fast corresponding to an exponential reduction of the contribution to the induced demagnetization of the direct photon absorption in the Cu layer. Above this thickness, we enter the second regime which could also be characterized by an exponential decay but with a much longer characteristic length of $150 - 200$ nm. In that case, demagnetization is only induced by hot electrons. Above 180 nm, a stronger attenuation seems to occur but the reason of this effect remains unclear and requires more experiments which is beyond the scope of this work. Moreover, the distinction between the direct photon and hot electron excitations vanishes when the laser power increases. In that case, the direct absorption becomes sufficient to induce a large demagnetization even for a thicker Cu layer.

To investigate in more details the role of hot electrons in the ultrafast demagnetization process, we collaborated with the group of Bert Koopmans from the Eindhoven University of Technology to implement hot electron ballistic transport within the Microscopic 3-temperatures model (M3TM) [53]. This model which was successfully used to reproduce laser induced magnetization dynamics for a wide range of ferromagnets, simulates transfer of angular momentum between the spin and the lattice based on Elliot-Yafet type of scattering with a probability a_{sf} that an electron flips its spin when absorbing or emitting a phonon (see reference [53] for more details). The time evolution of the electron and phonon temper-

atures and of the magnetization is derived using a set of coupled differential equations given by:

$$\begin{aligned} C_e[T_e](z)\frac{dT_e(z)}{dt} &= g_{ep}(T_p(z) - T_e(z)) + P(z,t), \\ C_p\frac{dT_p(z)}{dt} &= g_{ep}(T_e(z) - T_p(z)), \\ \frac{dm(z)}{dt} &= Rm(z)\frac{T_p(z)}{T_C}\left(1 - m(z)\coth\left(\frac{m(z)T_C}{T_e(z)}\right)\right), \end{aligned} \tag{2.1}$$

where T_C is the Curie temperature of the ferromagnetic layer. T_e and T_p are the electron and phonon temperatures respectively, and $P(z,t)$ represents the source of excitation as discussed below. Furthermore, $R = (8a_{sf}g_{ep}T_C^2)/(k_BT_D^2D_S)$ represents a prefactor controlling the demagnetization rate with k_B the Boltzmann constant, T_D the Debye temperature and D_S the atomic magnetic moment divided by μ_B. The coupling constant between the electron and phonon subsystem is given by $g_{ep} = (3\pi D_F^2 D_P k_B^2 T_D \lambda_{ep}^2)/(2\hbar)$ with D_F the density of states at the Fermi level, D_P the number of oscillators per atomic site and λ_{ep} the electron-phonon coupling constant.

Transfer matrix calculations were performed to calculate the laser absorption profile for relevant Cu spacer thicknesses (see supplementary information). All absorption in the buried Co/Pt layer $A_{CoPt}(t)$ is treated as a direct heating source $P_{dir}(t)$, with a Gaussian temporal profile $exp(-(t/t_p)^2)$, where t_p is determined by the laser pulse length. All absorption in the top Pt and Cu, $A_{Pt}(t)$ and $A_{Cu}(t)$ respectively, is assumed to be transferred to hot electrons. For sake of simplicity, and because of the short optical penetration depth, we approximate all hot electrons to be generated at t = 0 in a slab with infinitesimal thickness at the Pt/Cu interface. Hot electrons are assumed to travel ballistically at speed v_0, and with an isotropic orientational distribution, through the Cu of thickness d. Therefore, scattering that would widen the arrival time distribution is not taken into account. For this situation it is straightforward to derive the arrival time distribution at the Cu-Co/Pt interface. Furthermore we introduce a hot electron life time τ_{he} (related to the hot electron attenuation length via $\lambda_{he} = v_{he}/\tau_{he}$), and an efficiency F to transfer the energy flux at the interface into heating of the Co/Pt electronic system, which is treated as an indirect heating source term $P_{ind}(t)$ in Eq. (1). Thus we find:

$$P(t) = P_{dir}(t) + P_{ind}(t) \tag{2.2}$$

$$P_{ind}(t) = F(A_{Pt} + A_{Cu})(1 - \frac{d/v_{he}}{t^2})exp(-t/\tau_{he}), \text{if } t < d/v_{he}, \text{and 0 else} \tag{2.3}$$

In order to simulate the maximum demagnetization as a function of the power and the Cu thickness, we used a characteristic hot electron decay length of 200 nm, a hot electron velocity of 1×10^6 m/s and an efficiency parameter F of 0.8. The calculated evolution of the maximum demagnetization as a function of the Cu layer agrees very well with the experimental results (Figure 2.2 (b)). These results shed light on some of the questions that are still unanswered about ultrafast demagnetization. The first conclusion we can extract without ambiguity from this work is that the laser field is not a compulsory element to induce

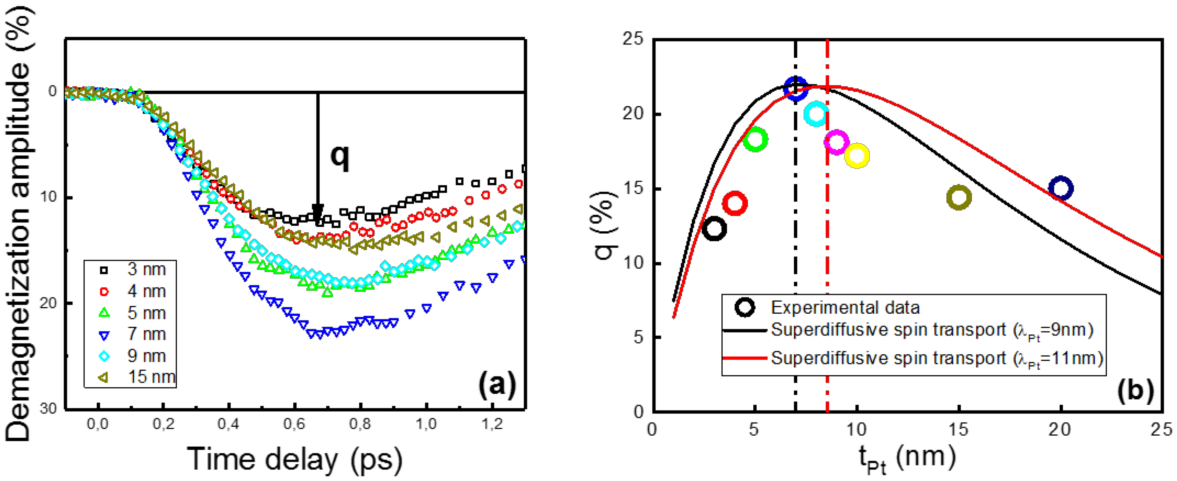

Figure 2.3: (a) Transient Kerr rotation measured in the pump-front/probe-back configuration upon hot-electron excitation as a function of the delay for different thicknesses of the Pt top layer. (b) Hot-electron-induced maximum demagnetization amplitude (q) as a function of the thickness of the Pt top layer.

ultrafast demagnetization [45, 46, 139]. Moreover, in order to induce demagnetization of the buried Co/Pt multilayer, the hot electron energy has to be transferred into the magnetic system. The generated unpolarized hot electrons in the Pt/Cu layers only act as a heating source, subsequently increasing the electron temperature by electron-electron interaction within the magnetic layer. We find very good agreement with experiments employing such a scenario and assuming a demagnetization process based on Elliot-Yafet mediated spin flip scattering, whereas in Eschenlohr's work [80], the hot electron induced demagnetization was claimed to be due to hot electron transport in the ferromagnetic layer itself. Despite the proven finite role of hot electron transport on ultrafast demagnetization, present consensus is that such demagnetization processes are predominantly driven by local dissipation of angular momentum [67].

In a subsequent study, we monitored the relative amplitude of the demagnetization induced by hot electrons in [Co/Pt] multilayers for different capping layers and a Cu thikcness of 100 nm [140]. We first showed that a Pt layer is more efficient than $[Co/Pt]_X$, Cu, or MgO layers in converting infrared (800 nm) photon pulses into hot-electron pulses at a given laser power. We then considered the influence of the Pt thickness on the maximum demagnetization of the [Co/Pt] multilayer. Figure 2.3 show the transient Kerr rotation upon hot-electron excitations as well as the maximum relative demagnetization amplitude q as a function of the thickness of the Pt capping layer for a constant laser power of 10 mW. Increasing the Pt thickness from 3 to 7 nm results in an increase of the demagnetization amplitude by $\sim 45\%$. However, the maximum demagnetization starts decreasing for larger thicknesses.

To elucidate the origin of the observed variation, we collaborated with Karel Carva from the Charles University of Prague. Using the superdiffusive model [59], they tracked the spatial diffusion of electrons excited to different energy levels, including secondary electron excitation due to electron-electron scattering. The simulations were thus run for FM(4)/Cu(100)/Pt(x) multilayers, where FM is a uniform ferromagnetic layer and the Pt

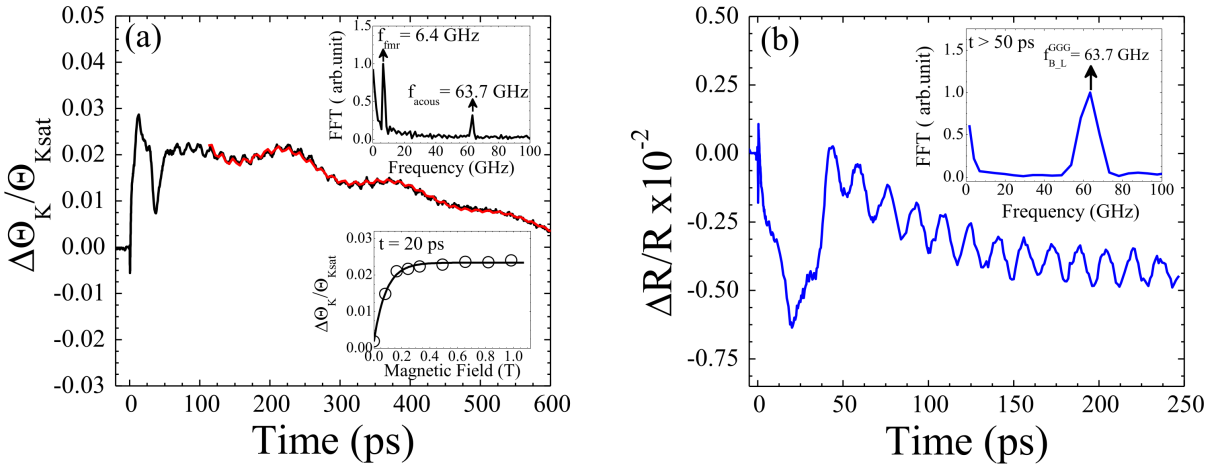

Figure 2.4: Dynamics of spin and reflectivity in the $Bi_2Y_1Fe_5O_{12}$/GGG(100) buried below a thick Pt/Cu bilayers. (a, b) $\Delta\Theta_K/\Theta_K sat$ and $\Delta R/R$ induced by a laser energy density of 11.3 mJ. cm^{-2} for H_{ext}= 0.33 T. Inset (a): Fourier transform spectrum of the $\Delta\Theta_K/\Theta_{Ksat}$ data for the time delay t $\geq$ 50 ps (top) and the $\Delta\Theta_K/\Theta_{Ksat}$ signals (bottom) measured at the time delay t = 20 ps as a function of H_{ext}. Inset (b): Fourier transform spectrum of the $\Delta R/R$ data for the time delay t $\geq$ 50 ps (top).

thickness x was varied in the range from 1 to 25nm. Their transport simulations employ the energy and spin-dependent electron velocities and life times, which were obtained from *ab initio* calculations for bulk Cu, Pt, and Co. Taking into account the laser fluence and the photon energy, they calculated the absorption within the sample assuming different penetration depths λ_{Pt} of the IR in the Pt layer. Theoretical calculations predict a maximum demagnetization for 8.5nm of Pt for λ_{Pt} = 11 nm and 7 nm of Pt for λ_{Pt} = 9 nm which is in good agreement with our experimental results. The optimum value of 7 nm of Pt to generate and propagate the highest number of hot electrons through the Cu layer is thus related to the competition between the penetration depth and the attenuation length within the Pt layer.

2.1.2 Using hot electrons to drive picosecond acoustic excitation in bismuth-substituted yttrium iron garnet

During the last decade, acoustic pulses have been proven to be an alternative way to control the spin dynamics with providing at least two advantages [141–143]. First, acoustic pulses can produce very high mechanical stress. As a result, a large modification of lattice parameter occurs and the magnetization can be therefore non thermally changed via the inverse magnetostriction effect. Second, acoustic pulses have a large propagation distance of several millimeters with low-energy dissipation [144, 145]. Consequently, they provide opportunity for nonthermal manipulation of spins in films deeply embedded in opaque heterostructure devices. While magnetization dynamics by picosecond acoustic pulse was achieved in GaMnAs ferromagnetic semiconductor [141] and ferromagnetic metals [142, 146, 147], an important

question in this context was the possibility to take advantage of picosecond acoustic pulse to trigger a magnetization dynamics in magnetic dielectrics.

To test this hypothesis, we explored the laser-induced ultrafast magnetization dynamics in bismuth-substituted yttrium iron garnets (Bi-YIG) buried below a thick Cu/Pt metallic bilayer [148]. This work was performed during the postdoctoral fellowship of Marwan Deb who had a long experience in studying these materials.

The experiments were performed on 140-nm-thick film of $Bi_2Y_1Fe_5O_{12}$, grown by pulsed laser deposition onto a gadolinium gallium garnet (GGG) (100) substrate. Longitudinal and polar Kerr measurements showed a normalized remanence of 0.45 and 0.05, respectively. The very weak polar remanence indicated that the easy axis of the magnetization is in the film plane.

In order to explore the effect of an ultrashort strain pulse on the magnetization dynamics in iron garnet, a thick Cu(100)/Pt(5) nonmagnetic metallic bilayer was deposited by dc magnetron sputtering on top of the garnet film. The time-resolved Kerr and reflectivity measurements were performed at 300 K with a front pump back probe configuration similar to what was presented in figure 2.1 (a).

Figure 2.4 shows the time-resolved Kerr effect measurement of the dynamics induced by a laser energy density of 11.3 mJ.cm^{-2} for an external applied magnetic field of H_{ext} = 0.33 T. We note that the TR-MOKE signal changes its sign when the direction of H_{ext} is reversed. In addition, the zero time delay corresponds to the arrivals of the hot-electron pulse at the back side of the Cu layer, as revealed by the TR-MOKE signals measured in areas with and without the Pt/Cu bilayers. Moreover, a strong peak in the TR-MOKE signal appears at t = 40 ps, corresponding to the time required for a longitudinal acoustic pulse to cross the Cu and Bi-YIG layers ($t = d_{Cu}/V^L_{Cu} + d_{Bi-YIG}/V^L_{Bi-YIG} \approx 46$ ps with d_i and V^L_i the thickness and longitudinale sound velocity of the layer i). Interestingly, after the acoustic pulse leaves the Bi-YIG layer, two resonance modes are clearly revealed by the oscillations shown in the time-resolved Kerr signal with the frequencies of 6.4 and 63.7 GHz, as seen in the Fourier transform spectrum displayed in the inset of Fig. 2.4(a). The first mode is the ferromagnetic resonance mode (f_{FMR}) observed via acoustic pulse induced changes of magnetocrystalline anisotropy, whereas the second mode (f_{acous}) results from the modulation of the Kerr effect by the propagation of the acoustic pulse in the GGG substrate.

The obtained results suggest that an acoustic strain excitation is at the origin of the observed resonance modes. The existence of such a strain pulse traveling through the sample has been experimentally confirmed by measuring the pump-induced changes in the reflectivity signal (Fig. 2.4 (b)), which shows clear oscillations for the time delay higher than 50 ps. Such oscillations were attributed to the so-called Brillouin oscillations, which are due to the interference between the probe beam reflected at the Bi-YIG interfaces and secondary beams reflected by the strain pulse propagating in the GGG substrate. The observation of such oscillations in the TR-MOKE signal can be related to a small difference in the reflection of $\sigma+$ and $\sigma-$ induced by the acoustic pulse when it propagates in the GGG. These results clearly demonstrate that an acoustic pulse can induce in a transparent medium a structure with a complex refractive index that allows the modulation of the magneto-optical effects at a frequency determined by the sound velocity.

On the other hand, the frequency of 6.4 GHz associated with the low-frequency mode is in the range of the ferromagnetic resonance (FMR) frequencies in Bi-YIG. In order to confirm

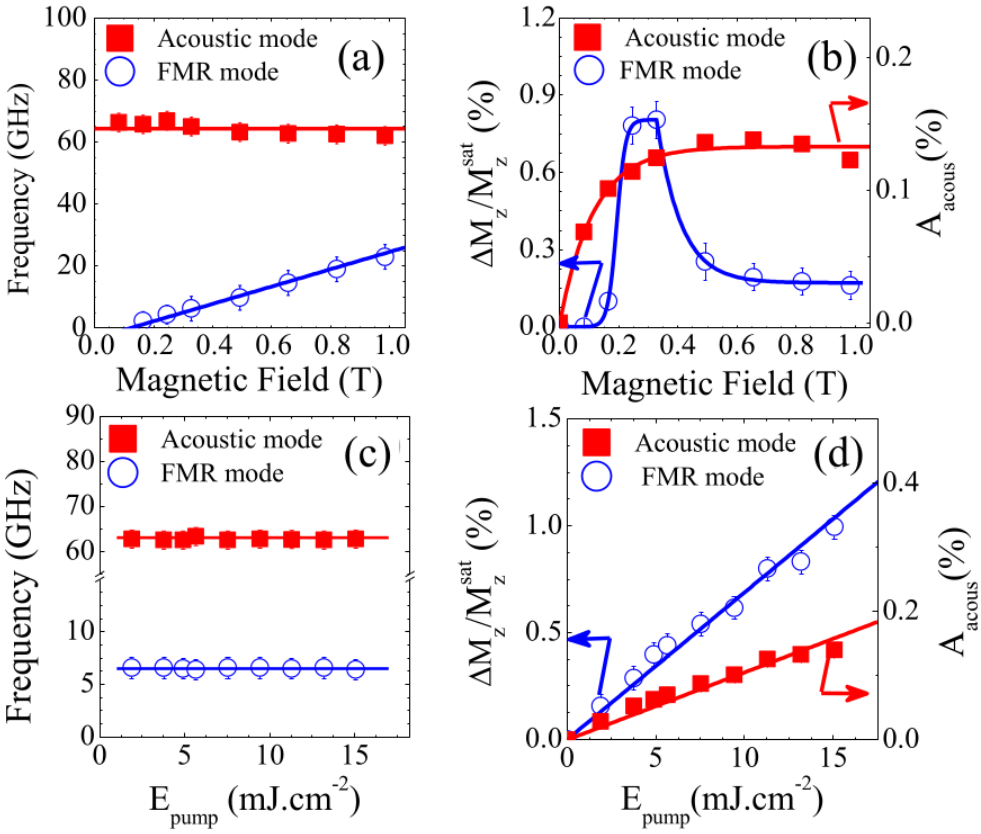

Figure 2.5: Field dependence of the precession frequencies (a) and amplitudes (b) associated with acoustic and FMR resonance modes. All measurements are obtained for a pump energy density of 11.3 mJ.cm-2. In (a) the solid line describing the FMR mode is a fit obtained using the Kittel formula, whereas the solid line for the acoustic mode is a guide to the eyes. Variation of the precession frequencies (c) and amplitudes (d) associated with acoustic and FMR resonance modes as a function of the laser energy density. All measurements are obtained for $H_{ext} = 0.33$ T applied along the direction perpendicular to the film. The solid lines in (c) and (d) are guides to the eyes.

the magnetic origin of this mode, we investigated the effect of the external magnetic field on the TR-MOKE signal. The field dependence of the oscillations frequency and amplitude are shown in figure 2.5 (a) and (b). The variation of the oscillations frequency of the low-frequency mode can be described by the Kittel formula adapted to the case of our experimental configuration. We also note that the initial precession amplitude for the low-frequency mode has a maximum near the saturating field $H_{sat} = 0.25$ T (Fig. 2.5(b)), which is also in a qualitative agreement with the typical behavior obtained for the FMR mode when H_{ext} is applied along a hard magnetization axis as in our experimental configuration. On the other hand, the frequency of the acoustic mode is independent on the magnetic field strength, once again proving that its origin is non-magnetic.

The excitation of the ferromagnetic resonance in our sample results from an ultrafast non-thermal modification of the magnetocrystalline anisotropy induced by the acoustic strain pulses via the inverse magnetostriction effect. Indeed, the field caused by the longitudinal

strain in the Bi-YIG layer is given by $H_z^{me} = 2b_1\epsilon_{zz}m_z$ [147] where $b_1 = 2.54$ T is a magnetoelastic coefficient of $Bi_2Y_1Fe_5O_{12}$, ϵ_{zz} is the strain components, and m_z is the normalized component of magnetization along the z direction . The coefficient b_1 is considered similar to the one of YIG due to the independence of the magnetostriction coefficient λ (100) to the composition of $Bi_xY_{3-x}Fe_5O_{12}$ [149]. By assuming that the strain component ϵ_{zz} generated here is similar to those usually reported in literature ($\sim 1.10^{-3}$) [142, 147], the field caused by the strain in the sample with an almost saturated magnetization along the z direction is $H_z^{me} \sim 5$mT.

To further investigate the two resonance modes, we performed TR-MOKE measurements as a function of the laser energy density E_{pump}. The pump energy density dependence of the oscillations frequency and amplitude are presented in Figs. 2.5 (c) and (d). The frequency of both modes is independent of the pump energy density. The behavior of f_{FMR} is similar to the one obtained by non-thermal effects induced magnetization precession [150, 151]. This is in agreement with our interpretation based on strain-induced changes of magnetic anisotropy via the inverse magnetostriction effect. Indeed, in the case of thermally induced spin precession a dependence of the frequency on E_{pump} is usually observed. On the other hand, the behavior of f_{acous} as a function of E_{pump} is also in agreement with the prediction that the frequency of acoustically-induced modulation of the magneto-optical effects is mainly defined by the speed of sound. Moreover, our experiments show that the oscillations amplitude of the two resonance modes increases linearly with the laser energy density within the probed range. This means that the amplitude of the spin precession is proportional to the amplitude of the strain pulse. Therefore, using an engineered structure that allows injecting a higher amplitude strain pulse into Bi-YIG can be used for further improving the magnetization precession amplitude or inducing a magnetization switching in magnetic garnet.

We then performed a similar study using this time a slightly different alloy of $Bi_1Y_2Fe_5O_{12}$ with a strong in plane anisotropy but still burried below a thick Cu/Pt metallic bilayer [152]. In this work, our collaboration with the group of Matias Bargheer allowed for measuring both the TR-MOKE as well as the ultrafast X-Ray diffraction (UXRD) on the same heterostructure. Figure 2.6 (a) and (b) depicts the UXRD study of the heterostructure. More precisely, Figure 2.6 (a) and (b) show the measured time-resolved average strains of the Cu layer and of the Bi-YIG layer.The time-resolved strain in Pt, Cu,and Bi-YIG were calculated using a two-temperature model in combination with a one-dimensional masses-and-springs model [153]. Results of the modeling are plotted as solid lines, indicating a reasonable agreement with the experimental data. Two distinct features are responsible for spatiotemporal dynamics of the lattice strain in the heterostructure. First, the Pt layer expands immediately after the optical excitation launching a strain pulse which propagates at the velocity of sound (not shown here) [138]. Second, the initial expansion of the Cu layer (Fig. 2.6 (a)) induces an immediate decrease of the strain in $Bi_1Y_2Fe_5O_{12}$ (Fig. 2.6 (b)), starting within less than 1 ps. At this time, the heat energy transported by the hot electrons through Cu arrived at the Bi-YIG interface. Moreover, the modeling showed that the heating of the Bi-YIG layer is strongly inhomogeneous which is mandatory for exciting high modes of standing spin waves (SSW). Although the temperature rose by more than 40 K during the first 100 ps in the first 10 nm behind the Cu interface, heat diffusion reached the back of the layer only after ~ 2 ns later.

Three important features characterized the time evolution of the Kerr signal plotted in

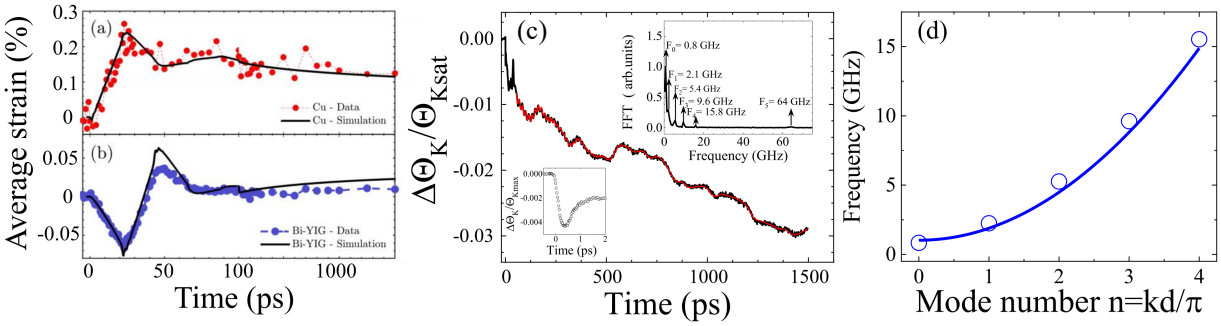

Figure 2.6: Laser-induced lattice dynamics in the Pt/Cu/ $Bi_1Y_2Fe_5O_{12}$/GGG heterostructure. Average strain in (a) the Cu layer and (b) BI-YIG layer as measured by ultrafast X-Ray diffraction (UXRD). The UXRD measurements were performed at room temperature with a pump wavelength of 800 nm, a pulse duration of 50 fs, and an incident pump energy density of 5 mJ/cm^2 . The solid lines in (a) and (b) are results of our modeling. (c) $\Delta\Theta_K/\Theta_{Ksat}$ induced by a pump energy density of 9.4mJ/cm^2 for H_{ext} = 164mT. Insets: (c) Fourier transform spectrum of the $\Delta\Theta_K/\Theta_{Ksat}$ data for the time delay t $\leq$ 50 ps (top) and a magnified view of the $\Delta\Theta_K/\Theta_{Ksat}$ signal (bottom) around the zero time delay. (d) Spin precession frequency as a function of the mode number. The solid line is the fit obtained using Eq. 2.4.

figure 2.6 (c). First, the signal shows a small ultrafast decrease within the first picosecond after the arrival of the hot electrons at the Bi-YIG/Cu interface. This ultrafast change of the magnetic order was attributed to an ultrafast modulation of the exchange interaction [154]. Second, a gradual slowly decrease of the signal startied at $\sim$ 5 ps and increasing up to 1500 ps. This slow demagnetization dynamic is consistent with the generation and propagation of incoherent phonons (heat) into the Bi-YIG layer together with the low magnon-phonon coupling characterizing iron garnets. Both these dynamics are thus induced by incoherent phonons. Third, very complex oscillations are superimposed on the slow exponential change of the signal. FFT analysis showed that the signal is composed of six different modes as shown in the top inset of figure 2.6 (c). The mode having the highest frequency of 64 GHz correspond to the previously described Brillouin oscillations. The lower frequencies of the other modes correspond to exchange SSW whose dispersion relation can be written in the case of our experimental configuration as:

$$\omega(k) = \omega_0 + \gamma D_{ex} k^2 \tag{2.4}$$

where ω is the angular precession frequency, ω_0 is the angular precession frequency of the fundamental mode, γ is the gyromagnetic ratio, D_{ex} is the exchange stiffness, and $k = n\pi/d$ represents the wave-vector of the SSW with d = 135 nm. Indeed a fit to the experimental data using equation 2.4 yields an excellent agreement with the experimental results (Fig. 2.6 (d)). It also shows that SSW with a frequency of 15 GHz can be excited. In previous papers, we showed that direct light excitations in similar Bi-YIG can also trigger high-frequency SSW [155]. Furthermore,their effective damping is about 40 times lower than the one of the fundamental mode [156].

2.2 Magnetization manipulation mediated by ultrafast spin transport

In the previous section, optical absorption of a femtosecond laser pulse was exploited to generate unpolarized hot electron and use them to manipulate the magnetization of a thin layer either by heat transfer or/and acoustic pulses. In the following I present the results we obtained regarding the generation and use of ultrafast polarized electron pulses and how they can be used to induce magnetization switching of a ferromagnetic layer.

2.2.1 Single-shot multi-level all-optical magnetization switching mediated by spin transport

The possibilities of deterministically manipulating the magnetization of a thin magnetic layer using an ultrafast pulses have attracted a lot of attention during the last 15 years as presented in the introduction. However, all-optical helicity independent switching was only reported for ferrimagnetic materials such as GdFeCo, [Co/Tb] multilayers or MnRuGa alloys [32, 97, 101] or GdFeCo/[Co/Pt] exchange coupled systems [157].However, in order to move towards ultrafast-spintronic applications, one needs to study and understand the fundamental mechanism not only for single layers, as it has been done in most study so far, but also in more complex structures like spin-valve structures, a key building block of modern spintronics. Selective magnetization switching in spin-valve structures or more complex heterostructures will enable multi-level magnetic storage and memories [158, 159]. In the following, I will show that the four possible magnetic configurations of a magnetic spin-valve structure ([Co/Pt]/Cu/GdFeCo) where both layers are magnetically decoupled, can be accessed using a sequence of single fs light pulses (Fig. 2.7 (a)) [160].

A schematic illustration of the Ta(5 nm)/$Gd_{23.3}(FeCo)_{76.7}$(5 nm)/Cu(9.3 nm)/[Co(0.6 nm)/Pt (1.0 nm)]4/Ta (5 nm)/Glass substrate spin-valve structure namely GdFeCo/Cu /[Co/Pt] is shown in Figure 2.7 (a). The GdFeCo and [Co/Pt] layers exhibit perpendicular magnetic anisotropy and are magnetically separated by a 9.3 nm continuous Cu layer. The ferrimagnetic GdFeCo layer is FeCo rich at room temperature for this composition as the net magnetization of the alloy is parallel to the magnetization of the FeCo sublattice and antiparallel to the magnetization of the Gd sublattice as shown by the hysteresis loop plotted in figure 2.7 (b). Moreover, four remanent magnetic configurations can be reached: two configurations where the magnetization of the two layers are parallel P+ and P- when the two magnetizations are along the positive and negative field direction, respectively, and two configurations where the two magnetizations are antiparallel AP+ and AP- when the magnetization of the [Co/Pt] is along the positive and negative field direction, respectively.

Figure 2.7 (c) shows magneto-optical Kerr microscopy images demonstrating that all four remanent magnetic configuration can be obtained after a single 35 fs laser pulse excitation under zero applied field. From these results, we can conclude that 0.5 μJ pulses switch both layers magnetization from P+ to P- and vice versa while 0.2 μJ pulses are only sufficient to exclusively switch the GdFeCo layer leaving the [Co/Pt] layer undisturbed. Moreover, starting from an AP state, only the GdFeCo magnetization is reversed. Finally, the P+ to P- and P- to P+ transitions clearly shows that the [Co/Pt] layer can be switched by a single

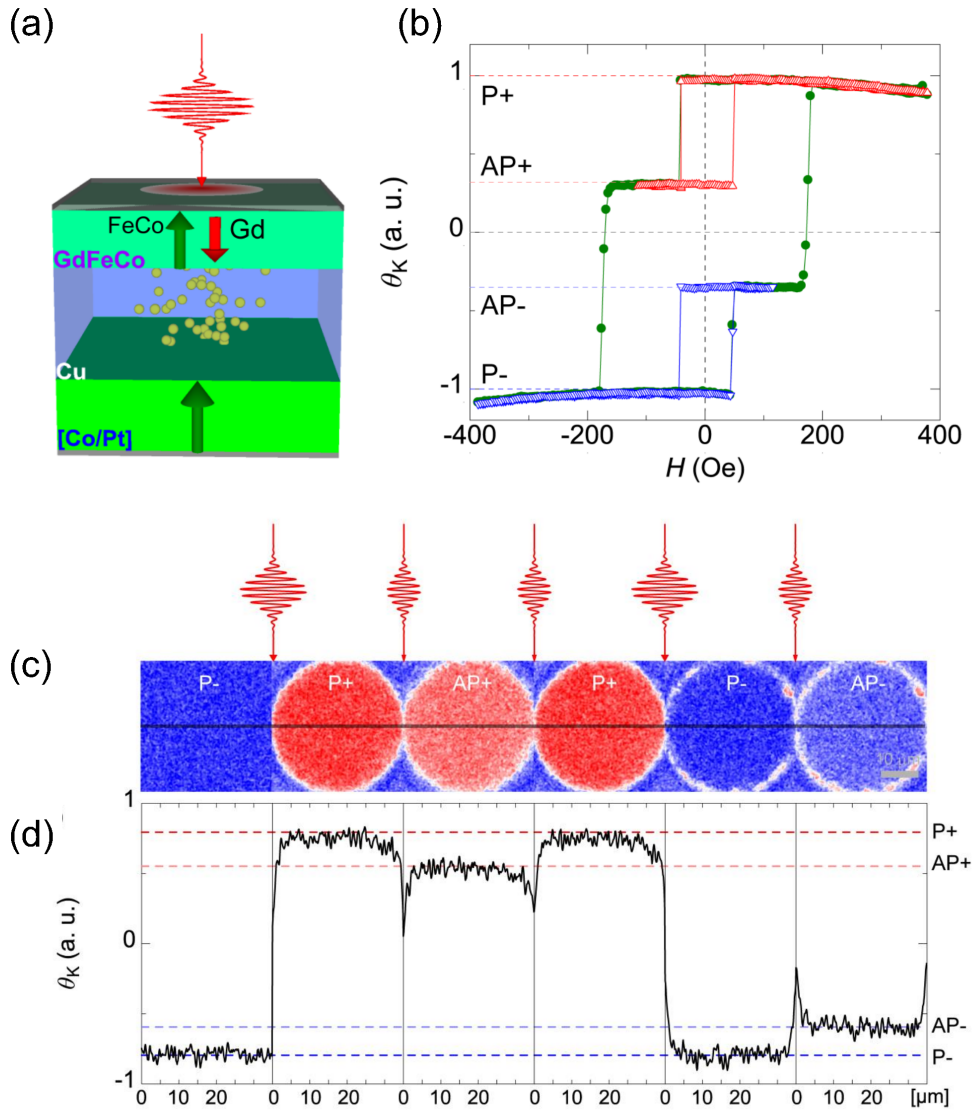

Figure 2.7: (a) Schematic representation of the Glass sub. / Ta (5 nm) / $Gd_{23.3}(FeCo)_{76.7}$ (9.3 nm) / Cu(9.3 nm) / $[Co(0.6\ nm)/Pt(1.0\ nm)]_4$ / Ta (5 nm) sample where the GdFeCo and [Co/Pt] magnetic layers showing perpendicular anisotropy are separated by a 9.3 nm thick Cu layer. (b) Normalized magneto-optical Kerr signal θ_K signal as a function of the magnetic field (H) applied perpendicular to the film plane. Red and blue open symbols are minor loop corresponding to the magnetization reversal of GdFeCo which are perfectly centered around the zero field axis. (c) 6 magnetic configurations obtained consecutively after a single pulse excitation. Starting from a saturated state P- (resp. P+), a single intense pulse (0.5 μJ) induces a switching toward the P+ state (resp. P-) . However a single moderate light pulse (0.2 μJ) induces a transition from a P- state (resp. P+) to an AP- (resp AP+) state. (d) Corresponding line scans of the normalized averaged magnetic contrast (black line shown on (c), averaged over a 5 μm width) allowing to descriminate between the four magnetic states (P+, P-, AP+, AP-).

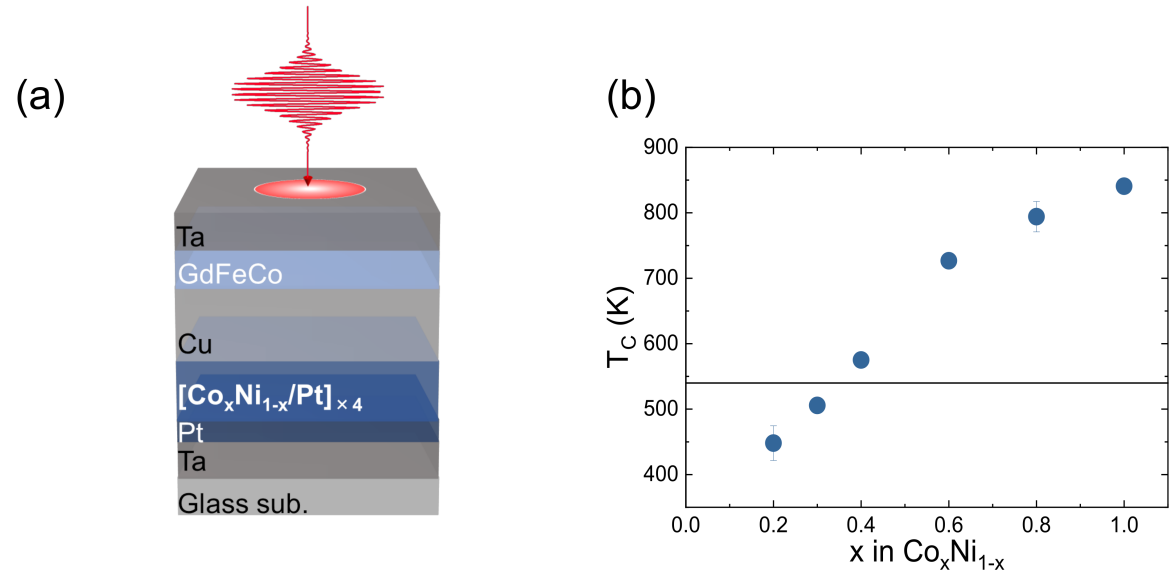

Figure 2.8: (a) Schematic presentation of the spin-valve structure. (b) Curie temperature measured for $[Co_xNi_{1-x}/Pt]$ multilayers plotted as a function of x. The line corresponds to T_C for GdFeCo [103, 105].

35 fs pulse.

After studying the effect of the GdFeCo concentration and of the spacer layer, we concluded that the final state of the magnetization switching of [Co/Pt] was mediated by spin currents. Surprisingly, the final state is dictated by the spin current generated by the Gd moment in the GdFeCo layer in agreement with the results of Choi *et al.* [90] (see section 1.1.3). These spin currents transfer their angular momenta, which, in combination with optical heating, are able to deterministically switch the magnetization of [Co/Pt]. This conclusion was supported by inserting Pt layers inside the Cu spacer layer of the spin-valve to depolarize the optically-induced spin current resulting in the thermal demagnetization of the [Co/Pt] layer.

This work was performed during the postdoctoral fellowships of Satoshi Iihama. It provided for the first time a new approach to deterministically switch the magnetization of a ferromagnetic layers using a single laser pulse [160]. It also opened the way to a complete new unexplored area of ultrafast spintronic.

2.2.2 Engineering single-shot all-optical switching of ferromagnetic materials

After that first work, the mechanism and the role of the magnetic properties of the ferromagnet as well as the time scale of the magnetization switching remained to be elucidated and many questions remained unanswered. For instance, how much polarized current is needed? How much heat has to be brought to the ferromagnetic layer? What type of ferro-

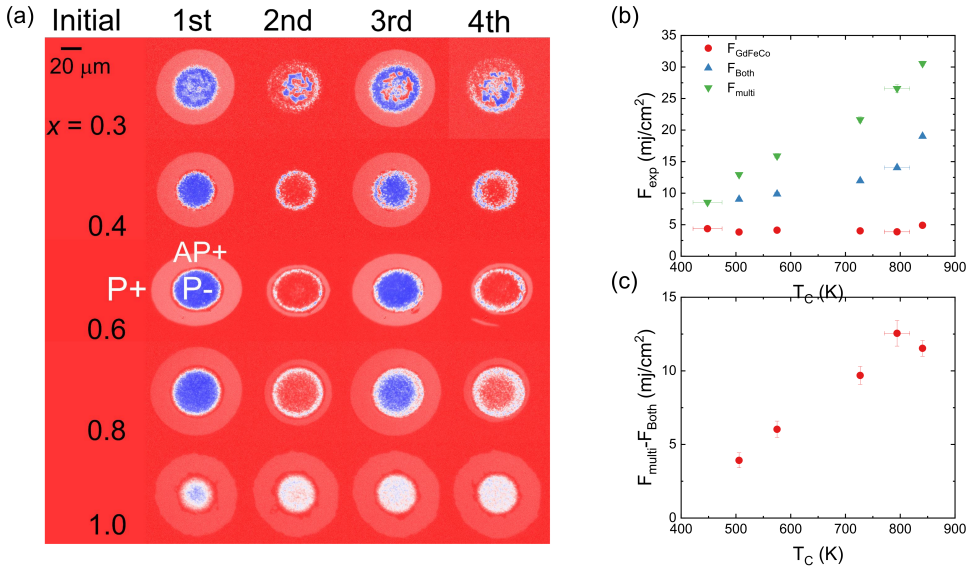

Figure 2.9: (a) MOKE images obtained after exciting the sample with one to four 35 fs laser pulses starting from a P+ initial sate. (b) Threshold fluences for reversing the GdFeCo magnetization (circles), both the GdFeCo and the ferromagnetic layers (triangles), and multidomain states (inverted triangles) as a function of the FM layer Curie temperature (T_C). (c) Difference in the threshold fluence for switching both layer (F_{both}) and multidomain states (F_{multi}) as a function of T_C.

magnet can be switched? What are the key ferromagnet characteristics needed to observe the switching? Does the Curie temperature of the FM play a role in the switching? What sets the fluence and the pulse duration needed to observe the single pulse reversal? These problems were tackled during the Ph.D. theses of Junta Igarashi and Quentin Remy [161, 162]. To start with, we investigated the switching of $[Co_xNi_{1-x}/Pt]$in GdFeCo/Cu/$[Co_xNi_{1-x}/Pt]$ spin-valve structure. $[Co_xNi_{1-x}]$ is a model system showing perpendicular anisotropy with a Curie temperature (T_C) that can be tuned from 400 K to about 850 K by adjusting the $[Co_xNi_{1-x}]$ concentration.

Ta (5)/$Gd_{23.3}FeCo_{76.7}$ (5)/Cu (10)/$[Co_xNi_{1-x}$ (1)/Pt (1)$]_4$/Pt (3)/ Ta (5) stacks were deposited on glass substrate by DC/RF magnetron sputtering as shown in figure 2.8 (a). The numbers in parentheses are nominal thicknesses in nm. A FeCo rich composition is used for the GdFeCo layer, meaning that net magnetization of the alloy is parallel to the magnetization of the FeCo sublattice. We prepared several samples with different Co compositions x (= 0.2, 0.3, 0.4, 0.6, 0.8, 1.0) in $[Co_xNi_{1-x}]$ to tune its Curie temperature (T_C) from $\approx$ 450 K up to about $\approx$ 850 K (Fig. 2.8 (b)).

Figure 2.9 (a) shows MOKE images obtained after shooting up to four single 35 fs laser pulses starting from a saturated P+ state for different samples. The sample is excited from the capping layer side and MOKE images are measured from the substrate side. The fluence used in the measurements shown in the figure are between 14 and 21 mJ/cm^2. A change in the MOKE images contrast from dark red (P+) to light red (AP+) indicates a switching of the GdFeCo magnetization only. Every single pulse leads to the reversal of the GdFeCo magnetization. The change of MOKE contrast from dark red (P+) to dark

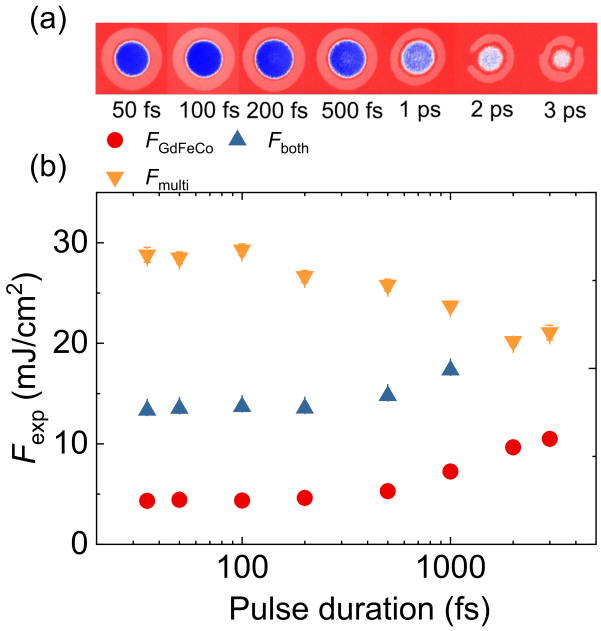

Figure 2.10: (a) MOKE images obtained after irradiation of one single laser pulse with a different optical pulse duration ranging from 50 fs to 3 ps. (b) Threshold fluences for reversing the magnetization of the GdFeCo layer only (circles), both the GdFeCo and the ferromagnetic layer magnetization (triangles), and forming multidomain states (inverted triangles) as a function of pulse duration.

blue (P-) proves that both the GdFeCo and the $[Co_xNi_{1-x}/Pt]$ magnetizations are switched. Single pulse reversal of both layers magnetization is possible for $0.4 \leq x \leq 0.8$, in agreement to the work of Iihama *et al.* [160]. The concentration of Co in the $[Co_xNi_{1-x}]$ does not modify the threshold fluence required for reversing the GdFeCo magnetization (F_{GdFeCo}) (Fig. 2.9 (b)). On the other hand, the threshold fluence for the switching of both layers (F_{both}) and the creation of a multidomain state (F_{multi}) increases with increasing the FM layer Curie temperature. Moreover, $F_{multi} - F_{both}$ increases with increasing T_C up to ≈ 800 K, indicating that there is a certain fluence window that allows the switching of both layers without generating a multidomain state and this window increases with T_C.

We can consider that the angular momentum carried by the spin current generated by the Gd sublattice demagnetization reaches a maximum for F_{GdFeCo} and no longer increases for higher fluences. Therefore, the increase in the threshold fluence required to switch the $[Co_xNi_{1-x}/Pt]$ multilayer with x is only due to the modification of the Curie temperature.

Furthermore, we performed single pulse magnetization switching measurements for various pulse duration ranging from 35 fs up to 3 ps (Fig. 2.10) (a)). These experiments were performed on a slightly modified spin-valve structure Ta (5)/$Gd_{23.3}FeCo_{76.7}$ (5)/Cu (10)/[Co (0.6)/ Pt (1)]$_4$/Pt (3)/Ta (5)/glass substrate. Clear single-shot switching of the both layers magnetization is obtained for pulse durations up to 500 fs while GdFeCo magnetization is switched for pulses as long as 3 ps. As presented in the introduction single GdFeCo layer shows AO-HIS for pulse up to 15 ps [105]. Figure 2.10 (b) shows the evolution of threshold fluences corresponding to the reversal of the GdFeCo magnetization, both layers magnetization, and the formation of a multidomain state as a function of the pulse duration. These threshold fluences do not change significantly when the pulse duration increases up to 200 fs. For pulses longer than 500 fs, a clear increase in the fluence required for switching the

GdFeCo and the Co/Pt magnetizations is observed while the fluence at which a multidomain state appears decereases. Both of these increases can be simply explained by the fact that as the pulse duration becomes longer, more energy is transferred to the lattice that does not contribute to the demagnetization or the switching. Surprisingly, the threshold energy to generate a multidomain state decreases with increasing the pulse duration. For a pulse duration of 2 ps, the fluence corresponding to the formation of a multidomain state becomes smaller than the one required for switching the magnetization of the Co/Pt, therefore impeding it. This can be explained by the fact that the spin generation rate given by $g_S = -dM/dt$ decreases when the pulse duration increases. Therefore, the temperature has to increase closer to T_C for obtaining the reversal of the [Co/Pt] magnetization. When the pulse becomes too long, there is not enough angular momentum transfer from the GdFeCo to the [Co/Pt] anymore before reaching the Curie temperature and thus ending in a multidomain state.

Finally, we studied the influence of the thickness of the Co layer at the interface with the Cu (the one absorbing the spin current) when excited with a single laser pulse of 35 fs. Once again, this does not affect the fluence required for switching the magnetization of the GdFeCo layer. However, a clear increase of about 50% is observed when increasing the Co thikcness from 0.2 to 1.0 nm. This indicates that the interface layer plays a major role in the single pulse switching mechanism. Once again, this can be understood by considering that the thinner the Co layer at the interface is, the lower the exchange coupling is within the layer. It will then be easier to reach the demagnetization threshold and consequently switch the magnetization. If the interface layer switches, the switching of the rest of the multilayer can then be explained by the propagation of the reversal due to the exchange coupling between the layer as reported in several systems [100, 157].

Once we knew that the Curie temperature of the FM layer plays an essential role in determining the required laser fluence to obtain magnetization switching, we engineered new samples with a thinner Co layer and different Gd_xFeCo_{1-x} alloys composition [162]. The full structure was glass/Ta (5)/Pt (4)/[Co (0,4)/Pt (1)]$_{x2/}$ Co (0,4)/Cu (10)/$Gd_x(FeCo)_{1-x}$ (5)/Cu (5)/Ta (5), with $x = 27.3\%$ (TM dominant) or 33% (RE dominant). AO-HIS of the GdFeCo layer could only be observed in the sample with a concentration of Gd $x = 27.3\%$. Surprisingly, single-shot switching of the Co/Pt multilayer could be obtained in both structures. This was the first demonstration that switching of the Co/Pt magnetization does not require a reversal of the GdFeCo magnetization. The fact that the Co/Pt multilayer's magnetization can be reversed without observing the reversal of the GdFeCo layer's magnetization in the sample with $x = 33\%$ can be explained by previous works [87,90,125]. Indeed, the key ingredient here is once again the spin current and the spin generation rate which is proportional to the magnetization decay ($-dM/dt$). The reversal process of the GdFeCo layer's magnetization (when it exhibits AO-HIS) is an ultrafast demagnetization followed by a slower reversal [27]. The fastest dynamics happens during the demagnetization and thus no full magnetization reversal is needed to generate the spin current. In order to observe the reversal of the ferromagnetic layer without switching the ferrimagnetic layer, it is then required to have a threshold fluence for AO-HIS higher than a threshold fluence for a sufficient demagnetization of the Co/Pt multilayer. We demonstrate here that this can be achieved by increasing the Gd concentration, which not only increases the spin current but also increases the threshold fluence required to observe AO-HIS or even makes it impossible

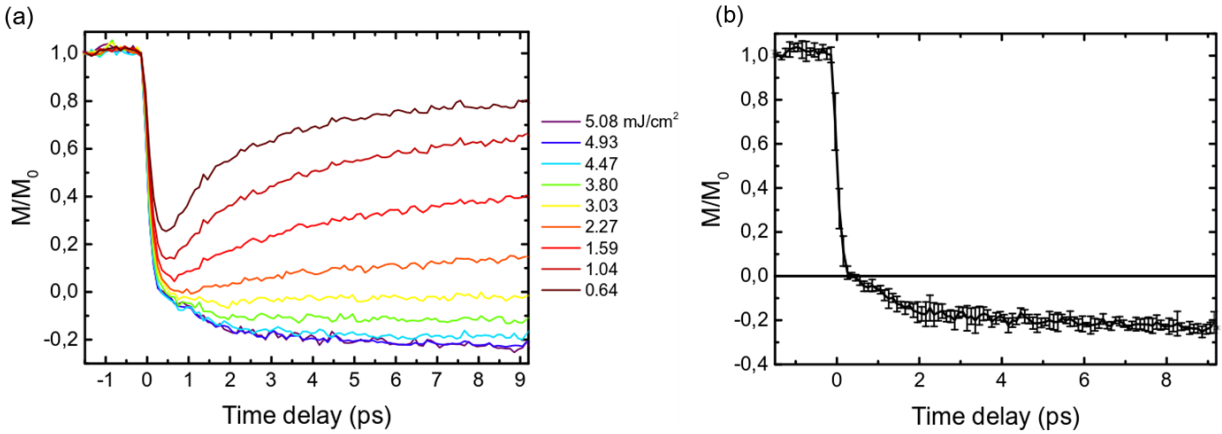

Figure 2.11: Normalized magnetization M/M_0 dynamics of [Co/Pt] for an initial P configuration, where M_0 is the magnetization at negative delay, as a function of pump-probe delay (a) for several fluences and (b) for a fluence of 5.08 ± 0.01 mJ/cm^2 (See Quentin Remy Ph.D. thesis for more details [164]).

to observe anymore as in the case of $x = 33\%$ here. Furthermore, a clear increase in the energy efficiency required for switching the Co/Pt magnetization of about $\approx 20\%$ of the threshold fluence was observed when increasing the Gd concentration by 5.7%. As demonstrated by Choi *et al.* and reported in figure 1.11 of the introduction [87], a small increase of only 3% of the Gd concentration could induce an increase of about a factor of 2 in the spin accumulation generated by the Gd demagnetization. Consequently, we attribute this difference in threshold fluences to the secondary spin current generated by the Gd sublattice demagnetization. Because this spin current carries more angular momentum in the sample with $x = 33\%$, less demagnetization is required to reverse the ferromagnetic layer.

2.2.3 Accelerating ultrafast magnetization reversal by non-local spin transfer

In order to access the switching time of the Co/Pt multilayers, TR-MOKE microscopy was performed on the following sample: Sapphire / Ta(5) / Pt(4) / $[Co(1)/Pt(1)]_2$ / Co(0,6) / $Gd33Fe_{60.3}Co_{6.7}(5)$ / Cu(10) / $[Co(0,6)/Pt(1)]_2$ / Ta(5) where the numbers represent the layer thicknesses in nm. In contrast to the investigated spin-valve structure discussed previously, a thick ferromagnetic layer was added at the bottom and exchange coupled to the GdFeCo layer to pin it in a given direction. This ensures two independent switching fields for both magnetic layers and gives access to four distinct remanent states (named P(AP) when the transition metal magnetizations of the free and pinned layers are parallel(anti-parallel) with a superscript + (-) when the free layer magnetization points up (down) at zero field). Depth-sensitive time-resolved magneto-optical Kerr effect microscopy was used to measure the magnetization dynamics in both P and AP configurations as a function of the pump fluence [163]. The setup was developed by Julius Hohlfeld and a complete description can be found in the thesis of Quentin Remy [164]. The time resolution is given by the probe pulse duration of 216 fs while the pump pulse duration was 100 fs.

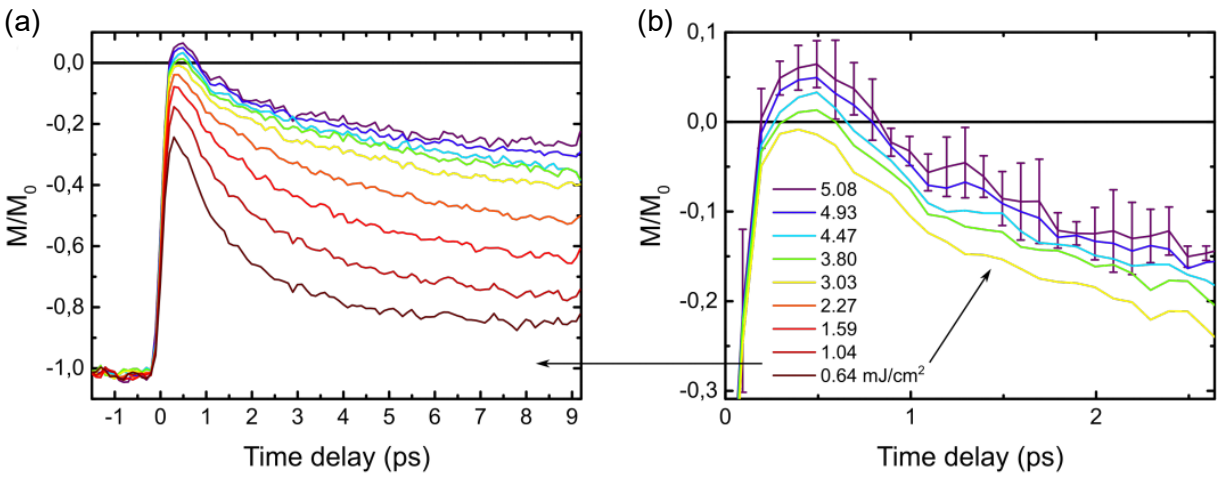

Figure 2.12: (a) Normalized magnetization M/M_0 dynamics of [Co/Pt] for an initial AP configuration, where M_0 is the magnetization at negative delay, as a function of pump-probe delay and for a fluence of 5.08 ± 0.01 mJ/cm^2 . (b) Zoom on the region around the magnetization overshoot.(See Quentin Remy Ph.D. thesis for more details [164]).

Figure 2.11 (a) shows the [Co/Pt] magnetization dynamics for various fluences starting from an initial P configuration. At low fluence, a standard ultrafast demagnetization curve with a fast reduction of magnetization is observed followed by a slower recovery. This is similar to standard demagnetization curves measured in single [Co/Pt] multilayers. At higher fluence, the behavior changes drastically. The magnetization goes to zero in around 400 fs before to slowly reverse its sign (Figure 2.11 (b)). Then the magnetization increases linearly at a rather large rate up to 2 ps before slowing down. This is attributed to the fact that before 2 ps, the magnetization is still not in equilibrium with the electronic system. Above 2 ps, the magnetization relaxes towards its initial state at a rate limited by heat dissipation out of the sample. Interestingly, even though the rate of magnetization change reduces slightly when crossing zero, we do not observe a critical slow down of the dynamics which usually happens when the net magnetization approaches zero [47,48,53,165,166] . This is explained by the presence of the spin current due to the Gd sublattice which prevents a complete spin disorder in the magnetic layer and will be discussed later.

We now focus on the dynamics of [Co/Pt] in the AP configuration (figure 2.12). At low fluence, the magnetization dynamics of [Co/Pt] in the AP configuration is similar to what is observed for ultrafast demagnetization. However, compared to the low fluence case in the P configuration, the magnetization recovery is sharper. At high fluence, a clear overshoot of the magnetization above zero is observed producing a transient reversal of the signal at around 200 fs (figure 2.12 (b)). This overshoot is attributed to the spin current generated by the CoFe sublattice while the sharper recovery is due to the one created by the Gd sublattice. Finally, the magnetization recovers and again, we do not observe a critical slow down of the magnetization dynamics.

Finally, we compared the results obtained for the magnetization dynamics of the [Co/Pt] within the spin-valve starting in the AP configuration with the dynamics of a reference sample where the second magnetic layer (i.e. [Co/Pt]/GdFeCo layer) has been removed.

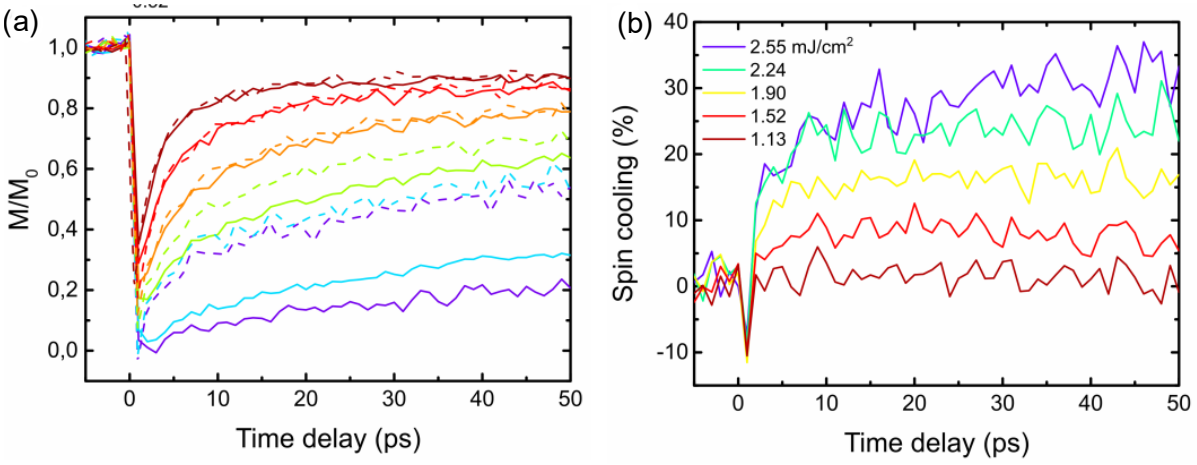

Figure 2.13: (a) Normalized magnetization dynamics for the reference sample (solid lines) and the spin valve sample in the AP configuration (dashed lines) as a function of pump-probe delay for several fluences (corresponding to the reference sample). (b) spin cooling, defined in the text, as a function of pump-probe delay for several for the same fluences (See Quentin Remy Ph.D. thesis for more details [164]).

Figure 2.13 shows the results obtained for both samples when the fluences where adjusted in order to have similar dynamics for low fluence excitation (i.e. when the effect of the spin accumulation is negligible). From figure 2.13 (a), a clear difference between both magnetization dynamics appears which keeps increasing as the fluence increases, showing again the increasing efficiency of the spin current generation (in the GdFeCo layer) and absorption (in the [Co/Pt] layer) as fluence increases. The injection of the spin current within the [Co/Pt] multilayer intensifies the cooling down of the magnetization. This spin cooling effect is plotted in figure 2.13 (b) and is given by $(|M_{AP}^{Co/Pt}(t)| - M_{single}^{Co/Pt}(t)|)/M_0$. At low fluences, there is no spin cooling but one can see an ultrashort transient spin heating (i.e. negative spin cooling) at 1 ps of around 10%. This spin heating is due to the already observed sharp onset on the magnetization recovery and it is attributed to the spin current coming from the TM sublattice of GdFeCo. At higher fluences, a spin cooling appears which can become larger than 30%.

In an attempt to draw conclusions about the mechanism governing the observed dynamics, Quentin Remy developed a model describing the out of equilibrium dynamics of a mean field two level model when it is exposed to spin polarized conduction electrons as derived by Beens *et al.* [167]. This was combined with a two temperature model and a spin accumulation generated by the ultrafast demagnetization of GdFeCo. The spin accumulation generated by the ferromagnetic multilayer itself was neglected. The magnetization dynamics of the Co/Pt layer is then described by the equation:

$$\frac{dm}{dt} = \frac{1}{\tau}\left(m - \frac{\Delta\mu}{2k_BT_C}\right)\left[1 - m\coth\left(\frac{2mk_BT_C - \Delta\mu}{2k_BT_C}\right)\right] \tag{2.5}$$

where m is the normalized magnetization, $\tau^{-1} \propto k_BT_C$ is the characteristic time for transfer of spin angular momentum between itinerant and localized electrons, $\Delta\mu$ is the

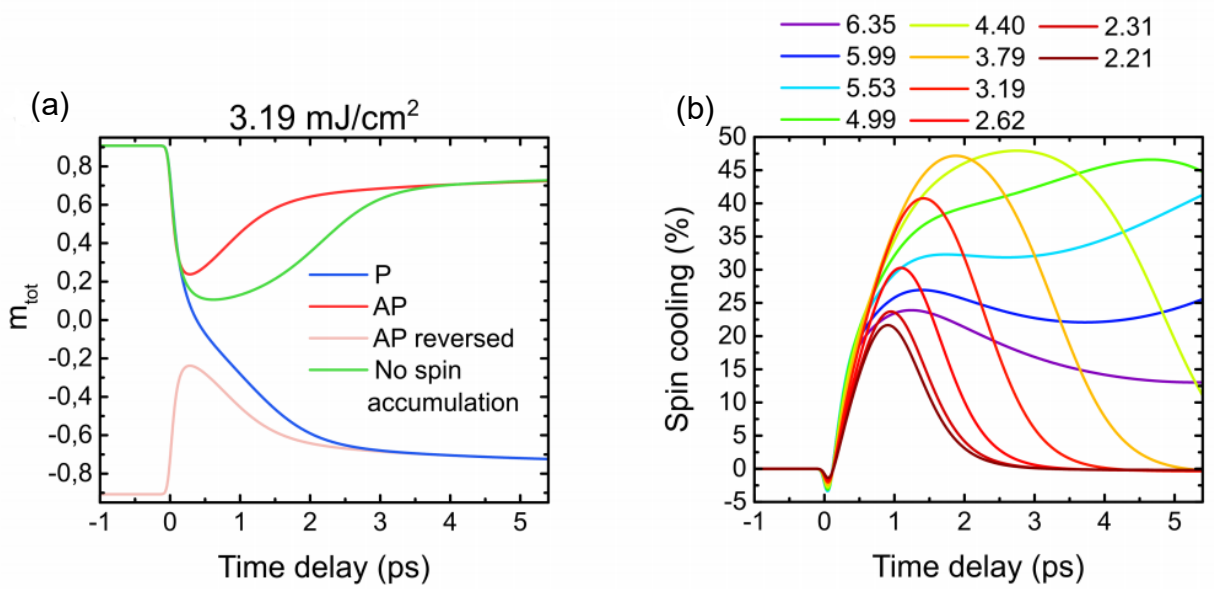

Figure 2.14: (a) Magnetization dynamics in the P and AP (standard and reversed) magnetic configurations as well as the magnetization dynamics without spin accumulation for a fluence of 3.19 mJ/cm^2. (b) Predicted spin cooling for this sample as a function of time delay for various fluences. (See Quentin Remy Ph.D. thesis for more details [164]).

spin accumulation, and k_B is the Boltzmann constant. It is interesting to see that when the magnetization approaches zero in the presence of a spin accumulation, its dynamics is governed by:

$$\frac{dm}{dt} = \left(\frac{-\Delta\mu}{2\tau k_B T_C} \right) \tag{2.6}$$

This shows that the magnetization regrows in a given direction depending on the sign of the spin accumulation at a rate given by how efficiently the angular momentum is transferred from the external bath to the spin system. However, in the absence of spin accumulation, the demagnetization rate tends toward zero triggering the critical slow down.

Predicted magnetization dynamics for the [Co/Pt] multilayer and different initial magnetic configurations are presented in figure 2.14 (a). We can see that the model reproduces the magnetization reversal when starting from a P state. The role of the spin accumulation is also witnessed in the dynamics calculated in the AP state. Indeed, it allows for a much faster recovery of the magnetization. The spin cooling is then calculated by subtracting the magnetization dynamics in the AP configuration with and without spin accumulation 2.14 (b). The simulated spin cooling present common features with the experimental results (Figure 2.13 (b)). For instance, it allows reproducing the spin heating observed as a negative peak just after the zero time delay. The behavior at longer time delays seems to be more complex. If the increase in spin cooling can be reproduced when the fluence becomes larger, at least during the first picoseconds, the model is not able to reproduce the long term dynamics. We incriminate the mean field approximation used in the model which cannot reproduce magnetization slow down due to out of equilibrium states that come with the

complex magnetic structures [48].

2.2.4 Sub-picosecond magnetization switching in ferromagnetic spin-valves

Up to now, we have seen that the presence of a GdFeCo ferrimagnetic layer was mandatory to allow for the reversal of the other FM layer within a spin-valve structure. This has been explained by the fact that most of the spin current entering the FM after its demagnetization is generated by the Gd sublattice. Nevertheless, during his postdoc fellowship, Junta Igarashi decided to evaluate the possibility to reverse the magnetization of a FM layer by using a second FM layer as a spin current source. These results will be presented in the rest of this section.

Our spin-valve structures consist of, Glass or Sapphire/Ta (5)/Pt (4)/[Co (1)/Pt (1)]$_3$/Co (1)/Cu (t_{Cu})/[Co (0.6)/Pt (1)]$_2$/Ta (5) in which we varied the Cu thickness from 5 to 80 nm. Here we define [Co (1)/Pt (1)]$_3$/Co (1) and [Co (0.6)/Pt (1)]$_2$ as the reference and free layers, respectively. As we have seen before, increasing the Co thickness and the number of repetitions lead to an increase of the Curie temperature. Therefore, the sample has been developed in order for the free layer to have a lower Curie temperature. Moreover, both layers possess different coercive fields for all Cu thicknesses as shown in figure 2.15 (a) and (c) for t_{Cu} = 10 and 80 nm.

Figures 2.15 (b)shows MOKE microscopy images obtained after exciting the sample with t_{Cu} = 10 nm from the capping layer side with a single linearly polarized femtosecond laser pulse of fluences F = 3.7 and 5.9 mJ/cm^2) and starting either from a parallel (P+) or an antiparallel (AP+) initial magnetic configuration. For the low fluence excitation (F=3.7 mJ/cm^2), a clear switching from the P to AP is observed while nothing happens when starting from the AP initial state. This result is rather surprising and unexpected. Indeed, it cannot be explained by the same argument used in our previous studies where the angular momentum carried by the spin current and generated by the Gd layer was always antiparallel to the magnetization of the FM layer. Furthermore, when increasing the fluence to 5.9 mJ/cm^2 and starting from a P state, the center of the excited area remains in P state while the surrounding, corresponding to a lower absorbed energy because of the Gaussian spot profile, switches to an AP state. Therefore, a low fluence excitation favors an antiparallel alignment of both magnetization while at larger fluences, a parallel alignment is preferred. The same result is obtained when increasing t_{Cu} to 80 nm for the low fluence case but only a demagnetization is observed in the center of the excited area when the fluence is increased.

The influence of the Cu thickness on the threshold fluences required to switch the free layer are reported in figure 2.16. The fluence required to switch from P to AP increases linearly with the Cu thickness and doubles when increases t_{Cu} from 5 to 80 nm. The threshold fluence for AP to P switching is larger and its thickness dependence is more pronounced since it doubles when increasing t_{Cu} from 5 to only 40 nm. Furthermore, it is not possible to switch from AP to P for Cu thicknesses larger than 60 nm because of the apparition of a multidomain state within the free layer. This is likely to be due to the fact that the free layer reaches its Curie temperature and remains demagnetized for a much longer time. The different evolution of the threshold fluences with the Cu thickness for P to AP and AP to P switching seems indicating that different mechanisms might be at work. This

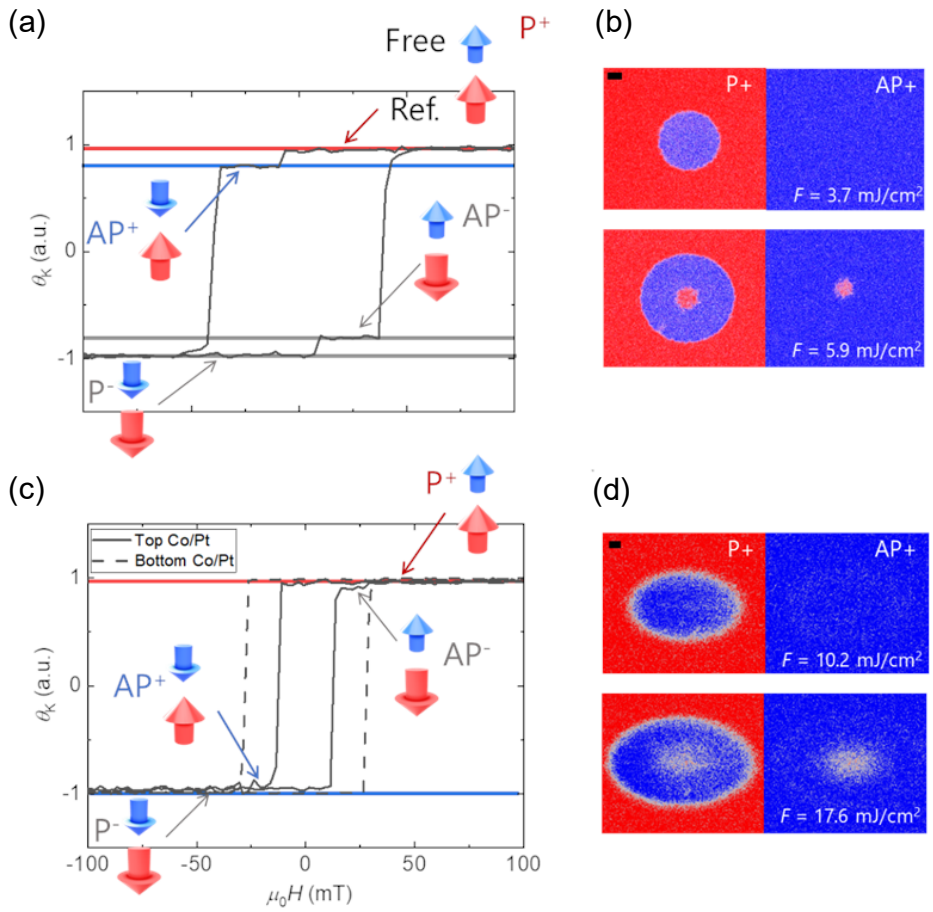

Figure 2.15: (a) MOKE hysteresis loop measured from the substrate side and (b) MOKE images obtained after irradiation of a fs-laser pulse starting from the P+(red) and AP+(blue) states for t_{Cu} = 10 nm, with F = 3.7 and 5.9 mJ/cm^2. (c) MOKE hysteresis loop measured from both sides of the sample and (d) MOKE images obtained after irradiation of a fs-laser pulse starting from the P+(red) and AP+(blue) states for t_{Cu} = 80 nm, with of 10.2 and 17.6 mJ/cm^2. The black line in (b) and (d) correspond to a 10 μm scale bar.

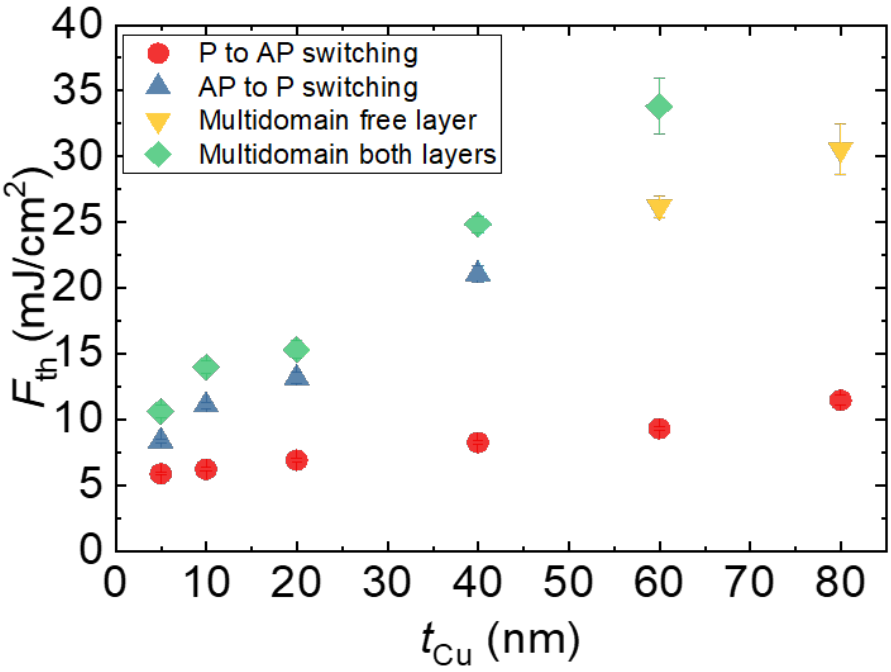

Figure 2.16: Evolution of the threshold fluences as a function of Cu thickness t_{Cu}. Red symbols correspond to the threshold fluence for P to AP switching. Blue symbols correspond to the threshold fluence for AP to P switching. Green symbols correspond to threshold fluence for forming multidomain in both layer. Yellow symbols correspond to threshold fluence for forming multidomain in free layer.

is also supported by the fact that P to AP switching can be observed for pulse durations up to 1 ps while AP to P switching is observed for pulses as long as 10 ps.

Finally, we measured the ultrafast evolution of the magnetization within the free and reference layer for t_{Cu} = 10 nm 2.17 (a). A reversal of the free layer magnetiation is observed for a fluence of 6.1 mJ/cm^2 but increasing it to 11.1 mJ/cm^2 only leads to a full demagnetization for at least 10 ps. When increasing the Cu thickness to 80 nm, we showed that the reversal of the magnetization of the free layer is only achieved when starting from a P state. In all cases, the reversal of the free layer from the P to AP state is taking place within 500 fs.

These counterintuitive results are really challenging our understanding of spin dynamics occurring on the ultrafast timescale in multilayer magnetic structures. Nevertheless, the P to AP switching observed at low fluence recalls the reversal of the free layer occuring within STT based devices. In this case, the minority spins within the spin polarized current generated by the free layer is reflected at the interface with the reference layer and bounces back. This allows for switching the free layer from P to AP when the current density is large enough [168]. We believe that a similar mechanism might take place in our experiments. Unfortunately, the existence of different possible mechanisms occurring at different timescales makes difficult a definitive interpretation. For instance, the creation of ultrafast spin currents can result from transient (charged) spin currents [169], the spin dependent Seebeck effect [88],

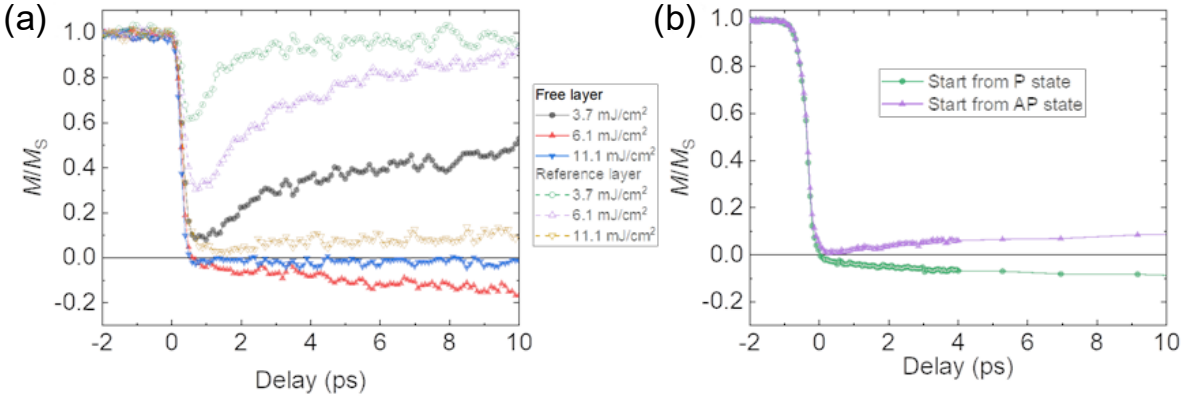

Figure 2.17: Magnetization dynamics measured by TR-MOKE. (a) Magnetization dynamics measured for t_{Cu} = 10 nm and several fluences. Utilizing a quarterwave plate enables separating the signal from the free layer and from the reference layer. An external magnetic field larger than the coercive field of the reference layer is applied during the measurement. (b) Magnetization dynamics for t_{Cu} = 80 nm starting from the P+ (green) and AP+ (purple) states with F = 10.4 mJ/cm^2. An external magnetic field (H) whose magnitude lies between the coercive fields (H_C) of the free and the reference layer (H_C of free layer < H < H_C of reference layer) is applied during the measurement.

or ballistic hot carriers transport [59, 170–172].

This work carried by Junta Igarashi during his postdoctoral fellowship provides new perspectives for ultrafast control of magnetism by further combining the area of spintronics and ultrafast magnetism.

Chapter 3

Magnetization reversal induced by ultrashort excitations

Since the discovery of laser induced AOS in 2007 [32], many researches have been carried on to determine the underlying microscopic mechanisms 1. Following the work of Mangin and Lambert [35, 36], we started studying multiple laser shots induced AOS in different magnetic materials as soon as I joined the group in 2013. In this chapter, I will start by focusing on HD-AOS occuring in ferrimagnetic alloys and ferromagnetic multilayers for a wide range of compositions and thicknesses.

3.1 Magnetization reversal mechanism leading to helicity-dependent all-optical switching

3.1.1 Domain size criterion for the observation of HD-AOS

The study presented in the following was motivated by the contradiction observed in the literature regarding the role of the saturation magnetization on the ability to trigger HD-AOS. Indeed, the previously reported low remanence criterion ($M_R \leq 220$ emu.cm^{-3}) for AO-HDS in ferrimagnetic materials [37,128,173] could not be satisfied in our observation of AO-HDS in ferromagnets with a high saturation magnetization ($M_S \geq 1400$ emu.cm^{-3}) and a magnetic thickness reduced to few nanometers [36]. This work was performed within the Ph.D. of Mohammed Salah El Hadri and more details can be found here [174–176].

In order to tackle this problem, we investigated ferrimagnetic thin films composed of Glass/Ta(3 nm)/Pt(5 nm)/ Tb_xCo_{1-x} (t)/Pt(5 nm). Two nominal concentrations of Tb have been used, namely 16% and 30%. However, changing the thickness of the TbCo alloy film strongly influences its effective concentration x. Therefore, the Tb atomic effective concentration x in the studied TbCo alloy films is ranging from 8% to 30%, while the thickness t varies from 1.5 to 20 nm. Further details can be found in the Ph.D. thesis of Mohammed Salah El Hadri [174] and in this review paper [176].

We also investigated two different ferromagnetic multilayer thin films, namely Glass/ Ta(3 nm)/Pt(3 nm)/$[$Pt(0.7 nm)/Co(0.6 nm)$]_N$/Pt(3.7 nm) multilayers and Glass/Ta(3 nm)/ Cu/$[$Co(0.2 nm)/Ni(0.6 nm)$]_N$/Cu/Pt(3 nm) multilayers. The number of repeats N varies

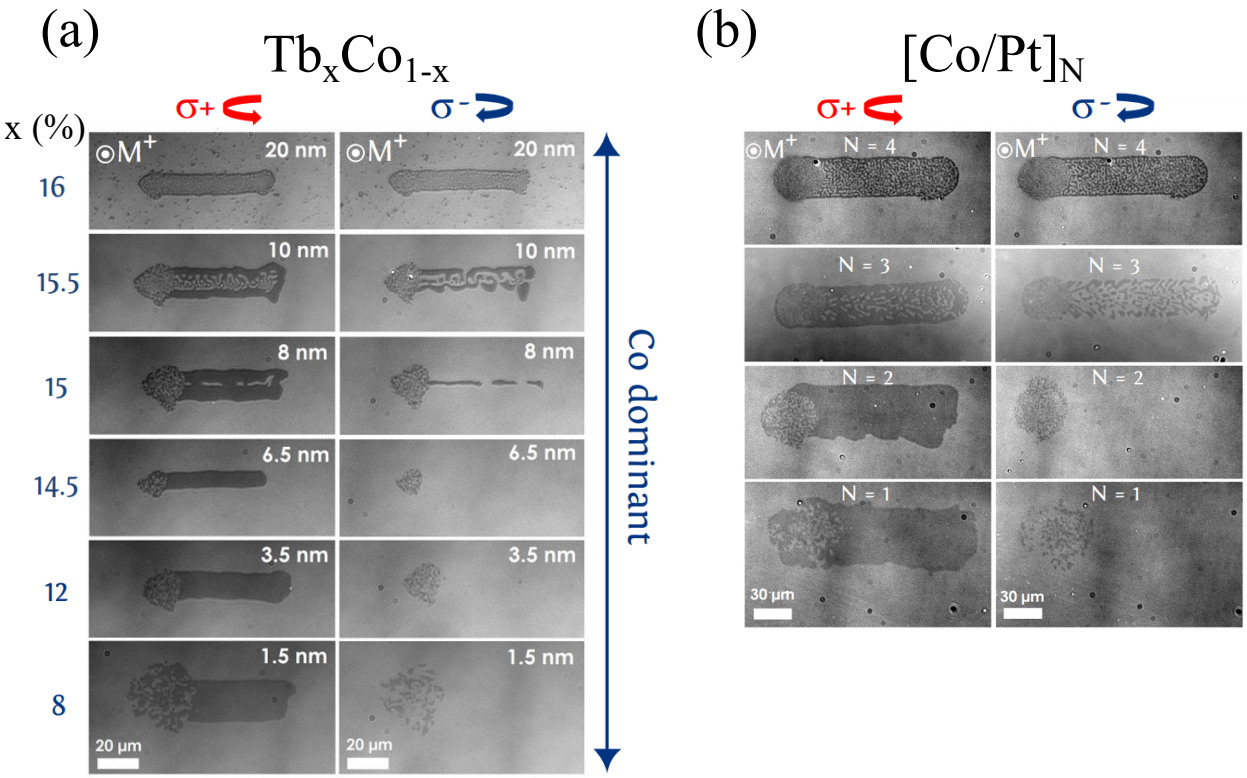

Figure 3.1: (a) Optical response for Tb_xCo_{1-x} alloys films for Tb concentration x ranging from 8 to 16 and alloy thickness varying from 1.5 nm to 20 nm and (b) for [Pt(0.7 nm)/Co(0.6 nm)]$_N$ multilayers for number of repeats N ranging for 1 to 4. The dark contrast corresponds to opposite directions of the magnetization. The laser power is ranging from 1.15 mW (for t < 8nm) to 1.5 mW (for t > 8 nm). Adapted from [174].

from 1 to 4 for Co/Pt multilayers and from 2 to 6 for Co/Ni multilayers. For [Co/Pt] multilayers, the saturation magnetization M_S increases from 1483, 1609, 2194 to 2217 kA/m when increasing N due to an increase of the spin polarization of Pt atoms by the adjacent Co layers. For the [Co/Ni] multilayers, the saturation magnetization is M_s = 1100 kA/m and barely changes with the number of repeats.

Thickness dependence of HD-AOS

The samples were excited through the glass substrate. Prior to being optically excited, the films were saturated with an external magnetic field applied perpendicular to the film plane. During optical excitation, no external magnetic field was applied. The fs laser beam is swept from right to left for both right-($\sigma+$) and left- ($\sigma-$) circular polarization. The sweeping speed was kept constant to about 10 μm.s^{-1}. Figure 3.1 shows the magneto-optical contrast corresponding to HD-AOS obtained for Tb_xCo_{1-x} alloys (Fig. 3.1 (a)) and [Co/Pt]$_N$ multilayers (Fig. 3.1 (b)).

Figure 3.1 (a) shows that the effect of helicity becomes more significant when reducing the thickness of the Tb_xCo_{1-x}. When decreasing the thickness from 20 nm down to 10 nm, the helicity induced reversal is more pronounced as shown by the larger rim. Moreover, the

domain in the demagnetized center area becomes larger. For $t = 8$ nm and $x = 15\%$, only a small non reversed stripe domain remains in the center of the sweept laser beam. For thinner layer, a complete HD-AOS is observed. For instance, the Co-dominated Tb_8Co_92 (1.5 nm) shows pure AO-HDS, even if this alloy does not present a compensation above RT and has a high saturation magnetization and remanence of 830 emu.cm^{-3}, thus contradicting the proposed low remanence criterion [128].

We also explored the AO-HDS ability in $[Co/Pt]_N$ multilayers. A pure AO-HDS is observed for N = 1 and 2 whereas only thermal demagnetization is obtained for N = 3 and 4 with the magnetic domains size increasing when reducing the number of repetitions. Therefore, the AO-HDS is achieved in both Co/Pt and Co/Ni (not shown here) multilayers by strongly reducing the magnetic thickness, similarly to what we observed for Co dominant TbCo alloy films.

Role of the domain size in HD-AOS

The results obtained previously when changing the thickness of the magnetic films brought us to consider the importance of the magnetic domain size. Indeed, the size of a stable magnetic domain in perpendicularly magnetized thin film strongly dependends on the film thickness [177, 178]. This results from the competition between the dipolar energy that stabilizes small domains and the domain wall energy that tends to reduce the length of the walls and so to stabilize big domains. It is therefore reasonable to infer that if the size of stable magnetic domains after the laser-induced heating is smaller than the size of the laser spot, thermal demagnetization will be observed because the system will break into small domains during cooling. Conversely, if the magnetic domain size is larger than the size of the laser spot, AO-HDS can be observed. As a result, the magnetic domain size can be considered as a relevant predictive parameter for the observation of AO-HDS.

The domain size was estimated using the model proposed by Kooy *et al.* for periodic stripe domains with a strong uniaxial anisotropy in an infinite plate [178]. The domain wall size is considered negligible compared to the magnetic domain size. By minimizing the total energy, the magnetic domain size D is given by

$$D = t \exp\left[\frac{\pi D_0}{2t} + \ln \pi - 1 + \mu\left(\frac{1}{2} - \ln 2\right)\right] \tag{3.1}$$

where $D_0 = \frac{\sigma}{E_d}$ is the dipolar length and $\mu = 1 + \frac{E_d}{K_u}$ is the magnetic susceptibility with K_u being the uniaxial perpendicular effective anisotropy. $E_d = 2\pi M_s^2$ is the demagnetizing energy per unit volume, $\sigma = 4\sqrt{A_{ex}K_u}$ is the domain wall energy per unit surface with A_{ex} being the exchange constant. Therefore, the domain size is determined by the material parameters, i.e. the saturation magnetization, the effective anisotropy and the exchange constant.

Figure 3.2 depicts the calculated evolution of the domain size D as a function of the magnetic thickness t at room temperature for the studied ferromagnetic multilayers and Tb_xCo_{1-x} alloys for x ranging from 8% to 13.5 % (all the details about the values of the different parameters can be found in references [174–176]). For all the investigated materials, the divergence of D for low thickness t can be understood from Eq. 3.1 and is due to the

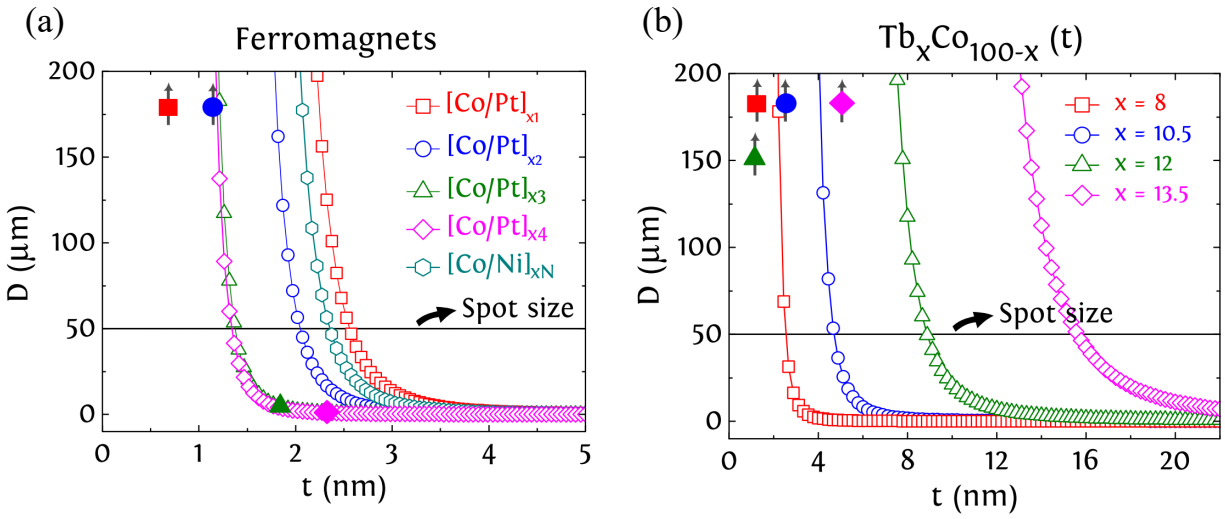

Figure 3.2: Estimation of the magnetic domain size D as a function of the magnetic thickness t at room temperature for (a) the studied ferro- and ferrimagnets [Pt (0.7 nm)/Co (0.6 nm)]$_N$ and [Co (0.2 nm)/Ni (0.6 nm)]$_N$ multilayers and (b) Tb_xCo_{1-x} alloys for x ranging from 8% to 13.5 %. Adapted from [174].

decrease of the demagnetizing energy. We defined a domain size threshold $D_{th} = 50\mu$m corresponding to the size of our laser spot used during the experiments.

In the case of [Co/Pt]$_N$, multilayers, the domain size at room temperature is much larger than D_{th} for N=1 and 2 while it becomes smaller when N$\leq$ 3. This is in agreement with our experimental results where HD-AOS is only observed for N=1 and 2. In the case of TbCo alloys with x = 8, 10.5, 12, 13.5 and t = 1.5, 2.5, 1.5, 5, respectively, D is always larger than D_{th} at room temperature. Again, this corroborates the observation of HD-AOS in these materials.

From our results, we concluded that HD-AOS could be observed only if the magnetic domains created after the fs excitation are larger than a threshold value close to the spot size during the full cooling process, otherwise a multidomain state would be reached. This criterion is common for both ferro- and ferri- magnetic materials.

As a follow up, we investigated the influence of He^+ ions irradiation on the HD-AOS observed previously in [Co/Pt]$_2$ multilayers [179]. Indeed, it is well known that the He^+ ion irradiation reduces the magnetic anisotropy and coercivity in perpendicularly magnetized Pt/Co/Pt sandwiches and [Pt/Co] multilayers [180]. The irradiation-induced intermixing at the interfaces makes them less abrupt, and leads to a strong decrease of the interface anisotropy. Moreover, another consequence of the intermixing is the increase of the effective magnetic thickness of Co/Pt multilayers. Therefore, modifying the effective anisotropy and magnetization as can be observed in figure 3.3 (a) should change the domain size and should influence the ability of AO-HDS. This is indeed what can be seen in figure 3.3 (b). By increasing the ion dose from 5.10^{14} He^+/cm^2 to 2.10^{15} He^+/cm^2, the effect of the helicity following the excitation in the irradiated [Co/Pt]$_2$ multilayers disappears gradually. At low ion dose, multiple domains start appearing in the scanned region and are stretched towards the center of the beam spot. This behavior was attributed to thermal-induced domain wall

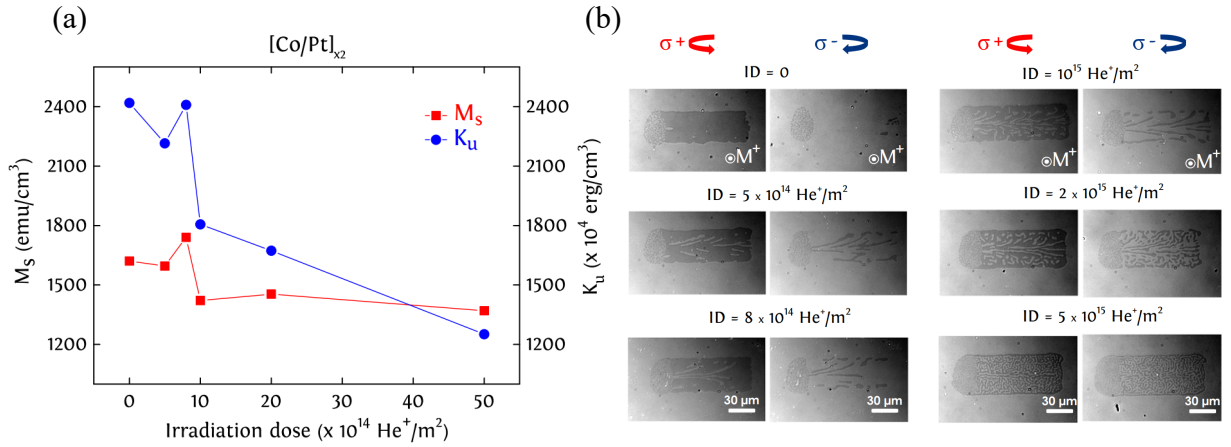

Figure 3.3: (a) M_S and K_u dependence on the irradiation dose ID at 15keV for [Co(0.6 nm)/Pt(0.7 nm)]$_2$ multilayers and (b) the effect on the laser induced HD-AOS. Adapted from [174].

motion. For the maximum ion dose 5.10^{15} He^+/cm^2, thermal demagnetization is obtained and the multiple domains in the scanned region get smaller.

To conclude this part, These results show that the AO-HDS ability is gradually lost upon increasing the irradiation dose due to a decrease of the magnetic anisotropy and thus the magnetic domain size. These findings confirm the large domain size criterion for the observation of AO-HDS demonstrated previously.

3.1.2 Using magneto-transport to investigate all-optical switching

To obtain more information about the magnetization reversal process following fs laser pulse excitation, we decided to investigate HD-AOS in in ferromagnetic Pt/Co/Pt and ferrimagnetic TbCo Hall crosses using the anomalous Hall effect [174, 181]. The sample was patterned into a 5 μm wide Hall cross using optical lithography (Figure 3.4 (a)). A DC current is injected along the x axis, and the Hall voltage is measured along the y direction in order to measure the z-component of magnetization within the Hall cross. The Hall voltage is given by:

$$V_{Hall} = \frac{\rho_{xy} I}{t} \tag{3.2}$$

with

$$\rho_{xy} = R_{AHE} \overrightarrow{M} \hat{e}_z \tag{3.3}$$

where R_{AHE} is the anomalous Hall coefficient, t is the magnetic thickness, I is the applied current, and ρ_{xy} is the Hall resistivity.

To study the magnetization switching within the Hall crosses, we adopted two different approaches. The first one, similar to the one used previously consisted in sweeping the laser beam over the Hall cross. In the second one, we kept the beam at a fixed position on the Hall cross as shown in figure 3.4 (b). For both approaches, the sample was saturated before

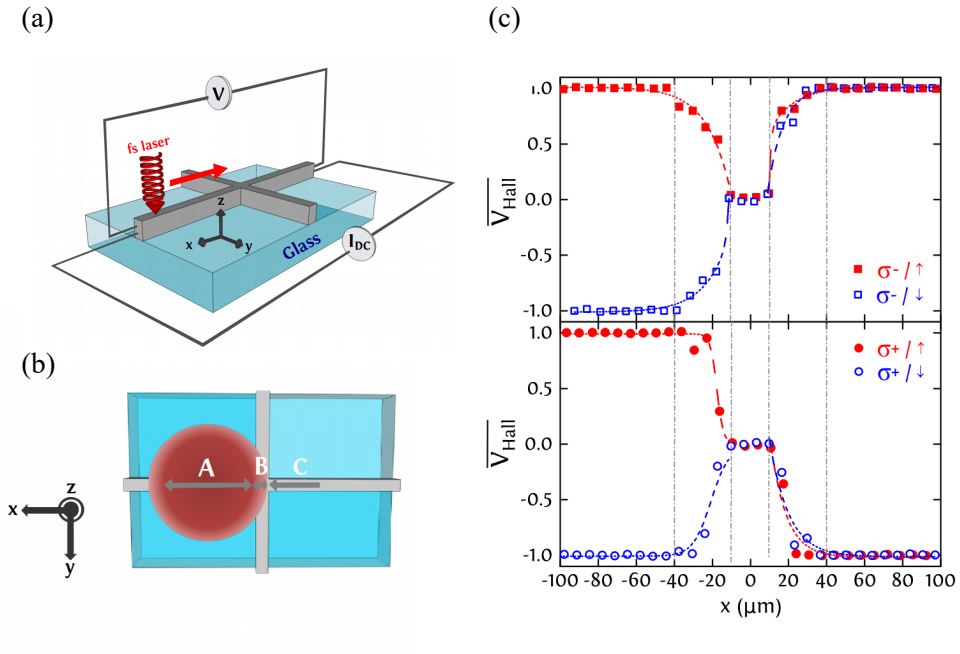

Figure 3.4: (a)Schematic representation of the resistance measurement with a swept beam: a DC current is applied along x axis, while the voltage is continuously measured along the y direction. The fs laser beam excites the samples perpendicularly to the film plane and is swept along the x axis. (b) Schematic representation of the different areas of the fs laser beam: "A" where multiple magnetic domains are obtained, "B" where HD-AOS is obtained, and "C" where no change of magnetization is induced. (c) Normalized Hall voltage as a function of the position of the beam x swept where (top)corresponds to left- handed circular polarization (σ-) and (b) to right-handed circular polarization (σ+). The values 1 and -1 of the Hall voltage correspond to both saturated magnetic states. The laser beam is swept over the whole x axis of Hall cross from position -100 μm to 100 μm, with a sweeping speed of 40 μm/s and a power of 0.95 mW. The experiment is repeated for both positive and negative saturation of the magnetization. The dashed lines are guides to the eyes. Adapted from [174].

any laser exposure to measure the Hall voltage for the two saturated magnetic state $\overrightarrow{M}\widehat{e}_z$ and $-\overrightarrow{M}\widehat{e}_z$. No magnetic field was applied during the laser excitation so the change in the Hall voltage reflects the laser induced magnetization modification within the Hall cross.

Static measurements of HD-AOS Hall crosses

The sweeping beam approach was first performed on a thin film of Glass/Ta(3 nm)/ Pt(3.7 nm)/Co(0.6 nm)/ Pt(3.7 nm) for the four possible configurations of circular helicity and saturation magnetization (figure 3.4 (c)). The laser beam was swept over a range of 200 μm centered on the Hall cross. Independently of the initial magnetic saturated state, the final state is only dictated by the circular polarization thus demonstrating the HD-AOS. When the beam gradually approaches the center of the Hall cross, a clear reduction of the Hall voltage is measured. We expected a magnetization reversal in the configuration shown in the area B of figure 3.4 (b) when sweeping from the left side but this was not the case. This can be explained by considering the small extension of the AOS rim of $\approx 2\mu$m and the low temporal resolution ($\approx$ 150 ms) used during these measurements. When the laser beam is centered over the Hall cross, the Hall voltage drops to zero because of the overheating leading to the formation of multiple domains. Finally, the helicity dependence starts appearing when the second parts of the AOS rim goes through the center of the Hall cross. As can be seen in figure 3.4 (c), a complete HD-AOS is obtained for a sweeping speed of 40 μm.s^{-1} and a laser power of 0.95 mW.

We then investigated the influence of the number of photons interacting with the Hall cross by either changing the laser power or by modifying the laser sweeping speed. All sweeping beam measurements were performed 20 times with a reset of magnetization to its initial state after each sweep in order to account for the stochastic nature of the HD-AOS. As can be seen in figure 3.5 (a), the threshold fluence at which the magnetization reversal starts taking place does not depend on the sweeping speed. However, increasing the sweeping speed results in a lower switching ratio of the Hall cross and an increase in the standard deviation and hence the stochasticity of the process. These results give indirect evidence that HD-AOS is a cumulative process and reproducible magnetization switching requires a certain number of pulses.

During the postdoctoral fellowship of Georgy Kichin, we demonstrated that tuning the pulse duration and the laser spot size, leads to a strong reduction of the number of pulses required to obtain a reliable HD-AOS. Using numerical calculations based on the three-temperature model, we found that the key parameter is the maximum spin temperature that has to reach a certain temperature without exceeding the Curie temperature of the material [182].

Similar results were obtained on a ferrimagnetic thin film of Glass/ Ta(5 nm)/$Tb_{27}Co_{73}$(20 nm)/Pt(3 nm) indicating that the same mechanisms are involved in ferromagnetic and ferrimagentic materials regarding HD-AOS. By comparing the results with the one obtained on the Pt/Co/Pt based Hall cross, we found that the laser beam helcity required for switching the magnetization depends on the orientation of the Co sublattice and not on the net magnetization. This finding is also a hint that a model based on the inverse Faraday effect (IFE) is less likely to explain the AO-HDS, since the reversal only depends on the absorption of the circular polarization by the Co sublattice and not on the direction of the net magnetization

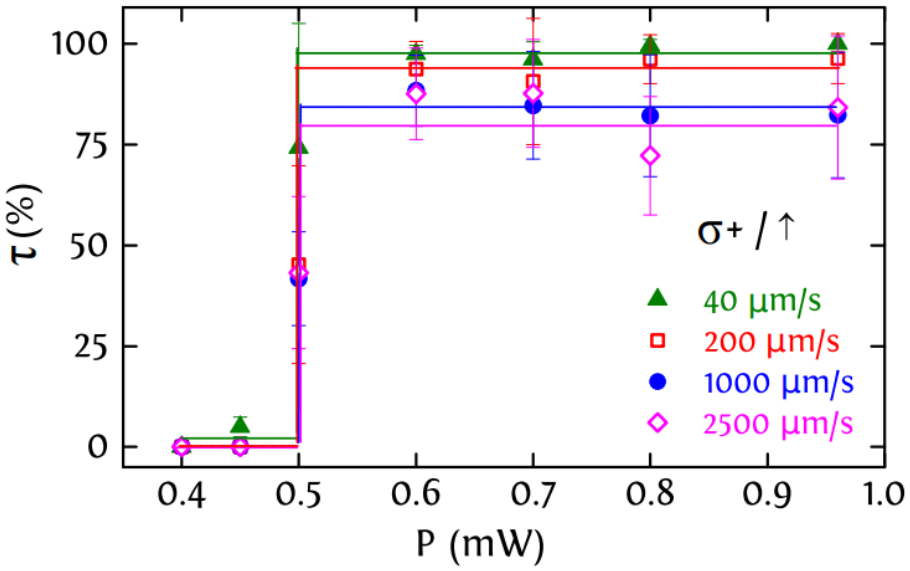

Figure 3.5: Switching ratio τ as a function of the laser power P for different sweeping speeds. The initial up magnetization saturation with $\sigma+$ sweeping is exemplarily shown. Adapted from [174].

of the alloy.

Dynamic measurements of HD-AOS Hall crosses

To further investigate the microscopic mechanisms involved in the magnetization switching of different materials, we combined direct imaging of the magnetic contrast after laser pulse excitation with a time-dependent electrical method by measuring the magnetization switching in Hall crosses via the anomalous Hall effect (AHE). This allows us to explore the magnetization dynamics over an intermediate and wide time scale ranging from 1μs to few seconds.

Three different samples were investigated under similar conditions. The samples consist of Glass/ Ta(3 nm)/$Gd_{28}Fe_{48}Co_{24}$(20 nm)/Ta(3 nm), Glass/ Ta(3 nm)/$Tb_{27}Co_{73}$(20 nm)/Ta(3 nm), and Glass/ Ta(3 nm)/ Pt(4.5 nm)/ Co(0.6 nm)/Pt(4.5 nm). All these three samples possess a perpendicular magnetique anisotropy.

Very distinct dynamics were obtained for GdFeCo and the other two Co/Pt and TbCo alloys. Figure 3.6 (a) shows the magnetization of the $Gd_{28}Fe_{48}Co_{24}$ Hall cross is totally reversed after the action of a single pulse, for each pulse in a set of ten pulses. The same behavior has been found for all six possible combinations of initial saturation and light polarization (Figure 3.6 (b)). The time reversal of the anomalous Hall signal is limited by the temporal resolution of our experiment which is 1 μs. These results are in agreement with the AO-HIS reported previously [27,38]. The anomalous Hall effect signal corresponding to the reversal of the Co/Pt magnetization can be decomposed in two phases occuring at distinct timescales: a helicity-independent drop induced by few pulses within the first ms

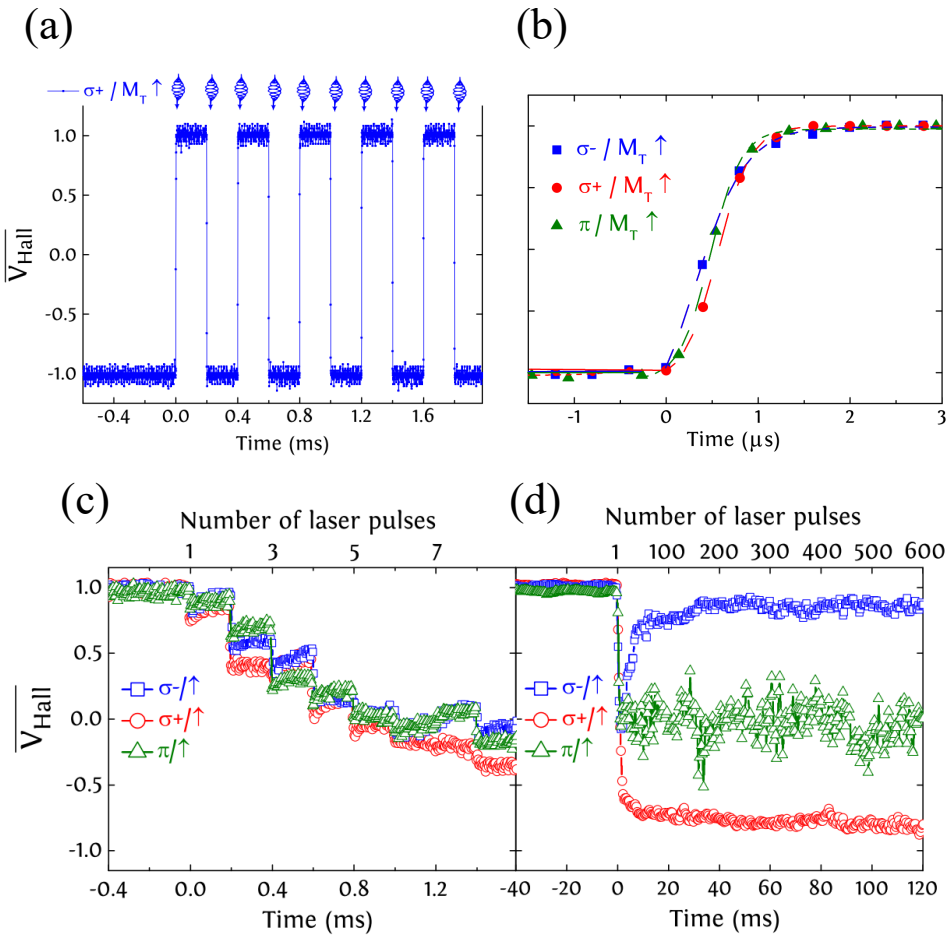

Figure 3.6: (a) Time evolution of the normalized Hall voltage of a 5 μm-wide $Gd_{28}Fe_{48}Co_{24}$ based Hall cross under the action of ten consecutive pulses as marked with the blue pulses in the upper row, with initial magnetization saturation up with $\sigma+$ polarization and a repetition rate of 5 kHz. Each of the ten laser pulses excites the same region of the Hall cross and reverses the magnetization within it. (b) Anomalous Hall voltage signal due to a single magnetization reversal obtained for three different polarizations with a fluence of 19 mJ/cm^2. (c) and (d) Time evolution of the anomalous Hall voltage of a 5 μm-wide Pt(4.5 nm)/Co(0.6 nm)/Pt(4.5 nm) Hall cross initially saturated up, under the action of a 35-fs laser beam with a 5 kHz repetition rate and a fluence of 10 mJ/cm^2 . The corresponding number of laser pulses is shown in the upper row. Adapted from [174].

and a helicity-dependent reversal of the Hall voltage on several tens of ms (Figure 3.6 (c) and (d)).

At first, each laser pulse excitation induces a reduction of the Hall voltage which follows a steplike process leading to a demagnetization of the Hall cross (Figure 3.6 (c)). This demagnetization process is actually independent of the helicity. One of the most interesting findings here is that the signature of the helicity starts appearing only after crossing the zero Hall voltage; i.e. after reaching a fully demagnetized multidomain state. Then, the complete switching of the Hall cross requires around 150 pulses. A similar response of the anomalous Hall voltage was obtained for TbCo alloys. Thus, these experiments demonstrate that the all-optical switching of ferromagnetic Pt/Co/Pt films is helicity dependent, cumulative, and only achieved after a steplike multiple-domain formation, and hence is drastically different from the GdFeCo switching mechanism.

A potential explanation of the remagnetization process would be a helicity dependent domain wall motion that could originate from the magnetic circular dichroism (MCD). The first pulses result in the nucleation of a multidomain state. However, due to different absorption within adjacent magnetic domains, a thermal gradient takes place whose sign depends on the helicity of the laser pulse therefore inducing an asymmetry in the domain wall displacement. This conclusion leads us to the next section of this manuscript focusing on helicity dependent domain wall motion and the role of magnetic circular dichroism.

3.1.3 The role of magnetic circular dichroism on HD-AOS

The work presented in this section was part of the Ph.D. thesis of Yassine Quessab [183] and was carried out in collaboration with the Center for Memory & Recording Research (CMRR) at the University of California San Diego (USA) where he spent some time as a visiting student. For more details we refer the interested reader to Yassine Quessab Ph.D. thesis [183] and to the related publications [184, 185].

Helicity-dependent all-optical domain wall motion in ferromagnetic thin films

To obtain a better understanding of the mechanism of HD-AOS, we started studying the optical response of a magnetic domain wall (DW) to an ultrashort laser pulse excitation [184]. The experimental protocol consisted in creating a single DW in a Pt/Co multilayer sample and measure its displacement after different excitation conditions. We varied the position of the laser spot compared to the DW and its helicity.

The action of exposing a DW in a Pt/Co/Pt single layer to 40 fs laser pulses with a fluence kept below the nucleation threshold is depicted in figure 3.7 (a). A clear displacement of the DW is only observed for two combinations (σ+, M^-) and (σ-, M^+) while the other combinations had no effect. Indeed, when the DW is excited by σ+ (resp. σ-) polarized laser pulses, this leads to an expansion of the M^+ (resp. M^-) magnetic domain. The effect of the light polarization is depicted in figure 3.7 (b). The maximum DW displacement is obtained when the light polarization is circular and no displacement is observed when it is linear. Moreover, the amplitude of the displacement is rather similar for both helicities.

While the effect of the polarization is pretty clear from the experiments, exciting the sample with a large number of pulses at a high repetition rate (5 kHz) leads to a modification

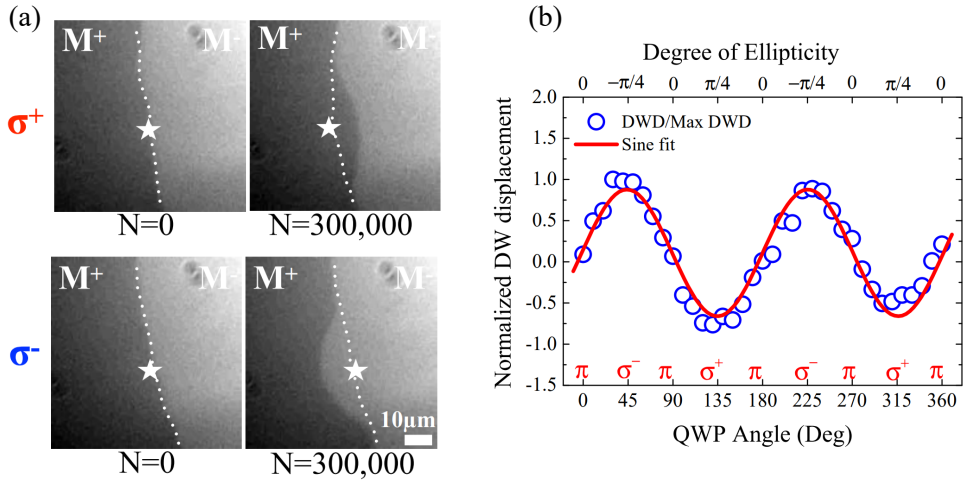

Figure 3.7: (a) Magneto-optical images of domain wall motion in Pt(4.5 nm)/Co(0.6 nm)/Pt(4.5 nm) induced by 40 fs 5 kHz laser pulses with right-circular (σ+) and left-circular (σ-) polarizations with an energy per pulse of 12.5 mJ/cm^2. The laser beam spot is centered on the DW. (b) Normalized DW displacement as a function of the angle of the quarter-wave plate and the degree of light ellipticity. Adapted from [183].

of the local temperature thus creating time dependent temperature gradients. During my first years in the Laboratoire de Physiques des Solides in Orsay, we reported that such a temperature gradient leads to a vortex wall displacement toward the hotter part of a in NiFe nanostrips [186]. As can be observed in figure 3.8, exciting the sample using a linearly polarized light triggers a motion of the DW towards the center of the laser spot in agreement with what we reported in NiFe. Therefore, the DW displacement under the action of laser pulses is the the summation of two different effects; one which is helicity dependent and tends to expand one magnetic domain to the detriment of the other, the other one being a pure thermal effect and therefore helicity independent which forces the DW to move to the center of the laser spot.

DW displacement under the excitation of polarized laser pulses can be understood when considering the magnetic circular dichroism effect. In our experiments, the laser beam spot overlaps with two domains of opposite magnetization directions. Therefore a difference in absorption in the M$^+$ and M$^-$ domains should result in the creation of temperature gradient across the DW. Taking into account a MCD of 2% [130] and using a two temperature model, we estimated a difference of temperature of 10 K between the two magnetic domains. In Co/Pt thin films, the domain wall width is typically in the range of 10 nm. Therefore, the temperature gradient across the DW due to MCD is of the order of 1 K/nm$^-$1. Using the same model as Torrejon *et al.* [186], we estimated that such a thermal gradient would result in a 7 mT effective magnetic field acting on the DW which is of the same order of magnitude that the field required to unpin a DW in such a sample. However, to confirm the role of MCD, it is important to know the actual direction of the temperature gradient and which magnetization state is the least absorbent for both helicities.

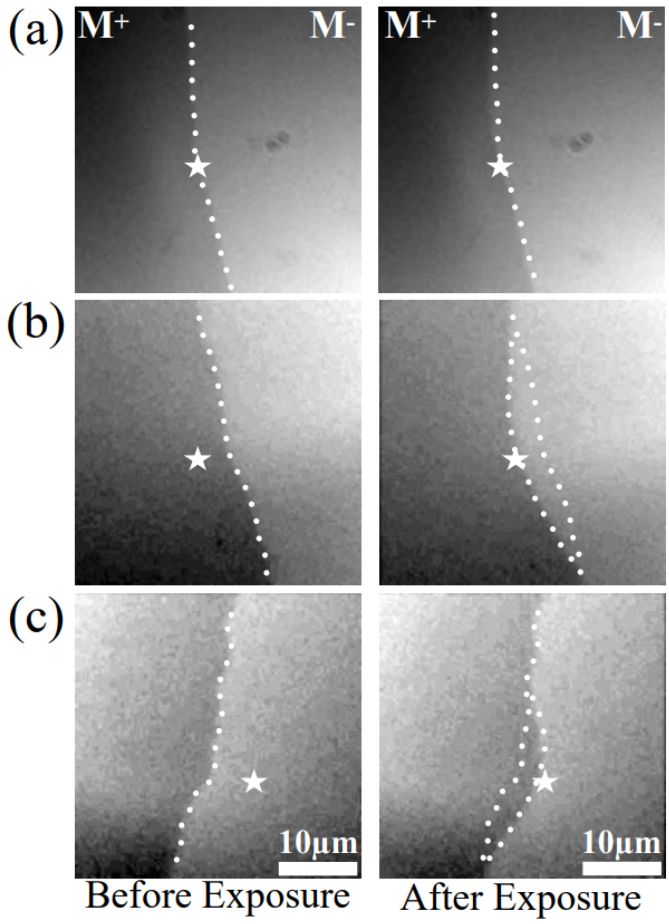

Figure 3.8: (a)-(c) Mageto-optical images of a DW in a Pt(4.5 nm)/Co(0.6 nm)/Pt(4.5 nm) thin film irradiated with 40 fs linearly polarized laser pulses with a fluence of 7 mJ/cm^2 . The center of the laser beam spot, represented by a white star, is on the DW (a) and off-centered in (b) and (c). Adapted from [183].

Resolving the role of magnetic circular dichroism in multishot helicity-dependent all-optical switching

In order to resolve the problem of the relevance of a purely thermal mechanism based on the MCD to explain HD-AOS and laser induced DW motion, we decided to perform time resolved magneto-optical Kerr measurements as a function of the helicity of the pump pulse [185]. The investigated sample is a ferrimagnetic alloy grown by DC magnetron sputtering with the structure Glass/Ta(2)/$Co_{70}Tb_{30}$(20)/Pt(2) (thickness in nm).

Since the ultrafast magnetization dynamics in metallic systems depends on the amount of absorbed light, it is therefore possible to extract the MCD from helicity dependent ultrafast magnetization dynamics measurements. In the linear regime, we can assume that the magnetization change is proportional to the absorbed laser fluence. Therefore, we can estimate the modification of the magnetization induced by a single laser pulse for all four combinations of light polarization (σ-, σ+) and initial magnetization direction (M^+, M^-):

$$\begin{aligned} M(\sigma-,+) &= (\Delta R + \delta R) + (\Delta M + \delta M) \\ M(\sigma-,-) &= (\Delta R - \delta R) - (\Delta M - \delta M) \\ M(\sigma+,+) &= (\Delta R - \delta R) + (\Delta M - \delta M) \\ M(\sigma+,-) &= (\Delta R + \delta R) - (\Delta M + \delta M) \end{aligned} \tag{3.4}$$

ΔM refers to the helicity independent and δM indicates the helicity dependent component of the magnetization change. By reversing the light helicity, the demagnetization rate changes by $\pm\delta M$, which is directly proportional to the MCD. The change of the reflectivity only depends on the helicity of the light. Linear combinations of the four equations allows us to extract both ΔM and δM. The convention used in Eqs. 3.4 yields δM proportional to [A(σ-, +) - A(σ-, -)] (equivalently to [A(σ+, -) - A(σ+, +)])with A being the light absorption. The results are plotted in figure 3.9

The helicity independent magnetization dynamics ΔM (figure 3.9 (a)) is actually similar to what would have been obtained using a linearly polarized light. Interestingly, the difference between the two magnetization dynamics due to the MCD represented by δM is clearly visible (figure 3.9 (b)). We can thus conclude that the amplitude of the MCD in our sample is about 1%. Moreover, since $\delta M < 0$, this implies that the MCD is negative. Therefore, pumping with a σ- polarization (respectively, σ+)more light is absorbed by the magnetic medium for the magnetization pointing down (respectively, up) leading to a higher demagnetization efficiency.

By combining these results with laser induced DW motion experiments performed on this sample, we unambiguously determined that the DW moves towards the hotter region. Therefore, the direction of the laser induced DW propagation is directly related to the direction of the temperature gradient. As it was shown previously that multishot HD-AOS involves a helicity independent domain nucleation followed by a helicity dependent DW motion, it results that thermal effects, e.g., the temperature gradient arising from the MCD, is probably the main driving force leading to HD-AOS.

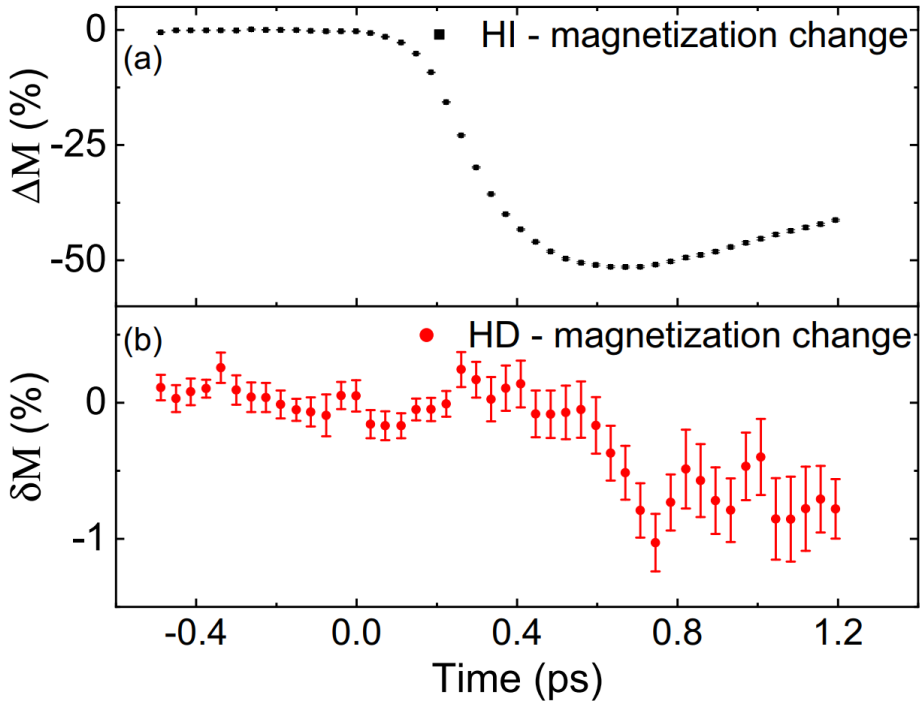

Figure 3.9: (Helicity-independent (ΔM) and (b) helicity- dependent (δM) magnetization dynamics induced by circularly polarized light. δM is proportional to the magnetic circular dichroism. Adapted from [185].

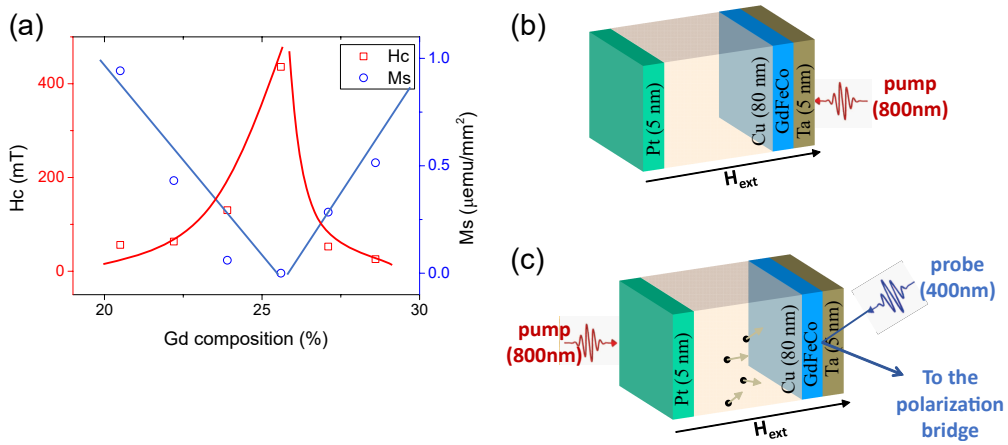

Figure 3.10: Quasistatic room temperature magnetic properties of Glass/ Ta (3 nm)/Pt (5 nm)/Cu (80 nm)/Gd_xFeCo_{1-x} (5 nm)/Ta (5 nm) films for ($20\% < x < 30\%$) and the pump–probe experimental configurations. (a) Variation of the coercive field HC and the saturation magnetization Ms as a function of the Gd content (x). (b)and (c) Sketch of the time resolved experimental configurations that enable to separately study of light pulse and hot electron pulse induced ultrafast magnetization dynamics. Adapted from [187].

3.1.4 All-optical helicity-independent switching in GdFeCo alloys

In this section, we will focus on the influence of the excitation parameters and the properties of GdFeCo on the HI-AOS process.

Hot-electron induced magnetization reversal in GdFeCo based heterostructures

As it was demonstrated in section 2.1, unpolarized hot electrons generated by the absorption of a femtosecond laser pulse could be used to demagnetize a Co/Pt multilayer buried under a 100 nm thick Cu layer due to ultrafast electronic transport. Wilson *et al.* have shown the possibility to use hot electrons to perform magnetization reversal in GdFeCo [188]. However, the timescale of such a magnetization reversal remains unknown, and this magnetization reversal was only reported for one composition of GdFeCo. These results triggered different fundamental questions: What is the timescale of this switching process? Is it similar to the one reported for the light-induced AO-HIS? Since the demagnetization timescale of rare earth and transition metal magnetic atoms are different, can hot electrons reverse the magnetization in both Gd-rich and FeCo-rich alloys? If yes, are the two reversal timescales similar? These questions were tackled by Marwan Deb and Yong Xu during their postdoctoral fellowships [187].

The study was carried on a series of 5 nm thick Gd_xFeCo_{1-x} layers made of an amorphous alloy with different concentrations of Gd ranging from 20% to 30%. The full multialyer structure was: Glass/Ta (3 nm)/Pt (5 nm)/Cu (80 nm)/Gd_xFeCo_{1-x} (5 nm)/Ta (5 nm). The static magnetic properties are summarized in figure 3.10 (a) where the coercive field and the saturation magnetization are plotted as a function of the Gd concentration. The magnetic compensation at which the magnetization of both sublattices are identical is obtained for a Gd concentration of $x_{comp} = 26\%$ leading to the vanishing of the net magnetization and the

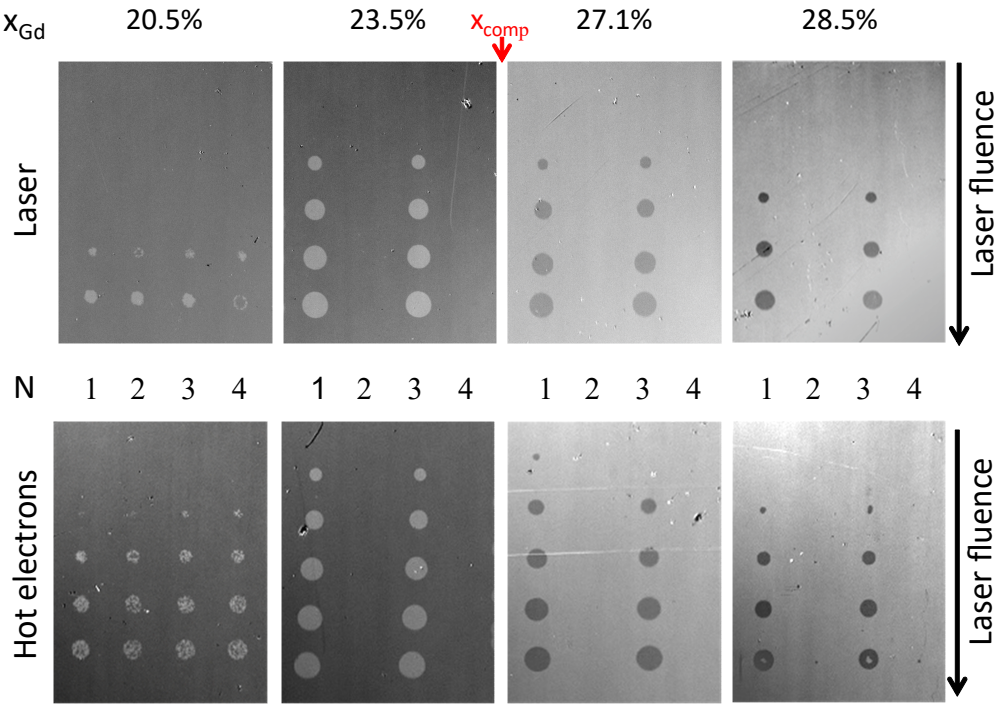

Figure 3.11: Magneto-optical Kerr images obtained after the excitation of Gd_xFeCo_{1-x} films by up to four direct light pulses for five different values of laser fluences ranging from 0.75 to 3.5 mJ.cm^{-2} and hot electron pulses for five different values of laser fluences ranging from 4 to 12.25 mJ.cm^{-2}. Adapted from [187].

divergence of the coercive field.

Using our engineered multilayer structures together with femtosecond laser pulses, we can investigate the ultrafast magnetization dynamics induced either by a direct optical excitation (figure 3.10 (b)) or by an indirect excitation induced only by hot electrons (figure 3.10 (c)). In this indirect configuration, the GdFeCo film is optically shielded by the 80 nm thick Cu layer. Both static MOKE imaging experiments as well as TRMOKE measurements were performed to study the light and hot electrons induced magnetization switching.

Single laser shot HI-AOS can be observed in samples with a Gd concentration ranging from 23% to 28% which surround the compensation concentration (figure 3.11 (top)). The images obtained for various laser fluences prove that samples having a composition closer to compensation require less power to switch. Moreover, the influence of the laser fluence on the switching confirms the existence of a power threshold which depends on the concentration. This point will be discussed in more detail in the next section. Similar results were obtained when using hot electrons to excite the GdFeCo layer (figure 3.11 (bottom)). However, the required laser fluence is four times higher than for direct optical excitation. These results prove once again that the ultrafast magnetization switching in GdFeCo has a purely thermal origin.

To further compare direct optical and hot electrons excitations, we performed TRMOKE measurements. Figure 3.12 clearly shows that both type of excitation lead to a similar magnetization dynamics and reversal. Here again, HI-AOS is obtained above a threshold fluence within a certain composition range around x_{comp} ($22 < x < 28$). In both cases, the

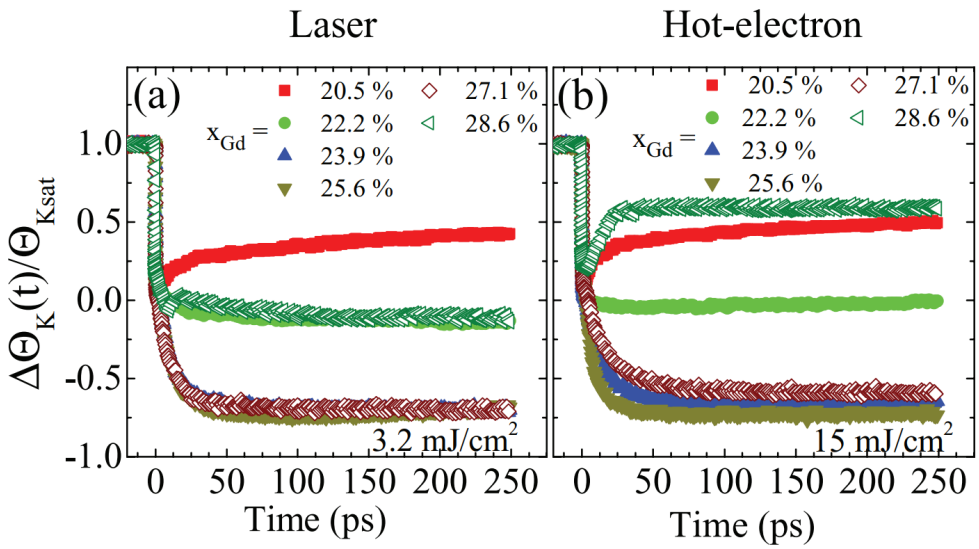

Figure 3.12: Comparison between the magnetization dynamics induced in 5 nm thick Gd_xFeCo_{1-x} films by (a) femtosecond laser and (b) hot-electron pulses excitations for six different concentrations around the compensation concentration and for laser fluencies of 3.2 and 15 mJ.cm^{-2}, respectively. The amplitude of the external magnetic field is adjusted to be slightly larger than the coercive field for each sample in order to ensure the same initial magnetic state. Adapted from [187].

femtosecond pulse generates a large increase of the electron bath temperature for a short time which leads to the magnetization reversal. Far from the compensation concentration, the magnetization dynamics looks similar to the one measured on ferromagnetic thin films.

These results demonstrated the possibility to deterministically reverse the magnetization of an embedded GdFeCo layer within few tens of picoseconds, opening up the possibility to integrate them in more complex spintronic devices.

Switching state diagram of GdFeCo

Despite the large number of investigations on single shot HI-AOS, the influence of the laser parameters such as fluence and pulse duration as well as the properties of the GdFeCo alloys such as the concentration and the thickness, has not been systematically investigated. We investigated the role of all these parameters during the Ph.D. thesis of Jiaqi Wei [189,190]. The investigated samples are deposited by DC magnetron sputtering onto a glass substrate according to the following multilayered structure: glass/Ta (3 nm)/Pt (5 nm)/$Gd_x(FeCo)_{1-x}$ (t nm)/Ta (5 nm). The GdFeCo thickness t was either 10 nm or 20 nm. All the samples exhibit perpendicular magnetic anisotropy and the magnetic compensation was obtained for a Gd concentration $24\% \leq x_{comp} \leq 25\%$.

Figure 3.13 present HI-AOS state diagram obtained on 20 nm $Gd_x(FeCo)_{1-x}$ alloys with $22\% \leq x \leq 27\%$. We observe that above a certain fluence defined as F_{switch}, the magnetization of the GdFeCo is reversed. Above a certain fluence F_{demag}, a multidomain state is observed in the middle of the spot. The state diagrams obtained for the different samples

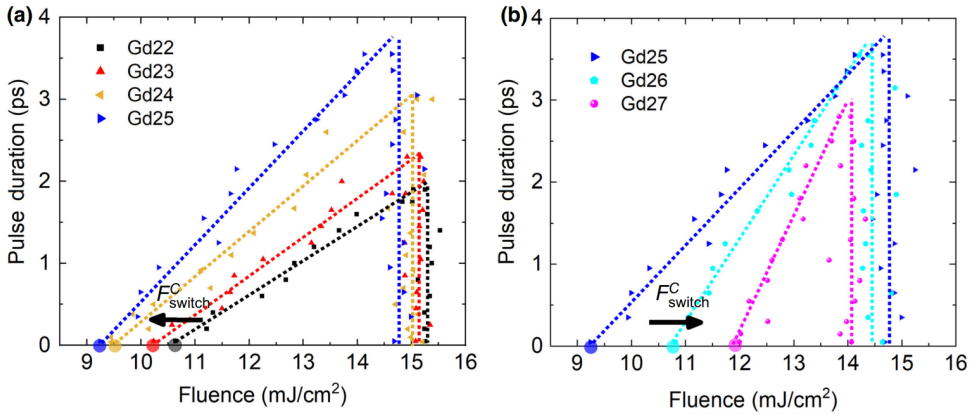

Figure 3.13: HI-AOS state diagrams of 20 nm $Gd_x(FeCo)_{1-x}$ for (a) $22\% \leq x \leq 25\%$ and (b) $25\% \leq x \leq 27\%$. The switching regions for different Gd concentrations are highlighted by colored dashed lines. Adapted from [189].

share similar outlines. Indeed, for all concentrations, F_{switch} increases linearly with the pulse duration while F_{demag} is independent of the pulse duration. However, notable variations can be observed as the alloy composition varies. For instance, the minimum switching fluence F^C_{switch} leading to HI-AOS decreases and the maximum pulse duration τ_{max} increases when approaching the compensation concentration. Furthermore, reducing the alloy thickness from 20 to 10 nm induces an increase of τ_{max} ujp to 11.8 ps for $x = 25\%$ and a decrease of F^C_{switch} by a factor of ≈ 2. The fact that F^C_{switch} scales with the layer thickness can be ascribed to the variation of the laser absorption and the total magnetic volume, indicating that a smaller thickness helps reaching higher energy efficiency for HI-AOS devices. Furthermore, calculations based on the atomistic spin model allowed reproducing the behaviors observed experimentally.

From our experimental results and the atomistic calculations, we concluded that the absence of variation of F_{demag} with the laser fluence is due to the phonon temperature reaching the Curie temperature of the alloy. Therefore, a higher Curie temperature should lead to an increase of τ_{max}. Moreover,the electronic excitation and the emperature seems to play a crucial role in HI-AOS. Indeed, shorter laser pulses allow reaching higher electronic temperature leading to a reduction of the fluence required for magnetization reversal to take place. These results provide a way to further develop this materials, which will be of great significance for the application of HI-AOS.

Role of the spin-lattice coupling in HI-AOS

The role of the spin-lattice coupling in the HI-AOS of ferrimagnetic alloys was studied during the postdoctoral fellowship of Wei Zhang [96]. To do so, we studied single-shot all optical switching phenomenon by tuning the Gd and Tb concentrations in $Gd_{1-x-y}Tb_yCo_x$ alloys. While Gd has no orbital mometum, the large orbital mometum of Tb induces a strong spin-orbit coupling therefore favoring the transfer of angular mometum to the lattice. The spin dynamics taking place from femtosecond to picosecond timescales was carefully measured using TRMOKE. The investigated multilayer structure was Glass/Ta(3

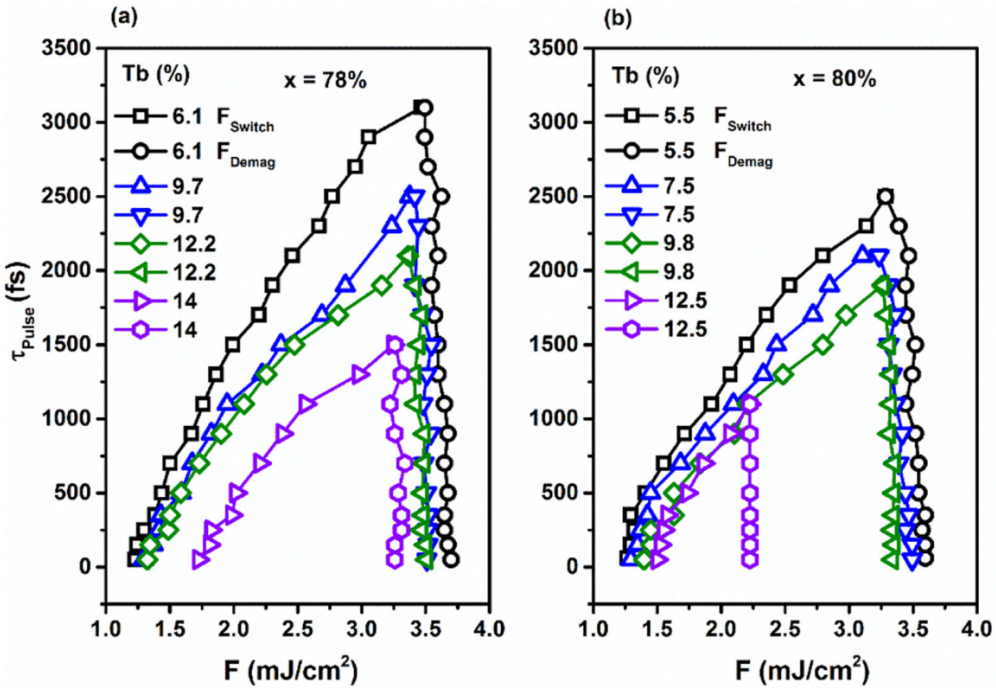

Figure 3.14: HI-AOS state diagrams for $Gd_{1-x-y}Tb_yCo_x$ thin films with $x = 78\%$ and 80%, while y varies from 6.1 to 14% and 5.5 to 12.5%, respectively. Adapted from [96].

nm)/Pt(5nm)/$Gd_{1-x-y}Tb_yCo_x$(5 nm)/Cu(3nm) /Ta(5nm).

In a first time, we determined the state diagrams for these alloys as done in the previous section (Figure 3.14. They present a similar shape as the one presented in the previous section for pure GdFeCo alloys [189]. However, F_{switch} and F_{demag} as well as τ_{max} strongly depend on the Tb concentration. Indeed, F_{switch} increases, while F_{demag} decreases for higher Tb concentration for a given pulse duration. We also found that the fluence range showing HI-AOS is larger and τ_{max} is longer for lower Tb concentrations.

The magnetization dynamics measured in $Gd_{15.9}Tb_{6.1}Co_{78}$ as a function of the laser fluence and for different pulse duration are displayed in figure 3.15. In the case of 60 fs pulse duration, above a fluence of 1.37 mJ/cm^2, a clear change of sign of the magneto-optical signal within the first 20 ps indicates a reversal of the magnetization. The maximum reversal amplitude is obtained for a fluence of 1.37 mJ/cm^2. Further increasing the fluence leads to the formation of a multidomain state within the center of the laser spot therefore decreasing the signal. When the pulse duration increases, the reversal of the signal becomes weaker and no reversal could be measured for a pulse duration $\leq$ 550 fs. Similar measurements were performed for samples with $x = 80\%$ and 84%. We found that the switching occurs for $x = 78\%$ and 80%, when the concentration of Tb y is lower than 12.2 and 9.8%, respectively. For $x = 84\%$, no switching could be observed whatever the Tb concentration, even at the shortest pulse duration. The difference in τ_{max} measured using signle pulse MOKE microscopy and TRMOKE might come from the presence of a significant DC heating due to the high laser repetition rate (5 kHz).

To better understand the role played by the Tb in the alloys, we performed atomistic simulations using the VAMPIRE software package [191]. We focused on the $Gd_{1-x-y}Tb_yCo_x$

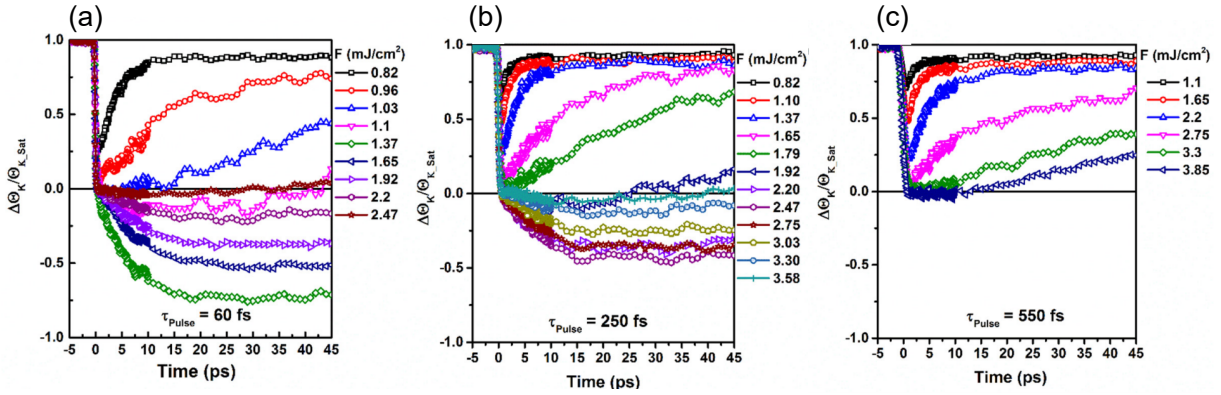

Figure 3.15: Ultrafast magnetization dynamics of $Gd_{15.9}Tb_{6.1}Co_{78}$ measured for different laser fluences and for various laser pulse duration pulse ranging from 60 to 550 fs. Adapted from [96].

alloy with $x = 80\%$ and $5.5\% \leq y \leq 12.5\%$. A specific damping was assigned to each constituent of the alloy instead of using a net damping of the system. This allows accounting for the different spin-lattice coupling between Gd and Tb. Here, we firstly fixed the element-specific damping values for the Tb to 0.08 to reproduce the experimental results, while the ones for Gd and Co were set to 0.02. Simulated magnetization dynamics and AO-HIS state diagram show very good qualitative agreement with the experimental results. Furthermore, we noticed a clear increase in the simulated critical fluence F_{switch} when increasing the Tb damping constant.

Based on our experiments and simulations, we concluded that the absence of AO-HIS observed when increasing the Tb concentration is due to an increase of angular momentum transfer to the lattice and therfore a reduction of the transfer to the Co sublattice. For more details, we refer the interested reader to [96].

Chapter 4

Perspectives

The results obtained during the last decade on ultrafast magnetization dynamics, ultrafast spin transport in magnetic multilayers, and laser induced magnetization switching showed that even though incredible progress have been made, a complete description of these phenomena remains elusive due to their intricacies.

Regarding ultrafast spin transport, many questions remain unanswered to this day. For instance, what are the spin-dependent scattering processes controlling superdiffusive spin transport? How do locally absorbed hot electrons when injected into a ferromagnet interact with magnons or phonons? Does the spin diffusion length of photoexcited hot electrons differ from the one measured at the Fermi energy? What is the role played by the interfaces? Can non-equilibrium spin current be filtered to improve the spin polarization? Why is Gd the main source of spin current in Gd based ferrimagnetic alloys? And finally, what are the microscopic processes responsible for magnetization reversal in ferromagnetic spin-valves (see section 2.2.4)?

Different approaches can be followed to try answering these questions. As I will present in the next chapter, we have just developed a new experimental setup allowing for measuring THz emission in magnetic multilayers. This new technique could prove useful in understanding ultrafast transport phenomena even though our first results tend to show that due to the high number of intricate conversion mechanisms, and most importantly, due to the high sensitivity to changes in the optical properties, extracting absolute numbers for spintronic phenomena remains extremely challenging [192]. Nevertheless, it remains a powerful characterization technique.

Information on ultrafast spin transport could also be obtained using the TRMOKE technique by measuring for instance the spin accumulation generated by the laser pulse excitation [87, 88, 193] and/or by using a crossed magnetization configuration to trigger spin transfer torque [87–89]. These experiments could help understanding the spin current generation in Gd based ferrimagnetic alloys and the difference with similar samples using Co/Gd bilayers.

The energy distribution of optically created hot carriers could be assessed by measuring the current injected from a mettalic multilayer into a semiconductor through a Schottky barrier [194]. Preliminary results seem to show that some excited carriers generated in a 5 nm thick Pt layer on top of a 100 nm thick Cu layer in contact with Si can cross the Schottky barrier at the Cu/Si interface when excited by a 35 fs, 800 nm laser pulse. This encouraging

results have to be reproduced and could open the way to studying the energy distribution and spin dependent ultrafast transport of optically excited hot electron.

Regarding laser induced magnetization switching, recent results obtained in collaboration with the group of SPINTEC on laser induced magnetization switching in Co/Tb multilayers led us to investigate once again RE-TM alloys with RE=Tb, Dy, and Ho and TM=Co and Fe. This study is actually carried out by Yi Peng during her Ph.D. thesis and indicates that single shot switching can be obtained within these alloys. However, the switching mechanism which we do not fully understand at the moment is clearly different than the one observed in Gd based systems. Furthermore, we do not have any information yet about the switching dynamics which could also help us understanding the magnetization reversal process. These alloys could prove useful in the development of ultrafast magnetic memories due to their much higher magnetic anisotropy compared to Gd based layers. This is an important aspect in order to use these materials in ultrafast functional memories and logic elements which become even more crucial when the bit size shrinks down to the tens of nm scale. Another approach we also follow consists in including Gd in Tb based alloys. Our recent results suggest that only few percent of Gd allows for observing a robust toggle switching while keeping a strong perpendicular anisotropy.

Our latest results about the possibility of switching the magnetization of ferromagnetic layers in spin valve structures on the picosecond timescale provide a new route for pushing spintronics down to the femtosecond timescale (see section 2.2.4). However, a complete microscopic mechanism is still lacking which is mainly due to the intricacy and the numerous different physical processes involved in the observed magnetization reversal. Indeed, the spin-polarized current leading to the magnetization reversal can have different origins. For instance, the laser pulse absorption leads to the creation of highly energetic electrons resulting in the appearance of a spin polarized current due to spin-dependent scattering and mobility. Another mechanism responsible for the creation of a spin current comes from the ultrafast demagnetization due to laser heating. In this case, it is assumed that electron-magnon coupling conserves spin angular momentum. Thus the spin loss during the demagnetization results in an out-of-equilibrium spin accumulation among itinerant electrons which can be transported by diffusion. Furthermore, the spin-dependent reflection and transmission of hot carriers at interfaces should also be taken into account. Therefore, engineered magnetic heterostructures with controlled bulk and interface properties will be required to improve our comprehension of this intringuing and complex problem.

Chapter 5

Research related activities

5.1 Experimental development

An important part of an experimental physicis work consists of developing and constantly improving or modifying experimental setups with the aim to make them easy to use and reliable. In the following, I will describe the experimental development I did since I entered the CNRS.

In 2010, I joined the group imaging and dynamics in magnetism of the Laboratory of Solid-State Physics (LPS) in Orsay as a full time CNRS researcher. The aim of my project was to study the ultrafast magnetization dynamics with a clear focus on the role played by hot electrons following laser excitation. For this purpose, I first obtained a regional grant (see section 5.4) to develop a TRMOKE setup at the LPS [79, 195]. At the same time, I was co-directing the Ph.D. of Nathan Beaulieu with Dr. Fausto Sirotti at the SOLEIL synchrotron on the TEMPO beamline where we setup for the firs time in SOLEIL time-resolved experiment combining laser excitation and soft X-Rays as a probe of the induced dynamics. This allowed us to study for instance the electronic and magnetization dynamics of Gd epitaxial thin films [196], multiphoton photoemission from Au(111) surface state with 800 nm laser pulses [197], and time resolved magnetic scattering of CoPd maultilayers [198].

In 2013, I joined the group SPIN at the Jean Lamour Institute in Nancy where I was given the opportunity to develop the topic of ultrafast magnetization dynamics together with Prof. Michel Hehn and Prof. Stéphane Mangin. To do so, I had to build up a full setup allowing for performing time resolved experiments as well as Kerr microscopy. I chose to purchase an amplified Ti:Sa laser (Legend Elite USX from COHERENT). This works at 5KHz repetition rate with pulse duration around 35 fs at the sample position and a pulse energy of 2.5 mJ at the laser output. The central wavelength is 800 nm but it can be tuned from 300 to 2600 nm using an optical parametric amplifier (TOPAS from LIGHT CONVERSION).

The TRMOKE setup was first developed with the help of Nicolas Bergeard during his postdoctoral fellowship. Since then, it was relocated in the IJL building and the actual setup is shown in figure 5.1 (a). In this experiment, the pulsed laser beam is split into two beams using a beam splitter. The pump beam is kept at a wavelength of 800 nm and is used to excite the dynamics we want to measure. Its spot size is usually in the 300-600 μm range. The frequency of the probe is doubled using a BBO crystal so its wavelength is 400 nm and its spot size is usually around 50 μm. This allows filtering the pump before the detection

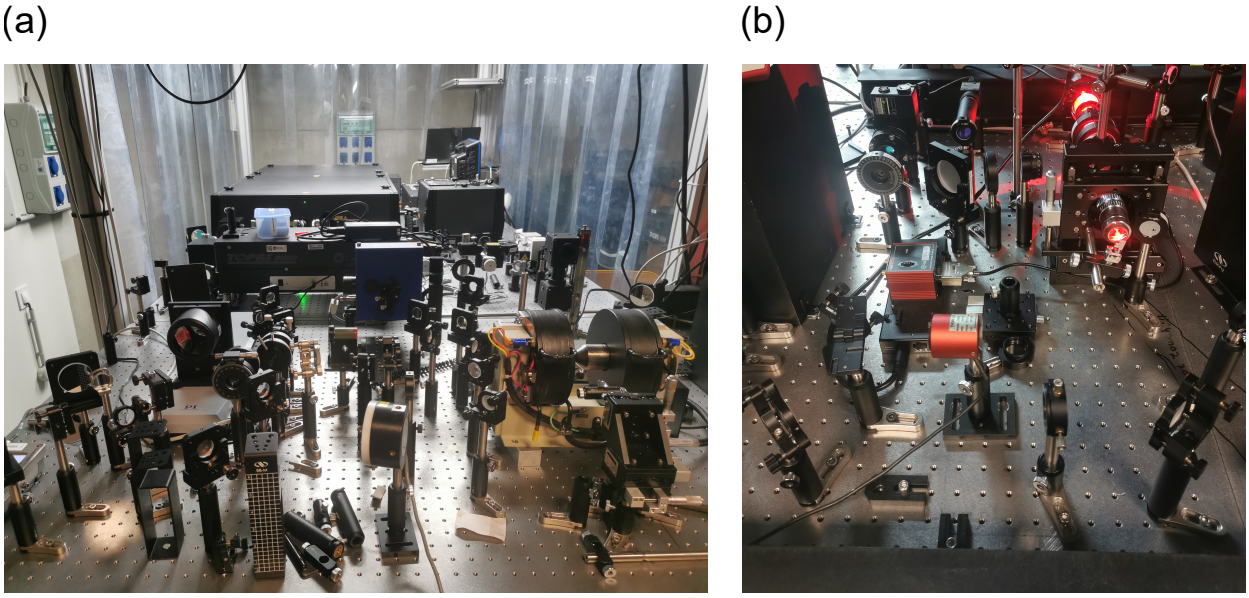

Figure 5.1: (a) TRMOKE and (b) MOKE microscopy setups.

performed by a balanced photodiodes detector and to avoid state filling effects. The time resolution is obtained by controlling the delay between the pump and probe pulses. To do so, we use a delay line with a maximum length of 30 cm which allows for a maximum delay of about 2 ns with a minimum incremental time of 6 fs. The setup can esaily be adjusted to perform front or back excitation through a transparent substrate. The sample is located within an electromagnet allowing applying magnetic field up to 1 T. The setup is fully interfaced using a Labview program we developed. This allows for measuring time resolved MOKE or reflectivity as well as hysteresis loops. The program was recently updated by Jon Gorchon in order to harmonise our different setups within the laboratory to facilitate their use by the students and postdocs.

The MOKE microscope combines the possibility to image the magnetic state of our sample after being excited by a certain number of 800 nm laser pulses. A pulse picker is used to vary the number of laser pulses from single pulse to continuous excitation. It also allows for controlling the duration between two subsequent pulses. The pulse is focused on the sample with a lens down to 50 μm. The excitation can be done at normal incidence when it is done through the substrate or under an angle of ≈ 45 degrees when exciting from the imaging side. The polarization of the laser pulse can be modified form linear to circular using an achromatic quarter-wave plate. Microscopy imaging is performed from the other side of the sample using a light emitting diode with a center wavelength around 630nm. We used a crossed polarizer-analyser configuration to measure the intensity change induced by the magnetic Kerr effect after the reflection of the light on the magnetic sample. The imaging is done by a charg coupled device (CCD) camera which is protected by a filter to avoid laser pulses to reach it. The magnetic contrast is usually obtained by subtracting a reference image obtained after saturation of the sample using a magnetic field from the image obtained after laser excitation. The imaging resolution is about 1 μm.

At the end of 2021, we built together with Jon Gorchon a THz time domain spectroscopy

setup. We used the same laser characteristic as for the TRMOKE experiments. Here again, the laser beam is split into two parts: a large (roughly 1mm FWHM) pump beam impinging on the sample at normal incidence is used to excite the magnetic multilayer and a probe beam which is used to detect the THz pulse via electro-optic sampling in a 1mm $\langle 111 \rangle$ ZnTe crystal [199, 200]. Our first study was recently published [192]. A new cryostat and an electromagnet will be installed by the end of the year in order to perform low temperature experiments.

During next year, a nitrogen-vacancy (NV) center microscope will also be installed on the optical tables. The microscope will be customized to allow direct excitation of the sample using our femtosecond laser. This will allow us to study in details the magnetic structures created by the laser excitation without any disturbance with a spatial resolution in the 25-50 nm.

5.2 Supervising responsibilities

1. Thesis

   During my carrier, I have been supervising many students involved in the ultrafast magnetization dynamics and reversal topic during the last twelve years. In the following I will only enumerate the Ph.D. thesis, Master thesis, and postdocoral fellowships I was officially (co-)directing.

   - 2011-2013: Nathan Beaulieu, Electronic and magnetic properties induced by laser excitation: from monocrystalline Gd to ferrimagnetic alloys, Univesrité Paris Sud, Orsay [196, 197]
   - 2014-2016: Mohammed Salah El Hadri, Magnetization reversal mechanism leading to all-optical helicity-dependent switching, Université de Lorraine, Nancy [174–176, 179, 181]
   - 2017-2020: Quentin Remy, Ultrafast spin dynamics and transport in magnetic metallic heterostructures, Université de Lorraine, Nancy [161, 162, 164]
   - 2017-2020:Philippe Scheid, Investigation of light – induced ultrafast magnetization dynamics using ab initio methods, Université de Lorraine, Nancy [129, 135, 201, 202]

2. Master M2

   - 2018: Boris Seng, Optically controlling the magnetization reversal of a ferromagnetic material using a single laser pulse, Université de Lorraine, Nancy

3. Postdoctoral fellowships

   - 2014-2016: Nicolas Bergeard studied the hot electrons induced ultrafast magnetization dynamics in [Co/Pt] multilayers [137, 140]

- 2016-2018: Marwan Deb mainly focused on laser and hot electrons induced magnetization dynamics in bismuth-substituted yttrium iron garnet [148,151,152,203]. He was also deeply involved in different other studies in collaboration with other postdocs or Ph.D. students [160, 185, 187]
- 2018-2019: Georgy Kichin investigated the influence of pulse duration, fluence, and laser spot size on all-optical helcity dependent switching in Pt/Co/Pt multilayers [182]
- 2018: Satoshi Iihama studied single-shot multi-level all-optical magnetization switching mediated by spin transport in ([Co/Pt]/Cu/GdFeCo) spin valve structures [160, 161]
- 2017-2019 Yong Xu focused on studying laser and hot electrons induced magnetization reversal in GdFeCo [187, 204]. He also participated in th ework of Boyu Zhang during his Ph.D. thesis [205–207]
- 2021- : Junta Igarashi, Investigation of ultrafast transport phenomena in magnetic multilayers, Université de Lorraine, Nancy

5.3 Collective responsibilities

5.3.1 Conference organization

1. Conference organizing committee

   - Colloque Louis Nèel, Sait-Dié des Vosges, France (2016)
   - Ultrafast Magnetism Conference, Nancy, France (2022)

2. Conference Session Chair

   - Joint European Magnetic Symposia, Conferecen session co-chair, Dublin, Ireland (2008)
   - Joint European Magnetic Symposia, Conferecen session co-chair on “Ultrafast laser-induced magnetization dynamics, magneto-optics and magnetoplasmonics”, Mainz, Germany (2018)
   - Joint MMM-Intermag Conference, Conference session chair on "Femtosecond Excitation of Magnetism", New Orleans, U.S.A. (2022)

5.3.2 Lab responsibilities

- 2017-2022 Member of the IJL scientific committee of the center of competence on optics and Lasers

5.3.3 Ph.D. examiner

- Davide Betto, New materials for Spin Electronics, November 2015, Trinity College Dublin, Dublin, Ireland
- Cyril Leveillé, November 2022, Synchrotron SOLEIL, Saint-Aubin, France
- Youri W. L. van Hees, Quick as a flick - All-optical control over ultrafast magnetization writing and spin transport, December 2022, Eindhoven University of Technology, Eindhoven, The Netherlands

5.4 Fundings

- 2010-2012: Laureat RTRA "Digiteo - Triangle de la Physique" Junior chair, LPS Orsay.
- 2014-2016: Laureat Excellent researcher Initiative, Université de Lorraine.
- 2014-2022: Programme Opérationnel FEDER-FSE Lorraine et massif des Vosges, Grand Est.
- 2015-2019: ANR UMAMI *Understanding the Mechanism of Ultrafast All Optical Magnetization Switching*, P.I. G. Malinowski, IJL Nancy
  Collaborations: LCPMR (Paris), LOA (Palaiseau).
- 2017-2019: ANR SWANGATE *Spin-WAve Nanochannels for reprogrammable logic GATEs*, P.I. M. Hehn, IJL Nancy
  Collaborations: IEF Bures-sur-Yvette,IPCMS Strasbourg.
- 2019-2022: CAP-MAT *CAPteurs intelligents pour la transformation des MATériaux (des ressources aux produits)* , P.I. S. Mangin, IJL Nancy.
- 2019-2022: Chair PLUS (PULSE LASER ULTRA-RAPIDE POUR STOCKER L'INFORMATIO
  Ultra-short laser pulse for data storage P.I. Julius Hohlfeld, IJL Nancy.
- 2020-2023: ANR UFO *UltraFast Opto-magneto-spintronics for Futur Nanotechnologies*, P.I. S. Mangin, IJL Nancy.
  Collaborations: SPINTEC Grenoble, LPCT Nancy.

Bibliography

[1] C. H. Back, D. Weller, J. Heidmann, D. Mauri, D. Guarisco, E. L. Garwin, and H. C. Siegmann. Magnetization Reversal in Ultrashort Magnetic Field Pulses. *Phys. Rev. Lett.*, 81(15):3251–3254, oct 1998.

[2] J. Katine, F. Albert, R. Buhrman, E. Myers, and D. Ralph. Current-Driven Magnetization Reversal and Spin-Wave Excitations in Co /Cu /Co Pillars. *Phys. Rev. Lett.*, 84(14):3149–3152, 2000.

[3] J. Grollier, D. Lacour, V. Cros, A. Hamzic, A. Vaurés, A. Fert, D. Adam, and G. Faini. Switching the magnetic configuration of a spin valve by current-induced domain wall motion. *J. Appl. Phys.*, 92(8):4825, 2002.

[4] K. Uchida, S. Takahashi, K. Harii, J. Ieda, W. Koshibae, K. Ando, S. Maekawa, and E. Saitoh. Observation of the spin Seebeck effect. *Nature*, 455(7214):778–781, oct 2008.

[5] G. E. W. Bauer, E. Saitoh, and B. J. van Wees. Spin caloritronics. *Nat. Mater.*, 11(5):391–399, 2012.

[6] Yoichi Shiota, Takayuki Nozaki, Frédéric Bonell, Shinichi Murakami, Teruya Shinjo, and Yoshishige Suzuki. Induction of coherent magnetization switching in a few atomic layers of FeCo using voltage pulses. *Nat. Mater.*, 11(1):39–43, 2012.

[7] T. Nozaki, Y. Shiota, S. Miwa, S. Murakami, F. Bonell, S. Ishibashi, H. Kubota, K. Yakushiji, T. Saruya, A. Fukushima, S. Yuasa, T. Shinjo, and Y. Suzuki. Electric-field-induced ferromagnetic resonance excitation in an ultrathin ferromagnetic metal layer. *Nat. Phys.*, 8(6):492–497, 2012.

[8] K. Roy, S. Bandyopadhyay, and J. Atulasimha. Hybrid spintronics and straintronics : A magnetic technology for ultra low energy computing and signal processing. *Appl. Phys. Lett.*, 99:063108, 2016.

[9] C. Vicario, C. Ruchert, F. Ardana-Lamas, P. M. Derlet, B. Tudu, J. Luning, and C. P. Hauri. Off-resonant magnetization dynamics phase-locked to an intense phase-stable terahertz transient. *Nat. Photonics*, 7(9):720–723, aug 2013.

[10] T. Kubacka, J. A. Johnson, M. C. Hoffmann, C. Vicario, S. de Jong, P. Beaud, S. Grubel, S.-W. Huang, L. Huber, L. Patthey, Y.-D. Chuang, J. J. Turner, G. L. Dakovski, W.-S. Lee, M. P. Minitti, W. Schlotter, R. G. Moore, C. P. Hauri, S. M.

Koohpayeh, V. Scagnoli, G. Ingold, S. L. Johnson, and U. Staub. Large-Amplitude Spin Dynamics Driven by a THz Pulse in Resonance with an Electromagnon. *Science (80-.).*, 343(6177):1333–1336, mar 2014.

[11] E. Beaurepaire, J.-C. Merle, A. Daunois, and J.-Y. Bigot. Ultrafast Spin Dynamics in Ferromagnetic Nickel. *Phys. Rev. Lett.*, 76(22):4250, may 1996.

[12] J. Hohlfeld, E. Matthias, R. Knorren, and KH Bennemann. Nonequilibrium magnetization dynamics of nickel. *Phys. Rev. Lett.*, 78(25):4861–4864, 1997.

[13] J. Güdde, U. Conrad, V. Jähnke, J. Hohlfeld, and E. Matthias. Magnetization dynamics of Ni and Co films on Cu (001) and of bulk nickel surfaces. *Phys. Rev. B*, 59(10):6608–6611, 1999.

[14] H. Regensburger, R. Vollmer, and J. Kirschner. Time-resolved magnetization-induced second-harmonic generation from the Ni(110) surface. *Phys. Rev. B*, 61:716–722, 2000.

[15] K. H. Bennemann. Theory for nonlinear magnetooptics in metals. *J. Magn. Magn. Mater.*, 200(1-3):679–705, 1999.

[16] A. Melnikov, I. Razdolski, T. O. Wehling, E. Th. Papaioannou, V. Roddatis, P. Fumagalli, O. Aktsipetrov, A. I. Lichtenstein, and U. Bovensiepen. Ultrafast Transport of Laser-Excited Spin-Polarized Carriers in Au/Fe/MgO(001). *Phys. Rev. Lett.*, 107(7):076601, 2011.

[17] Cong Chen, Zhensheng Tao, Adra Victoria Carr, Piotr Matyba, Tibor Szilvasi, Sebastian Emmerich, Martin Piecuch, Mark Keller, Dmitriy Zusin, Steffen Eich, Markus Rollinger, Wenjing You, Stefan Mathias, Uwe Thumm, Manos Mavrikakis, Martin Aeschlimann, Peter M. Oppeneer, Henry Cornelius Kapteyn, and Margaret M. Murnane. Distinguishing Attosecond Electron-Electron Scattering and Screening in Transition Metals. *Proc. Natl. Acad. Sci. U. S. A.*, pages 1–8, 2017.

[18] Uwe Bovensiepen. Coherent and incoherent excitations of the Gd(0001) surface on ultrafast timescales. *J. Phys. Condens. Matter*, 19(8):083201, 2007.

[19] M. Sultan, A. Melnikov, and U. Bovensiepen. Ultrafast magnetization dynamics of Gd(0001): Bulk versus surface. *Phys. Status Solidi B*, 248:2323–2329, 2011.

[20] A. Scholl, L. Baumgarten, R. Jacquemin, and W. Eberhardt. Ultrafast Spin Dynamics of Ferromagnetic Thin Films Observed by fs Spin-Resolved Two-Photon Photoemission. *Phys. Rev. Lett.*, 79(25):5146, dec 1997.

[21] H.-S. Rhie, H. A. Dürr, and W. Eberhardt. Femtosecond electron and spin dynamics in Ni/W (110) films. *Phys. Rev. Lett.*, 90(24):247201, 2003.

[22] Robert Carley, Kristian Döbrich, Björn Frietsch, Cornelius Gahl, Martin Teichmann, Olaf Schwarzkopf, Philippe Wernet, and Martin Weinelt. Femtosecond Laser Excitation Drives Ferromagnetic Gadolinium out of Magnetic Equilibrium. *Phys. Rev. Lett.*, 109(5):057401, jul 2012.

[23] Phoebe Tengdin, Wenjing You, Cong Chen, Xun Shi, Dmitriy Zusin, Yingchao Zhang, Christian Gentry, Adam Blonsky, Mark Keller, Peter M. Oppeneer, Henry Kapteyn, Zhensheng Tao, and Margaret Murnane. Critical Behavior within 20fs Drives the Out-of-Equilibrium Laser-induced Magnetic Phase Transition in Nickel. *Sci. Adv.*, 4(March):1–9, 2018.

[24] C. Stamm, T. Kachel, N. Pontius, R. Mitzner, T. Quast, K. Holldack, S. Khan, C. Lupulescu, E. F. Aziz, M. Wietstruk, H a Dürr, and W. Eberhardt. Femtosecond modification of electron localization and transfer of angular momentum in nickel. *Nat. Mater.*, 6(10):740–3, oct 2007.

[25] C. Boeglin, E. Beaurepaire, V. Halte, V. Lopez-Flores, C. Stamm, N. Pontius, H. A. Durr, and J.-Y. Bigot. Distinguishing the ultrafast dynamics of spin and orbital moments in solids. *Nature*, 465(7297):458–461, may 2010.

[26] M. Wietstruk, A. Melnikov, C. Stamm, T. Kachel, N. Pontius, M. Sultan, C. Gahl, M. Weinelt, H. A. Dürr, and U. Bovensiepen. Hot-Electron-Driven Enhancement of Spin-Lattice Coupling in Gd and Tb 4f Ferromagnets Observed by Femtosecond X-Ray Magnetic Circular Dichroism. *Phys. Rev. Lett.*, 106(12):127401, mar 2011.

[27] I. Radu, K. Vahaplar, C. Stamm, T. Kachel, N. Pontius, H. A. Dürr, T. A. Ostler, J. Barker, R. F. L. Evans, R. W. Chantrell, A. Tsukamoto, A. Itoh, A. Kirilyuk, Th Rasing, and A. V. Kimel. Transient ferromagnetic-like state mediating ultrafast reversal of antiferromagnetically coupled spins. *Nature*, 472(7342):205–208, apr 2011.

[28] N Bergeard, V López-Flores, V Halté, M Hehn, C Stamm, N Pontius, E Beaurepaire, and C Boeglin. Ultrafast angular momentum transfer in multisublattice ferrimagnets. *Nat. Commun.*, 5:3466, jan 2014.

[29] K. Holldack, N. Pontius, E. Schierle, T. Kachel, V. Soltwisch, R. Mitzner, T. Quast, G. Springholz, and E. Weschke. Ultrafast dynamics of antiferromagnetic order studied by femtosecond resonant soft x-ray diffraction. *Appl. Phys. Lett.*, 97:062502, 2010.

[30] E. Jal, V. López-Flores, N. Pontius, C. Schuessler-Langeheine, T. Ferté, N. Bergeard, C. Boeglin, B. Vodungbo, J. Lüning, and N. Jaouen. Structural dynamics during laser induced ultrafast demagnetization. *Phys. Rev. B*, 95:184422, 2017.

[31] A. V. Kimel, A. Kirilyuk, P. A. Usachev, R. V. Pisarev, A. M. Balbashov, and Th Rasing. Ultrafast non-thermal control of magnetization by instantaneous photomagnetic pulses. *Nature*, 435:655–657, 2005.

[32] C. D. Stanciu, F. Hansteen, A. V. Kimel, A. Kirilyuk, A. Tsukamoto, A. Itoh, and Th. Rasing. All-Optical Magnetic Recording with Circularly Polarized Light. *Phys. Rev. Lett.*, 99(4):047601–4, 2007.

[33] Sabine Alebrand, Matthias Gottwald, Michel Hehn, Daniel Steil, Mirko Cinchetti, Daniel Lacour, Eric E. Fullerton, Martin Aeschlimann, and Stéphane Mangin. Light-induced magnetization reversal of high-anisotropy TbCo alloy films. *Applied Physics Letters*, 101(16):162408, oct 2012.

[34] Alexander Hassdenteufel, Birgit Hebler, Christian Schubert, Andreas Liebig, Martin Teich, Manfred Helm, Martin Aeschlimann, Manfred Albrecht, and Rudolf Bratschitsch. Thermally Assisted All-Optical Helicity Dependent Magnetic Switching in Amorphous Fe 100- x Tb x Alloy Films. *Advanced Materials*, 25(22):3122–3128, jun 2013.

[35] S Mangin, M Gottwald, C-h Lambert, D Steil, V Uhlíř, L Pang, M Hehn, S Alebrand, M Cinchetti, G Malinowski, Y Fainman, M Aeschlimann, and E E Fullerton. Engineered materials for all-optical helicity-dependent magnetic switching. *Nature Materials*, 13(3):286–292, mar 2014.

[36] C.-H. Lambert, S. Mangin, B. S. D. C. S. Varaprasad, Y. K. Takahashi, M. Hehn, M. Cinchetti, G. Malinowski, K. Hono, Y. Fainman, M. Aeschlimann, and E. E. Fullerton. All-optical control of ferromagnetic thin films and nanostructures. *Science*, 345:1337, 2014.

[37] C. Schubert, a. Hassdenteufel, P. Matthes, J. Schmidt, M. Helm, R. Bratschitsch, and M. Albrecht. All-optical helicity dependent magnetic switching in an artificial zero moment magnet. *Applied Physics Letters*, 104:082406, 2014.

[38] T.a. Ostler, J. Barker, R.f.l. Evans, R.w. Chantrell, U. Atxitia, O. Chubykalo-Fesenko, S. El Moussaoui, L. Le Guyader, E. Mengotti, L.j. Heyderman, F. Nolting, A. Tsukamoto, A. Itoh, D. Afanasiev, B.a. Ivanov, A.m. Kalashnikova, K. Vahaplar, J. Mentink, A. Kirilyuk, Th. Rasing, and A.v. Kimel. Ultrafast heating as a sufficient stimulus for magnetization reversal in a ferrimagnet. *Nature Communications*, 3:666, 2012.

[39] Grégory Malinowski, Nicolas Bergeard, Michel Hehn, and Stéphane Mangin. Hot-electron transport and ultrafast magnetization dynamics in magnetic multilayers and nanostructures following femtosecond laser pulse excitation. *The European Physical Journal B*, 91:98, 2018.

[40] A. Vaterlaus, T. Beutler, and F. Meier. Spin-lattice relaxation time of ferromagnetic gadolinium determined with time-resolved spin-polarized photoemission. *Physical Review Letters*, 67(23):3314–3317, 1991.

[41] W. Hübner and K. H. Bennemann. Simple theory for spin-lattice relaxation in metallic rare-earth ferromagnets. *Physical Review B*, 53(6):3422, feb 1996.

[42] U. Conrad, J. Güdde, V. Jähnke, and E. Matthias. Ultrafast electron and magnetization dynamics of thin Ni and Co films on Cu(001) observed by time-resolved SHG. *Applied Physics B: Lasers and Optics*, 68:511–517, 1999.

[43] M. Aeschlimann, M. Bauer, S. Pawlik, W. Weber, R. Burgermeister, D. Oberli, and H. C. Siegmann. Ultrafast Spin-Dependent Electron Dynamics in fcc Co. *Physical Review Letters*, 79(25):5158, dec 1997.

[44] Chan La-O-Vorakiat, Mark Siemens, Margaret M. Murnane, Henry C. Kapteyn, Stefan Mathias, Martin Aeschlimann, Patrik Grychtol, Roman Adam, Claus M. Schneider, Justin M. Shaw, Hans Nembach, and T. J. Silva. Ultrafast demagnetization dynamics at the M edges of magnetic elements observed using a tabletop high-harmonic soft X-ray source. *Phys. Rev. Lett.*, 103(25):257402, 2009.

[45] J.-Y. Bigot, M. Vomir, and E. Beaurepaire. Coherent ultrafast magnetism induced by femtosecond laser pulses. *Nat. Phys.*, 5(7):515–520, 2009.

[46] Hélène Vonesch and Jean-Yves Bigot. Ultrafast spin-photon interaction investigated with coherent magneto-optics. *Phys. Rev. B*, 85(18):180407, may 2012.

[47] U. Atxitia, O. Chubykalo-Fesenko, J. Walowski, A. Mann, and M. Münzenberg. Evidence for thermal mechanisms in laser-induced femtosecond spin dynamics. *Phys. Rev. B*, 81(17):174401, may 2010.

[48] N. Kazantseva, U. Nowak, R. W. Chantrell, J. Hohlfeld, and a. Rebei. Slow recovery of the magnetisation after a sub-picosecond heat pulse. *EPL (Europhysics Lett.*, 81(2):27004, 2008.

[49] B. Koopmans, J. J. M. Ruigrok, F. Dalla Longa, and W. J. M. de Jonge. Unifying Ultrafast Magnetization Dynamics. *Phys. Rev. Lett.*, 95(26):267207, dec 2005.

[50] M. Cinchetti, M. Sánchez Albaneda, D. Hoffmann, T. Roth, J.-P. Wüstenberg, M. Krauß, O. Andreyev, H. C. Schneider, M. Bauer, and M. Aeschlimann. Spin-Flip Processes and Ultrafast Magnetization Dynamics in Co: Unifying the Microscopic and Macroscopic View of Femtosecond Magnetism. *Phys. Rev. Lett.*, 97(17):177201, oct 2006.

[51] E. Carpene, E. Mancini, C. Dallera, M. Brenna, E. Puppin, and S. De Silvestri. Dynamics of electron-magnon interaction and ultrafast demagnetization in thin iron films. *Phys. Rev. B*, 78(17):174422, nov 2008.

[52] M. Krauß, T. Roth, S. Alebrand, D. Steil, M. Cinchetti, M. Aeschlimann, and H. C. Schneider. Ultrafast demagnetization of ferromagnetic transition metals: The role of the Coulomb interaction. *Phys. Rev. B*, 80(18):180407, nov 2009.

[53] B. Koopmans, G. Malinowski, F. Dalla Longa, D. Steiauf, M. Fähnle, T. Roth, M. Cinchetti, and M. Aeschlimann. Explaining the paradoxical diversity of ultrafast laser-induced demagnetization. *Nat. Mater.*, 9(3):259–265, mar 2010.

[54] A. B. Schmidt, M. Pickel, M. Donath, P. Buczek, A. Ernst, V. P. Zhukov, P. M. Echenique, L. M. Sandratskii, E. V. Chulkov, and M. Weinelt. Ultrafast Magnon Generation in an Fe Film on Cu(100). *Phys. Rev. Lett.*, 105(19):197401, nov 2010.

[55] K. Carva, M. Battiato, D. Legut, and P. M. Oppeneer. Ab initio theory of electron-phonon mediated ultrafast spin relaxation of laser-excited hot electrons in transition-metal ferromagnets. *Phys. Rev. B*, 87(18):184425, may 2013.

[56] B. Y. Mueller, a. Baral, S. Vollmar, M. Cinchetti, M. Aeschlimann, H. C. Schneider, and B. Rethfeld. Feedback Effect during Ultrafast Demagnetization Dynamics in Ferromagnets. *Phys. Rev. Lett.*, 111(16):167204, oct 2013.

[57] V. P. Zhukov, E. V. Chulkov, and P. M. Echenique. Lifetimes and inelastic mean free path of low-energy excited electrons in Fe, Ni, Pt, and Au: Ab initio GW+T calculations. *Phys. Rev. B*, 73:125105, 2006.

[58] A. Alekhin, I. Razdolski, N. Ilin, J. P. Meyburg, D. Diesing, V. Roddatis, I. Rungger, M. Stamenova, S. Sanvito, U. Bovensiepen, and A. Melnikov. Femtosecond Spin Current Pulses Generated by the Nonthermal Spin-Dependent Seebeck Effect and Interacting with Ferromagnets in Spin Valves. *Phys. Rev. Lett.*, 119:017202, 2017.

[59] M. Battiato, K. Carva, and P. M. Oppeneer. Superdiffusive Spin Transport as a Mechanism of Ultrafast Demagnetization. *Phys. Rev. Lett.*, 105(2):027203, 2010.

[60] S. D. Brorson, J. G. Fujimoto, and E. P. Ippen. Femtosecond electronic heat-transport dynamics in thin gold films. *Phys. Rev. Lett.*, 59(17):1962–1965, 1987.

[61] T. Juhasz, H. E. Elsayed-Ali, G. O. Smith, C. Suárez, and W. E. Bron. Direct measurements of the transport of nonequilibrium electrons in gold films with different crystal structures. *Phys. Rev. B*, 48(20):15488–15491, nov 1993.

[62] J. Hohlfeld, S. S. Wellershoff, J. Güdde, U. Conrad, V. Jähnke, and E. Matthias. Electron and lattice dynamics following optical excitation of metals. *Chemical Physics*, 251(1-3):237–258, jan 2000.

[63] R. Knorren, K. H. Bennemann, R. Burgermeister, and M. Aeschlimann. Dynamics of Excited Electrons in Copper and Ferromagnetic Transition Metals: Theory and Experiment. *Phys. Rev. B*, 61:9427, 2000.

[64] M. Aeschlimann, M. Bauer, S. Pawlik, R. Knorren, G. Bouzerar, and K.H. Bennemann. Transport and dynamics of optically excited electrons in metals. *Applied Physics A: Materials Science and Processing*, 71(5):485–491, nov 2000.

[65] G. Malinowski, F. Dalla Longa, J. H. H. Rietjens, P. V. Paluskar, R. Huijink, H. J. M. Swagten, and B. Koopmans. Control of speed and efficiency of ultrafast demagnetization by direct transfer of spin angular momentum. *Nat. Phys.*, 4(11):855–858, sep 2008.

[66] M. Battiato, K. Carva, and P. M. Oppeneer. Theory of laser-induced ultrafast superdiffusive spin transport in layered heterostructures. *Phys. Rev. B*, 86(2):024404, jul 2012.

[67] A. J. Schellekens, W. Verhoeven, T. N. Vader, and B. Koopmans. Investigating the contribution of superdiffusive transport to ultrafast demagnetization of ferromagnetic thin films. *Appl. Phys. Lett.*, 102(25):252408, 2013.

[68] V. Shokeen, M. Sanchez Piaia, J.-Y. Bigot, T. Müller, P. Elliott, J.FIXMEK. Dewhurst, S. Sharma, and E.FIXMEK.FIXMEU. Gross. Spin Flips versus Spin Transport in Nonthermal Electrons Excited by Ultrashort Optical Pulses in Transition Metals. *Phys. Rev. Lett.*, 119(10):107203, 2017.

[69] M. Hofherr, P. Maldonado, O. Schmitt, M. Berritta, U. Bierbrauer, S. Sadashivaiah, A. J. Schellekens, B. Koopmans, D. Steil, M. Cinchetti, B. Stadtmüller, P. M. Oppeneer, S. Mathias, and M. Aeschlimann. Speed and efficiency of femtosecond spin current injection into a nonmagnetic material. *Phys. Rev. B*, 96(10):100403, 2017.

[70] J. Wieczorek, A. Eschenlohr, B. Weidtmann, M. Rösner, N. Bergeard, A. Tarasevitch, T. O. Wehling, and U. Bovensiepen. Separation of ultrafast spin currents and spin-flip scattering in Co/Cu(001) driven by femtosecond laser excitation via the complex MOKE. *Phys. Rev. B*, 92:174410, 2015.

[71] E. Turgut, C. La-o vorakiat, J. M. Shaw, P. Grychtol, H. T. Nembach, D. Rudolf, R. Adam, M. Aeschlimann, C. M. Schneider, T. J. Silva, M. M. Murnane, H. C. Kapteyn, and S. Mathias. Controlling the Competition between Optically Induced Ultrafast Spin-Flip Scattering and Spin Transport in Magnetic Multilayers. *Phys. Rev. Lett.*, 110(19):197201, may 2013.

[72] W. He, T. Zhu, X.-Q. Zhang, H.-T. Yang, and Z.-H. Cheng. Ultrafast demagnetization enhancement in CoFeB/MgO/CoFeB magnetic tunneling junction driven by spin tunneling current. *Sci. Rep.*, 3:2883, jan 2013.

[73] F Schleicher, U Halisdemir, D Lacour, M Gallart, S Boukari, G Schmerber, V Davesne, P Panissod, D Halley, H Majjad, Y Henry, B Leconte, a Boulard, D Spor, N Beyer, C Kieber, E Sternitzky, O Cregut, M Ziegler, F Montaigne, E Beaurepaire, P Gilliot, M Hehn, and M Bowen. Localized states in advanced dielectrics from the vantage of spin- and symmetry-polarized tunnelling across MgO. *Nature communications*, 5:4547, jan 2014.

[74] D. Rudolf, C. La-O-Vorakiat, M. Battiato, R. Adam, J. M. Shaw, E. Turgut, P. Maldonado, S. Mathias, P. Grychtol, H. T. Nembach, T. J. Silva, M. Aeschlimann, H. C. Kapteyn, M. M. Murnane, C. M. Schneider, and P. M. Oppeneer. Ultrafast magnetization enhancement in metallic multilayers driven by superdiffusive spin current. *Nat. Commun.*, 3:1037, sep 2012.

[75] A. J. Schellekens, N. de Vries, J. Lucassen, and B. Koopmans. Exploring laser-induced interlayer spin transfer by an all-optical method. *Phys. Rev. B*, 90(10):104429, sep 2014.

[76] B. Pfau, S. Schaffert, and L. Müller. Ultrafast optical demagnetization manipulates nanoscale spin structure in domain walls. *Nat. ...*, 3:1100, oct 2012.

[77] B. Vodungbo, J. Gautier, G. Lambert, A. Barszczak Sardinha, M. Lozano, S. Sebban, M. Ducousso, W. Boutu, K. Li, B. Tudu, M. Tortarolo, R. Hawaldar, R. Delaunay,

V. Lopez-Flores, J. Arabski, C. Boeglin, H. Merdji, P. Zeitoun, and J. Luning. Laser-induced ultrafast demagnetization in the presence of a nanoscale magnetic domain network. *Nat. Commun.*, 3:999, aug 2012.

[78] K. C. Kuiper, T. Roth, a. J. Schellekens, O. Schmitt, B. Koopmans, M. Cinchetti, and M. Aeschlimann. Spin-orbit enhanced demagnetization rate in Co/Pt-multilayers. *Appl. Phys. Lett.*, 105:202402, nov 2014.

[79] N. Moisan, G. Malinowski, J. Mauchain, M. Hehn, B. Vodungbo, J. Lüning, S. Mangin, E. E. Fullerton, and a. Thiaville. Investigating the role of superdiffusive currents in laser induced demagnetization of ferromagnets with nanoscale magnetic domains. *Sci. Rep.*, 4:1–6, apr 2014.

[80] A. Eschenlohr, M. Battiato, P. Maldonado, N. Pontius, T. Kachel, K. Holldack, R. Mitzner, A. Föhlisch, P. M. Oppeneer, and C. Stamm. Ultrafast spin transport as key to femtosecond demagnetization. *Nat. Mater.*, 12(4):332–336, apr 2013.

[81] M. Battiato, G. Barbalinardo, K. Carva, and P. M. Oppeneer. Beyond linear response theory for intensive light-matter interactions: Order formalism and ultrafast transient dynamics. *Phys. Rev. B*, 85(4):045117, jan 2012.

[82] B. Vodungbo, B. Tudu, J. Perron, R. Delaunay, L. Müller, M. H. Berntsen, G. Grübel, G. Malinowski, C. Weier, J. Gautier, G. Lambert, P. Zeitoun, C. Gutt, E. Jal, A. H. Reid, P. W. Granitzka, N. Jaouen, G. L. Dakovski, S. Moeller, M. P. Minitti, A. Mitra, S. Carron, B. Pfau, C. von Korff Schmising, M. Schneider, S. Eisebitt, and J. Lüning. Indirect excitation of ultrafast demagnetization. *Sci. Rep.*, 6:18970, 2016.

[83] A. R. Khorsand, M. Savoini, A. Kirilyuk, and Th. Rasing. Optical excitation of thin magnetic layers in multilayer structures. *Nat. Mater.*, 13(2):101, jan 2014.

[84] G. Salvatella, R. Gort, K. B??hlmann, S. D??ster, A. Vaterlaus, and Y. Acremann. Ultrafast demagnetization by hot electrons: Diffusion or super-diffusion? *Struct. Dyn.*, 3(5):7–13, 2016.

[85] L. Berger. Emission of spin waves by a magnetic multilayer traversed by a current. *Phys. Rev. B*, 54(13):9353, oct 1996.

[86] J. C. Slonczewski. Current-driven excitation of magnetic multilayers. *J. Magn. Magn. Mater.*, 159(1-2):L1–L7, 1996.

[87] G.-M. Choi, B.-C. Min, K.-J. Lee, and D. G. Cahill. Spin current generated by thermally driven ultrafast demagnetization. *Nat. Commun.*, 5(30):4334, 2014.

[88] G.-M. Choi, C.-H. Moon, B.-C. Min, K.-J Lee, and D. G. Cahill. Thermal spin-transfer torque driven by the spin-dependent Seebeck effect in metallic spin-valves. *Nat. Phys.*, 11(June):576, 2015.

[89] A. J. Schellekens, K. C. Kuiper, R. R. J. C. de Wit, and B. Koopmans. Ultrafast spin-transfer torque driven by femtosecond pulsed-laser excitation. *Nat. Commun.*, 5:4333, jul 2014.

[90] Gyung-Min Choi and Byoung-Chul Min. Laser-driven spin generation in the conduction bands of ferrimagnetic metals. *Physical Review B*, 97(1):014410, 2018.

[91] I. Razdolski, A. Alekhin, N. Ilin, J. P. Meyburg, V. Roddatis, D. Diesing, U. Bovensiepen, and A. Melnikov. Nanoscale confinement of ultrafast spin transfer torque exciting non-uniform spin dynamics by femtosecond spin current pulses. *Nat. Commun.*, 8:15007, 2017.

[92] M. L. M. Lalieu, P. L. J. Helgers, and B. Koopmans. Absorption and generation of femtosecond laser-pulse excited spin currents in noncollinear magnetic bilayers. *Phys. Rev. B*, 96:014417, 2017.

[93] A. R. Khorsand, M. Savoini, A. Kirilyuk, A. V. Kimel, A. Tsukamoto, A. Itoh, and Th. Rasing. Role of Magnetic Circular Dichroism in All-Optical Magnetic Recording. *Physical Review Letters*, 108:127205, mar 2012.

[94] Amal El-Ghazaly, Brandon Tran, Alejandro Ceballos, Charles Henri Lambert, Akshay Pattabi, Sayeef Salahuddin, Frances Hellman, and Jeffrey Bokor. Ultrafast magnetization switching in nanoscale magnetic dots. *Applied Physics Letters*, 114:232407, 2019.

[95] Alejandro Ceballos, Akshay Pattabi, Amal El-Ghazaly, Sergiu Ruta, Christian P. Simon, Richard F.L. Evans, Thomas Ostler, Roy W. Chantrell, Ellis Kennedy, Mary Scott, Jeffrey Bokor, and Frances Hellman. Role of element-specific damping in ultrafast, helicity-independent, all-optical switching dynamics in amorphous (Gd,Tb)Co thin films. *Physical Review B*, 103:24438, 2021.

[96] Wei Zhang, Jun Xiao Lin, Tian Xun Huang, Gregory Malinowski, Michel Hehn, Yong Xu, Stéphane Mangin, and Weisheng Zhao. Role of spin-lattice coupling in ultrafast demagnetization and all optical helicity-independent single-shot switching in Gd 1 - x - y Tb y Co x alloys. *Physical Review B*, 105:054410, 2022.

[97] C Banerjee, N Teichert, K E Siewerska, Z Gercsi, G Y P Atcheson, P Stamenov, K Rode, J M D Coey, and J Besbas. Single pulse all-optical toggle switching of magnetization without gadolinium in the ferrimagnet Mn2RuxGa. *Nature Communications*, 11:4444, 2020.

[98] M L M Lalieu, M J G Peeters, S R R Haenen, R Lavrijsen, and B Koopmans. Deterministic all-optical switching of synthetic ferrimagnets using single femtosecond laser pulses. *Physical Review B*, 96:220411, 2017.

[99] M L M Lalieu, R Lavrijsen, and B Koopmans. Integrating all-optical switching with spintronics. *Nature Communications*, 10:1–6, 2019.

[100] M. Beens, M. L.M. Lalieu, A. J.M. Deenen, R. A. Duine, and B. Koopmans. Comparing all-optical switching in synthetic-ferrimagnetic multilayers and alloys. *Physical Review B*, 100:220409, 2019.

[101] L. Avilés-Félix, L. Álvaro-Gómez, G. Li, C. S. Davies, A. Olivier, M. Rubio-Roy, S. Auffret, A. Kirilyuk, A. V. Kimel, Th Rasing, L. D. Buda-Prejbeanu, R. C. Sousa, B. Dieny, and I. L. Prejbeanu. Integration of Tb/Co multilayers within optically switchable perpendicular magnetic tunnel junctions. *AIP Advances*, 9:125328, 2019.

[102] L. Avilés-Félix, A. Olivier, G. Li, C. S. Davies, L. Álvaro-Gómez, M. Rubio-Roy, S. Auffret, A. Kirilyuk, A. V. Kimel, Th Rasing, L. D. Buda-Prejbeanu, R. C. Sousa, B. Dieny, and I. L. Prejbeanu. Single-shot all-optical switching of magnetization in Tb/Co multilayer-based electrodes. *Scientific Reports*, 10:1038, 2020.

[103] Thomas A. Ostler, Richard F.L. Evans, Roy W. Chantrell, Unai Atxitia, Oksana Chubykalo-Fesenko, Ilie Radu, Radu Abrudan, Florin Radu, Arata Tsukamoto, A. Itoh, Andrei Kirilyuk, Theo Rasing, and Alexey Kimel. Crystallographically amorphous ferrimagnetic alloys: Comparing a localized atomistic spin model with experiments. *Physical Review B - Condensed Matter and Materials Physics*, 84:024407, 2011.

[104] K. Vahaplar, A. M. Kalashnikova, A. V. Kimel, S. Gerlach, D. Hinzke, U. Nowak, R. Chantrell, A. Tsukamoto, A. Itoh, A. Kirilyuk, and Th. Rasing. All-optical magnetization reversal by circularly polarized laser pulses: Experiment and multiscale modeling. *Physical Review B*, 85(10):104402, mar 2012.

[105] J. Gorchon, R. B. Wilson, Y. Yang, A. Pattabi, J. Y. Chen, L. He, J. P. Wang, M. Li, and J. Bokor. Role of electron and phonon temperatures in the helicity-independent all-optical switching of GdFeCo. *Physical Review B*, 94(18):19–24, 2016.

[106] C. S. Davies, T. Janssen, J. H. Mentink, A. Tsukamoto, A. V. Kimel, A. F.G. Van Der Meer, A. Stupakiewicz, and A. Kirilyuk. Pathways for Single-Shot All-Optical Switching of Magnetization in Ferrimagnets. *Physical Review Applied*, 13:024064, 2020.

[107] F. Jakobs, T. A. Ostler, C. H. Lambert, Y. Yang, S. Salahuddin, R. B. Wilson, J. Gorchon, J. Bokor, and U. Atxitia. Unifying femtosecond and picosecond single-pulse magnetic switching in Gd-Fe-Co. *Physical Review B*, 103:104422, 2021.

[108] Daniel Steil, Sabine Alebrand, Alexander Hassdenteufel, Mirko Cinchetti, and Martin Aeschlimann. All-optical magnetization recording by tailoring optical excitation parameters. *Physical Review B*, 84(22):224408, dec 2011.

[109] Y. Yang, R. B. Wilson, J. Gorchon, C.-H. Lambert, S. Salahuddin, and J. Bokor. Ultrafast magnetization reversal by picosecond electrical pulses. *Science Advances*, 3(11):e1603117, 2017.

[110] K Mistry, C Allen, C Auth, B Beattie, D Bergstrom, M Bost, M Brazier, M Buehler, A Cappellani, R Chau, C Choi, G Ding, K Fischer, T Ghani, R Grover, W Han, D Hanken, M Hattendorf, J He, J Hicks, R Huessner, D Ingerly, P Jain, R James, L Jong, S Joshi, C Kenyon, K Kuhn, K Lee, H Liu, J Maiz, B Mcintyre, P Moon, J Neirynck, S Pae, C Parker, D Parsons, C Prasad, L Pipes, M Prince, P Ranade, T Reynolds, J Sandford, L Shifren, J Sebastian, J Seiple, D Simon, S Sivakumar,

P Smith, C Thomas, T Troeger, P Vandervoorn, S Williams, and K Zawadzki. A 45nm Logic Technology with High-k+Metal Gate Transistors, Strained Silicon, 9 Cu Interconnect Layers, 193nm Dry Patterning, and 100Packaging. *IEEE International Electron Devices Meeting*, pages 247–250, 2007.

[111] Amal El-Ghazaly, Jon Gorchon, Richard B. Wilson, Akshay Pattabi, and Jeffrey Bokor. Progress towards ultrafast spintronics applications. *Journal of Magnetism and Magnetic Materials*, 502(January):166478, 2020.

[112] Sicong Wang, Chen Wei, Yuanhua Feng, Hongkun Cao, Wenzhe Li, Yaoyu Cao, Bai-ou Guan, Arata Tsukamoto, Andrei Kirilyuk, Alexey V Kimel, and Xiangping Li. Dual-shot dynamics and ultimate frequency of all-optical magnetic recording on GdFeCo. *Light: Science & Applications*, 10:8, 2021.

[113] Felix Steinbach, Nele Stetzuhn, Dieter Engel, Unai Atxitia, Clemens von Korff Schmising, and Stefan Eisebitt. Accelerating double pulse all-optical write/erase cycles in metallic ferrimagnets. *Applied Physics Letters*, 120(11):112406, 2022.

[114] Youri L.W. Van Hees, Bert Koopmans, and Reinoud Lavrijsen. Toward high all-optical data writing rates in synthetic ferrimagnets. *Applied Physics Letters*, 120(25), 2022.

[115] Youri L. W. van Hees, Paul van de Meugheuvel, Bert Koopmans, and Reinoud Lavrijsen. Deterministic all-optical magnetization writing facilitated by non-local transfer of spin angular momentum. *Nature Communications*, 11(1):3835, dec 2020.

[116] G Bonfiglio, K Rode, G Y P Atcheson, P Stamenov, J M D Coey, A V Kimel, Th Rasing, and A Kirilyuk. Sub-picosecond exchange-relaxation in the compensated ferrimagnet Mn₂Ru _x Ga. *J Phys Condens Matter*, 33:135804, 2021.

[117] R. Medapalli, I. Razdolski, M. Savoini, A. Khorsand, A. Kirilyuk, A. Kimel, Th. Rasing, A. Kalashnikova, A. Tsukamoto, and A. Itoh. Efficiency of ultrafast laser-induced demagnetization in gdfeco alloys. *Physical Review B*, 86(5):054442, aug 2012.

[118] C. E. Graves, A. H. Reid, T. Wang, B. Wu, S. de Jong, K. Vahaplar, I. Radu, D. P. Bernstein, M. Messerschmidt, L. Müller, R. Coffee, M. Bionta, S. W. Epp, R. Hartmann, N. Kimmel, G. Hauser, A. Hartmann, P. Holl, H. Gorke, J. H. Mentink, A. Tsukamoto, A. Fognini, J. J. Turner, W. F. Schlotter, D. Rolles, H. Soltau, L. Strüder, Y. Acremann, A. V. Kimel, A. Kirilyuk, Th Rasing, J. Stöhr, A. O. Scherz, and H. A. Dürr. Nanoscale spin reversal by non-local angular momentum transfer following ultrafast laser excitation in ferrimagnetic GdFeCo. *Nat. Mater.*, 12:293–298, mar 2013.

[119] Martin Hennecke, Ilie Radu, Radu Abrudan, Torsten Kachel, Karsten Holldack, Rolf Mitzner, Arata Tsukamoto, Stefan Eisebitt, and Max-born-institut Nichtlineare. Angular Momentum Flow During Ultrafast Demagnetization of a Ferrimagnet. *Physical Review Letters*, 122(15):157202, 2019.

[120] JH Mentink, J. Hellsvik, and DV Afanasiev. Ultrafast spin dynamics in multisublattice magnets. *Physical Review Letters*, 108(5):057202, jan 2012.

[121] U. Atxitia, P. Nieves, and O. Chubykalo-Fesenko. Landau-Lifshitz-Bloch equation for ferrimagnetic materials. *Physical Review B*, 86(10):104414, sep 2012.

[122] U Atxitia, J Barker, and R W Chantrell. Controlling the polarity of the transient ferromagneticlike state in ferrimagnets. *Physical Review B*, 89:224421, 2014.

[123] AJ Schellekens and B. Koopmans. Microscopic model for ultrafast magnetization dynamics of multisublattice magnets. *Physical Review B*, 87(2):020407, jan 2013.

[124] Alexander Baral and Hans Christian Schneider. Magnetic switching dynamics due to ultrafast exchange scattering: A model study. *Physical Review B*, 91(10):1–5, 2015.

[125] V N Gridnev. Ultrafast heating-induced magnetization switching in ferrimagnets. *Journal of Physics: Condensed Matter*, 28:476007, 2016.

[126] A. M. Kalashnikova and V. I. Kozub. Exchange scattering as the driving force for ultrafast all-optical and bias-controlled reversal in ferrimagnetic metallic structures. *Physical Review B*, 93(5):1–11, 2016.

[127] S. Wienholdt, D. Hinzke, K. Carva, P. M. Oppeneer, and U. Nowak. Orbital-resolved spin model for thermal magnetization switching in rare-earth-based ferrimagnets. *Physical Review B*, 88(2):020406, jul 2013.

[128] Alexander Hassdenteufel, Johannes Schmidt, Christian Schubert, Birgit Hebler, Manfred Helm, Manfred Albrecht, and Rudolf Bratschitsch. Low-remanence criterion for helicity-dependent all-optical magnetic switching in ferrimagnets. *Physical Review B*, 91(10):104431, mar 2015.

[129] Philippe Scheid, Quentin Remy, Sébastien Lebègue, Gregory Malinowski, and Stéphane Mangin. Light induced ultrafast magnetization dynamics in metallic compounds. *Journal of Magnetism and Magnetic Materials*, 560:169596, 2022.

[130] J. Gorchon, Y. Yang, and J. Bokor. Model for multishot all-thermal all-optical switching in ferromagnets. *Physical Review B*, 94:020409, 2016.

[131] Matthew O.A. Ellis, Eric E. Fullerton, and Roy W. Chantrell. All-optical switching in granular ferromagnets caused by magnetic circular dichroism. *Scientific Reports*, 6:300522, 2016.

[132] L P Pitaevskii. Electric Forces in a Transparent Dispersive Medium. *J. Exptl. Theoret. Phys. (U.S.S.R.)*, 12(5):1450, 1961.

[133] T D Cornelissen, R Córdoba, and B Koopmans. Microscopic model for all optical switching in ferromagnets. *Applied Physics Letters*, 108:142405, 2016.

[134] Marco Berritta, Ritwik Mondal, Karel Carva, and Peter M. Oppeneer. Ab Initio Theory of Coherent Laser-Induced Magnetization in Metals. *Physical Review Letters*, 117:137203, 2016.

[135] Philippe Scheid, Gregory Malinowski, Stéphane Mangin, and Sébastien Lebègue. Ab initio theory of magnetization induced by light absorption in ferromagnets. *Physical Review B*, 100(21):214402, 2019.

[136] M. Bauer, a. Marienfeld, and M. Aeschlimann. Hot electron lifetimes in metals probed by time-resolved two-photon photoemission. *Prog. Surf. Sci.*, 90(3):319–376, 2015.

[137] N. Bergeard, M. Hehn, S. Mangin, G. Lengaigne, F. Montaigne, M. L. M. Lalieu, B. Koopmans, and G. Malinowski. Hot-Electron-Induced Ultrafast Demagnetization in Co/Pt Multilayers. *Phys. Rev. Lett.*, 117(14):147203, 2016.

[138] Jan-etienne Pudell, Maximilian Mattern, Michel Hehn, Grégory Malinowski, Marc Herzog, and Matias Bargheer. Heat Transport without Heating ?— An Ultrafast X-Ray Perspective into a Metal Heterostructure. *Advanced functional Materials*, page 2004555, 2020.

[139] G. P. Zhang, W. Hübner, Georgios Lefkidis, Yihua Bai, and Thomas F. George. Paradigm of the time-resolved magneto-optical Kerr effect for femtosecond magnetism. *Nature Physics*, 5(7):499–502, jun 2009.

[140] N Bergeard, M Hehn, K Carva, P Baláž, S Mangin, and G Malinowski. Tailoring femtosecond hot-electron pulses for ultrafast spin manipulation. *Applied Physics Letters*, 117:222408, 2020.

[141] A V Scherbakov, A S Salasyuk, A V Akimov, X Liu, M Bombeck, C Bruggemann, V F Sapega, J K Furdyna, and M Bayer. Coherent Magnetization Precession in Ferromagnetic (Ga , Mn) As Induced by Picosecond Acoustic Pulses. *Physical Review Letters*, 105:117204, 2010.

[142] Ji-Wan Kim, Mircea Vomir, and Jean-Yves Bigot. Ultrafast Magnetoacoustics in Nickel Films. *Physical Review Letters*, 109:166601, oct 2012.

[143] Oleksandr Kovalenko, Thomas Pezeril, and Vasily V. Temnov. New concept for magnetization switching by ultrafast acoustic pulses. *Physical Review Letters*, 110:266602, 2013.

[144] H. Y. Hao and H. J. Maris. Study of phonon dispersion in silicon and germanium at long wavelengths using picosecond ultrasonics. *Physical Review Letters*, 84(24):5556–5559, 2000.

[145] Otto L. Muskens and Jaap I. Dijkhuis. High Amplitude, Ultrashort, Longitudinal Strain Solitons in Sapphire. *Physical Review Letters*, 89(28):285504, 2002.

[146] Ji Wan Kim, Mircea Vomir, and Jean Yves Bigot. Controlling the spins angular momentum in ferromagnets with sequences of picosecond acoustic pulses. *Scientific Reports*, 5:8511, 2015.

[147] T. L. Linnik, V. N. Kats, J. Jager, A. S. Salasyuk, D. R. Yakovlev, A. W. Rushforth, A. V. Akimov, A. M. Kalashnikova, M. Bayer, and A. V. Scherbakov. The effect of dynamical compressive and shear strain on magnetic anisotropy in a low symmetry ferromagnetic film. *Physica Scripta*, 92:054006, 2017.

[148] Marwan Deb, Elena Popova, Michel Hehn, Niels Keller, Stéphane Mangin, and Gregory Malinowski. Picosecond acoustic excitation driven ultrafast magnetization dynamics in dielectric Bi-substituted yttrium iron garnet. *Physical Review B*, 98:174407, 2018.

[149] P. Hansen, K. Witter, and W. Tolksdorf. Magnetic and magneto-optic properties of lead- and bismuth-substituted yttrium iron garnet films. *Physical Review B*, 27:6608–6625, 1983.

[150] Marwan Deb, Mircea Vomir, Jean Luc Rehspringer, and Jean Yves Bigot. Ultrafast optical control of magnetization dynamics in polycrystalline bismuth doped iron garnet thin films. *Applied Physics Letters*, 107:252404, 2015.

[151] Marwan Deb, Pierre Molho, Bernard Barbara, and Jean Yves Bigot. Temperature and magnetic field dependence of rare-earth - iron exchange resonance mode in a magnetic oxide studied with femtosecond magneto-optical Kerr effect. *Physical Review B*, 94:1054422, 2016.

[152] Marwan Deb, Elena Popova, Steffen Peer Zeuschner, Michel Hehn, Niels Keller, Stéphane Mangin, Gregory Malinowski, and Matias Bargheer. Generation of spin waves via spin-phonon interaction in a buried dielectric thin film. *Physical Review B*, 103:024411, 2021.

[153] D. Schick, A. Bojahr, M. Herzog, R. Shayduk, C. Von Korff Schmising, and M. Bargheer. UDKM1DSIM - A simulation toolkit for 1D ultrafast dynamics in condensed matter. *Computer Physics Communications*, 185(2):651–660, 2014.

[154] Sebastian F. Maehrlein, Ilie Radu, Pablo Maldonado, Alexander Paarmann, Michael Gensch, Alexandra M. Kalashnikova, Roman V. Pisarev, Martin Wolf, Peter M. Oppeneer, Joseph Barker, and Tobias Kampfrath. Dissecting spin-phonon equilibration in ferrimagnetic insulators by ultrafast lattice excitation. *Science Advances*, 4(7):5164, 2018.

[155] Marwan Deb, Elena Popova, Michel Hehn, Niels Keller, Matias Bargheer, Stéphane Mangin, and Grégory Malinowski. Femtosecond Laser-Excitation-Driven High Frequency Standing Spin Waves in Nanoscale Dielectric Thin Films of Iron Garnets. *Physical Review Letters*, 123:027202, 2019.

[156] Marwan Deb, Elena Popova, Michel Hehn, Niels Keller, Sébastien Petit-watelot, Matias Bargheer, Stéphane Mangin, and Gregory Malinowski. Damping of Standing Spin Waves in Bismuth-Substituted Yttrium Iron Garnet as Seen via the Time-Resolved Magneto-Optical Kerr Effect. *Physical Review Applied*, 12:044006, 2019.

[157] Jon Gorchon, Charles Henri Lambert, Yang Yang, Akshay Pattabi, Richard B. Wilson, Sayeef Salahuddin, and Jeffrey Bokor. Single shot ultrafast all optical magnetization switching of ferromagnetic Co/Pt multilayers. *Applied Physics Letters*, 111:042401, 2017.

[158] R. Lavrijsen, J.H. Lee, A. Fernandez-Pacheco, D.C.M.C. Petit, R. Mansell, and R.P. Cowburn. Magnetic ratchet for three-dimensional spintronic memory and logic. *Nature*, 493:647–650, 2013.

[159] Shilei Zhang, Jingyan Zhang, Alexander A. Baker, Shouguo Wang, Guanghua Yu, and Thorsten Hesjedal. Three dimensional magnetic abacus memory. *Scientific Reports*, 4:06109, 2014.

[160] Satoshi Iihama, Yong Xu, Marwan Deb, Grégory Malinowski, Michel Hehn, Jon Gorchon, Eric E Fullerton, and Stéphane Mangin. Single-Shot Multi-Level All-Optical Magnetization Switching Mediated by Spin Transport. *Advanced Materials*, 30:1804004, 2018.

[161] Junta Igarashi, Quentin Remy, Satoshi Iihama, Gregory Malinowski, Michel Hehn, Jon Gorchon, Julius Hohlfeld, Shunsuke Fukami, Hideo Ohno, and Stéphane Mangin. Engineering Single-Shot All-Optical Switching of Ferromagnetic Materials. *Nano Letters*, 20:8654–8660, 2020.

[162] Quentin Remy, Junta Igarashi, Satoshi Iihama, Grégory Malinowski, Michel Hehn, Jon Gorchon, Julius Hohlfeld, Shunsuke Fukami, Hideo Ohno, and Stéphane Mangin. Energy Efficient Control of Ultrafast Spin Current to Induce Single Femtosecond Pulse Switching of a Ferromagnet. *Advanced Science*, page 2001996, 2020.

[163] J. Hamrle, J. Ferré, M. Nývlt, and Š. Višňovský. In-depth resolution of the magneto-optical Kerr effect in ferromagnetic multilayers. *Phys. Rev. B*, 66(22):1–16, 2002.

[164] Quentin Remy. *Ultrafast spin dynamics and transport in magnetic metallic heterostructures*. PhD thesis, Université de Lorraine, 2020.

[165] A. Manchon, Q. Li, L. Xu, and S. Zhang. Theory of laser-induced demagnetization at high temperatures. *Physical Review B*, 85(6):064408, feb 2012.

[166] Lei Xu and Shufeng Zhang. Magnetization dynamics at elevated temperatures. *Physica E: Low-Dimensional Systems and Nanostructures*, 45:72–76, 2012.

[167] M. Beens, R. A. Duine, and B. Koopmans. S-d model for local and nonlocal spin dynamics in laser-excited magnetic heterostructures. *Physical Review B*, 102:054442, 2020.

[168] E. B. Myers, D. C. Ralph, J. A. Katine, R. N. Louie, and R. A. Buhrman. Current-Induced Switching of Domains in Magnetic Multilayer Devices. *Science*, 285:867–870, 1999.

[169] D. M. Nenno, S. Kaltenborn, and H. C. Schneider. Boltzmann transport calculation of collinear spin transport on short timescales. *Phys. Rev. B*, 94:115102, 2016.

[170] J. Chen, U. Bovensiepen, A. Eschenlohr, T. Müller, P. Elliott, E. K.U. Gross, J. K. Dewhurst, and S. Sharma. Competing Spin Transfer and Dissipation at Co/Cu (001) Interfaces on Femtosecond Timescales. *Physical Review Letters*, 122(6):67202, 2019.

[171] Wen-Tian Lu and Zhe Yuan. Spin accumulation and dissipation excited by an ultrafast laser pulse. *Physical Review B*, 104:214404, 2021.

[172] F. Töpler, J. Henk, and I. Mertig. Ultrafast spin dynamics in inhomogeneous systems: A density-matrix approach applied to Co/Cu interfaces. *New Journal of Physics*, 23:033042, 2021.

[173] Birgit Hebler, Alexander Hassdenteufel, Patrick Reinhardt, Helmut Karl, and Manfred Albrecht. Ferrimagnetic Tb–Fe alloy thin films: Composition and thickness dependence of magnetic properties and all-optical switching. *Frontiers in Materials*, 3(February):1–8, 2016.

[174] Mohammed Salah El Hadri. *Magnetization reversal mechanism leading to all-optical helicity-dependent switching*. PhD thesis, Université de Lorraine, 2016.

[175] Mohammed Salah El Hadri, Michel Hehn, Philipp Pirro, Charles-henri Lambert, Grégory Malinowski, Eric E. Fullerton, and Stéphane Mangin. Domain size criterion for the observation of all-optical helicity-dependent switching in magnetic thin films. *Physical Review B*, 94(6):064419, aug 2016.

[176] M. S. El Hadri, M. Hehn, G. Malinowski, and S. Mangin. Materials and devices for all-optical helicity-dependent switching. *J. Phys. D: Appl. Phys.*, 50:133002, 2017.

[177] Charles Kittel. Theory of the structure of ferromagnetic domains in films and small particles. *Physical Review*, 70(11-12):965–971, 1946.

[178] C. Kooy and U. Enz. Experimental and theoretical study of the domain configuration in thin layers of $BaFe_{12}O_{19}$. *Philips Res. Rep.*, 15:7, 1960.

[179] Mohammed Salah El Hadri, Michel Hehn, Grégory Malinowski, Cyrille Beigné, Eric E. Fullerton, Dafiné Ravelosona, and Stéphane Mangin. Suppression of all-optical switching in He + -irradiated Co / Pt multilayers : influence of the domain-wall energy. *Journal of Physics D: Applied Physics*, 51:215004, 2018.

[180] C. Chappert, H. Bernas, J. Ferré, V. Kottler, J.-P. Jamet, Y. Chen, E. Cambril, T. Devolder, F. Rousseaux, V. Mathet, and H. Launois. Planar Patterned Magnetic Media Obtained by Ion Irradiation. *Science*, 280(5371):1919–1922, 1998.

[181] M S El Hadri, P Pirro, C Lambert, N Bergeard, M Hehn, G Malinowski, F Montaigne, R Medapalli, E E Fullerton, and Mangin. Electrical characterization of all-optical helicity-dependent switching in ferromagnetic Hall crosses. *Applied Physics Letters*, 108:092405, 2016.

[182] G Kichin, M Hehn, J Gorchon, G Malinowski, J Hohlfeld, and S Mangin. From Multiple- to Single-Pulse All-Optical Helicity-Dependent Switching in Ferromagnetic Co / Pt Multilayers. *Physical Review Applied*, 12:024019, 2019.

[183] Yassine Quessab. *Mechanism and size effects of helicity-dependent all-optical magnetization switching in ferromagnetic thin*. PhD thesis, Université de Lorraine, 2018.

[184] Y. Quessab, R. Medapalli, M. S. El Hadri, M. Hehn, G. Malinowski, E. E. Fullerton, and S. Mangin. Helicity-dependent all-optical domain wall motion in ferromagnetic thin films. *Physical Review B*, 97:054419, 2018.

[185] Y Quessab, M Deb, J Gorchon, M Hehn, G Malinowski, and S Mangin. Resolving the role of magnetic circular dichroism in multishot helicity-dependent all-optical switching. *Physical Review B*, 100:024425, 2019.

[186] J. Torrejon, G. Malinowski, M. Pelloux, R. Weil, A. Thiaville, J. Curiale, D. Lacour, F. Montaigne, and M. Hehn. Unidirectional Thermal Effects in Current-Induced Domain Wall Motion. *Physical Review Letters*, 109(10):106601, sep 2012.

[187] Y. Xu, M. Deb, G. Malinowski, M. Hehn, W. Zhao, and S. Mangin. Ultrafast Magnetization Manipulation Using Single Femtosecond Light and Hot-Electron Pulses. *Advanced Materials*, 29:1703474, 2017.

[188] R. B. Wilson, J. Gorchon, YY. Yang, C.-H. Lambert, S. Salahuddin, and J. Bokor. Ultrafast magnetic switching of GdFeCo with electronic heat currents. *Phys. Rev. B*, 95(18):180409, 2017.

[189] Jiaqi Wei, Boyu Zhang, Michel Hehn, Wei Zhang, Gregory Malinowski, Yong Xu, Weisheng Zhao, and Stéphane Mangin. All-optical Helicity-Independent Switching State Diagram in Gd - Fe - Co Alloys. *Physical Review Applied*, 15:054065, 2021.

[190] Jiaqi Wei. *Magnetization manipulation induced by spin current and ultrafast laser*. PhD thesis, Université de Lorraine, 2021.

[191] R. F.L. Evans, W. J. Fan, P. Chureemart, T. A. Ostler, M. O.A. Ellis, and R. W. Chantrell. Atomistic spin model simulations of magnetic nanomaterials. *Journal of Physics Condensed Matter*, 26(10):103202, 2014.

[192] Jon Gorchon, Stéphane Mangin, Michel Hehn, and Grégory Malinowski. Is terahertz emission a good probe of the spin current attenuation length ? Is terahertz emission a good probe of the spin current attenuation length ? *Applied Physics Letters*, 121:012402, 2022.

[193] G.-M. Choi, R. B. Wilson, and David G. Cahill. Indirect heating of Pt by short-pulse laser irradiation of Au in a nanoscale Pt/Au bilayer. *Phys. Rev. B - Condens. Matter Mater. Phys.*, 89:064307, 2014.

[194] E. Monteblanco, F. Donatini, M. Hehn, D. Lacour, Y. Lassailly, J. Peretti, and N. Rougemaille. Transmission of high-energy electrons through metal-semiconductor Schottky junctions. *Physical Review B*, 100(20):205301, nov 2019.

[195] J. Gorchon, J. Curiale, A. Lemaître, N. Moisan, M. Cubukcu, G. Malinowski, C. Ulysse, G. Faini, H. J. von Bardeleben, and V. Jeudy. Stochastic Current-Induced Magnetization Switching in a Single Semiconducting Ferromagnetic Layer. *Physical Review Letters*, 112(2):026601, jan 2014.

[196] Nathan Beaulieu, Gregory Malinowski, Azzedine Bendounan, Mathieu G. Silly, Christian Chauvet, Damjan Krizmancic, and Fausto Sirotti. Probing ultrafast dynamics in electronic structure of epitaxial Gd(0001) on W(110). *Journal of Electron Spectroscopy and Related Phenomena*, 189(2013):40–45, aug 2013.

[197] Fausto Sirotti, Nathan Beaulieu, Azzedine Bendounan, Mathieu G. Silly, Christian Chauvet, Gregory Malinowski, Guido Fratesi, Valérie Véniard, and Giovanni Onida. Multiphoton <math xmlns="http://www.w3.org/1998/Math/MathML"><mi>k</mi></math>-resolved photoemission from gold surface states with 800-nm femtosecond laser pulses. *Physical Review B*, 90(3):035401, jul 2014.

[198] Mathieu G. Silly, Tom Ferté, Marie Agnes Tordeux, Debora Pierucci, Nathan Beaulieu, Christian Chauvet, Federico Pressacco, Fausto Sirotti, Horia Popescu, Victor Lopez-Flores, Marina Tortarolo, Maurizio Sacchi, Nicolas Jaouen, Philippe Hollander, Jean Paul Ricaud, Nicolas Bergeard, Christine Boeglin, Bharati Tudu, Renaud Delaunay, Jan Luning, Gregory Malinowski, Michel Hehn, Cédric Baumier, Franck Fortuna, Damjan Krizmancic, Luigi Stebel, Rudi Sergo, and Giuseppe Cautero. Pump-probe experiments at the TEMPO beamline using the low-α operation mode of Synchrotron SOLEIL. *Journal of Synchrotron Radiation*, 24(4):886–897, jul 2017.

[199] Bradley Ferguson and Xi-cheng Zhang. Materials for terahertz science and technology. *Nature Materials*, 1:26–33, 2002.

[200] Masayoshi Tonouchi. Cutting-edge terahertz technology. *Nature Photonics*, 1:97–105, 2007.

[201] Philippe Scheid, Gregory Malinowski, Stéphane Mangin, and Sébastien Lebègue. Ab initio study of electronic temperature effects on magnetic materials properties. *Phys. Rev. B*, 99:174415, 2019.

[202] Philippe Scheid, Sangeeta Sharma, Gregory Malinowski, Stéphane Mangin, and Sébastien Lebègue. Ab Initio Study of Helicity-Dependent Light-Induced Demagnetization: From the Optical Regime to the Extreme Ultraviolet Regime. *Nano Letters*, 21:1943–1947, 2021.

[203] M. Deb, P. Molho, B. Barbara, and J.-Y. Bigot. Temperature and magnetic field dependence of rare-earth iron exchange resonance mode in a magnetic oxide studied with femtosecond magneto-optical Kerr effect. *Phys. Rev. B*, 94(5):054422, 2016.

[204] Yong Xu, Michel Hehn, Weisheng Zhao, Xiaoyang Lin, Grégory Malinowski, and Stéphane Mangin. From single to multiple pulse all-optical switching in GdFeCo thin films. *Physical Review B*, 100:064424, 2019.

[205] Boyu Zhang, Yong Xu, Weisheng Zhao, Daoqian Zhu, Xiaoyang Lin, Michel Hehn, Gregory Malinowski, Dafiné Ravelosona, and Stéphane Mangin. Energy-Efficient Domain-Wall Motion Governed by the Interplay of Helicity-Dependent Optical Effect and Spin-Orbit Torque. *Physical Review Applied*, 11:034001, 2019.

[206] Boyu Zhang, Yong Xu, Weisheng Zhao, Daoqian Zhu, Huaiwen Yang, Xiaoyang Lin, Michel Hehn, Gregory Malinowski, Nicolas Vernier, Dafiné Ravelosona, and Stéphane Mangin. Domain-wall motion induced by spin transfer torque delivered by helicity-dependent femtosecond laser. *Physical Review B*, 99:144402, 2019.

[207] Boyu Zhang, Daoqian Zhu, Yong Xu, Xiaoyang Lin, Michel Hehn, Gregory Malinowski, Weisheng Zhao, and Stéphane Mangin. Optoelectronic domain-wall motion for logic computing. *Applied Physics Letters*, 116:252403, 2020.